REPORT DOCUMENTATION PAGE

Form Approved
OMB No. 0704-0188

PLEASE DO NOT RETURN YOUR FORM TO THE ABOVE ADDRESS.

1. REPORT DATE *(DD-MM-YYYY)*	2. REPORT TYPE	3. DATES COVERED *(From - To)*
21-06-2007	Final	27-03-2007 --- 30-09-2008

4. TITLE AND SUBTITLE

A Megawatt Power Module for Ship Service - Supplement
Volume 1 Program Technical Report

5a. CONTRACT NUMBER

N00014-07-C-0361

5b. GRANT NUMBER

5c. PROGRAM ELEMENT NUMBER

6. AUTHOR(S)

Herbst, John D.
Gattozzi, Angelo L.
Hebner, Robert E

5d. PROJECT NUMBER

5e. TASK NUMBER

5f. WORK UNIT NUMBER

7. PERFORMING ORGANIZATION NAME(S) AND ADDRESS(ES)

The University of Texas at Austin, Center for Electromechanics
10100 Burnet Road, Bldg 133
Austin, TX 78758-4497

8. PERFORMING ORGANIZATION REPORT NUMBER

RF280 Volume 1

9. SPONSORING/MONITORING AGENCY NAME(S) AND ADDRESS(ES)

Office of Naval Research
875 North Randolph Street
Arlington, VA 22203-1995

10. SPONSOR/MONITOR'S ACRONYM(S)

ONR

11. SPONSOR/MONITOR'S REPORT NUMBER(S)

12. DISTRIBUTION/AVAILABILITY STATEMENT

Approved for Public Release; distribution is Unlimited.

13. SUPPLEMENTARY NOTES

14. ABSTRACT

This report is Volume 1 of a three volume Final Report on ONR Contract N00014-07-C-0361. Activities documented in this report were performed as a supplement to ONR Grant N00014-06-01-0886. The two programs address the use of energy storage and high speed power generation to reduce fuel consumption of DDG51 Arleigh Burke class ship service generation system by improving efficiency and permitting safe operation on one gas turbine generator set. In the event of turbine failure, the energy storage unit will provide power for critical loads until a second gas turbine generator set can be brought online. Volume 1 of the Final Report documents trade studies and preliminary design of the energy storage flywheel and associated motor/generator, the final system topology, high fidelity modeling and simulation activities, and top level platform integration issues. Volume 2 of the Final Report is a User's Manual for the high fidelity MatLab Simulink system simulation model. Volume 3 of the Final Report documents projected fuel savings, a preliminary interface control matrix, a ship installation study, and a technology development plan.

15. SUBJECT TERMS

16. SECURITY CLASSIFICATION OF:			17. LIMITATION OF ABSTRACT	18. NUMBER OF PAGES	19a. NAME OF RESPONSIBLE PERSON
a. REPORT	b. ABSTRACT	c. THIS PAGE			Herbst, John D.
U	U	U	UU	106	19b. TELEPHONE NUMBER *(Include area code)* 512-232-1645

Reset

Standard Form 298 (Rev. 8/98)
Prescribed by ANSI Std. Z39.18

Megawatt Power Module for Ship Service Supplement

ONR Contract N00014-07-C-0361

Final Report

Volume 1

Program Technical Report

Submitted by:

J.D. Herbst, A.L. Gattozzi, and R.E. Hebner

RF 280

Center for Electromechanics
The University of Texas at Austin
1 University Station, R7000
Austin TX 78712

January 2009

Contents

Executive Summary 1

Program Overview 3
Background 3

Flywheel Motor/Generator 5
Trade Study 5
Existing AC Induction MG with Separate Excitation Circuit 5
Permanent Magnet M/G 6
Wound Field Synchronous M/G 7
Homopolar Inductor Alternator M/G 8
Motor/Generator Technology Comparison 11
HIA Machine Concept Integration 12
Preliminary 1 MW HIA Performance Analysis 15
Field Coil Design Check 19

Flywheel Energy Storage 22
Flywheel Rotordynamic Analysis 22
FW Point Design Options for Ship Integration 26
Preliminary Evaluation of FW and Motor Generator Integration 29
Flywheel Bearing Loads due to Ship Motion 32
Flywheel Discharge Sequence Option Evaluation 35

Baseline 1.25 MW Flywheel Motor Generator and Power Electronics 39
1.25 MW HIA Design 39
1.25 MW Power Electronic Modules 40
Flywheel Motor Generator Rotor Stress Analysis 40
Number of Flywheels and System Package Modeling 42
Flywheel System Component Technical Specifications 45

System Modeling with Simulink 47
Background 47
Rationalization of the Model 47
High Fidelity Turbine Model 50
Realistic Load Models 54
Improved VFD Model 61
Extended System Simulations 62
Control System Upgrade 64
Modeling Summary 78

Technology Demonstration and Development Planning 79
System Definition 79
Demonstration of Flywheel Discharge 83
Starting Gas Turbine in Laboratory 84

Flywheel System Reliability and Maintenance Estimation 85
Background 85
Energy Storage System 85
Flywheel Design Life 85

Flywheel Magnetic Bearing Control System MTBF 88
Flywheel Motor Generator System Life 88
Flywheel Motor Generator Electrical Insulation Life 89
Flywheel Motor Generator Shaft Encoder MTBF 89
Flywheel Motor Generator Bearing MTBF 90
Appendix 1. Homopolar Inductor Alternator Technology Literature Search 97

Tables

Table 1. Evaluation of MG topologies based on technical risk issues 11
Table 2. Evaluation of MG topologies based on overall assessment 12
Table 3. HIA motor generator design example dimensions 17
Table 4. HIA motor generator design example performance predictions 18
Table 5. HIA motor generator field coil magnetic circuit calculations 20
Table 6. HIA motor generator field coil sizing 21
Table 7. Long flywheel design parameters 24
Table 8. Flywheel operating speeds vs. flexible mode results 24
Table 9. Flywheel point designs for multi unit installations 26
Table 10. Motor generator physical and electrical parameters 30
Table 11. Radial and axial bearing reaction forces for several sea state conditions 33
Table 12. Nominal flywheel ratings for discharge sequence options (4 FW, 5 min. discharge at 2.5 MW) 35
Table 13. Motor generator physical and electrical parameters 39
Table 14. Physical characteristics for 2.5 MW, 10 minute UPS energy storage system 45
Table 15. Electrical characteristics for 2.5 MW, 10 minute UPS energy storage system 46
Table 16. Representative simulation scenario for system modeling 50
Table 17. Load profiles for extended duration simulation. 63

Table 18. Summary of calculated and estimated flywheel system maintenance data 91
Table 19. Summary of maintenance issues for flywheel energy storage system 92
Table 20. List of spare parts inventory for flywheel energy storage system 93
Table 21. System level characteristics for 10 minute and 5 minute UPS duration 94
Table 22. Component characteristics for 10 minute UPS duration 96

Figures

Figure 1. Notional megawatt power module 4
Figure 2. Section view of homopolar inductor alternator 9
Figure 3. Comparison of induction (left) and HIA (right) geometry 13
Figure 4. Results of preliminary stress analysis to determine feasibility of assumed HIA rotor geometry 14
Figure 5. HIA motor generator section 17
Figure 6. HIA motor generator flux path and magnetic circuit model 19
Figure 7. Deflected mode shape results for 2nd flexible mode of rotor (free-free) 24
Figure 8. XLRotor model of rotor for rotor dynamic analysis 25
Figure 9. Variation of rotor modes with operating speed 25
Figure 10. Comparison of rotor sizes for 4 FW and 8 FW installation cases 26
Figure 11. Section of 210 MJ flywheel rotor model showing reduced thrust bearing 27
Figure 12. Section of flywheel including all main internal components 29
Figure 13. Integrated 210 MJ flywheel and 525 kW HIA motor generator package 31
Figure 14. Flywheel system depicted in representative integrated electric power system 31
Figure 15. Mathcad document for calculating bearing reaction forces 34
Figure 16. Flywheel system discharge sequence for parallel flywheel configuration 36

Figure 17. Flywheel system discharge sequence for parallel / series flywheel configuration 37
Figure 18. Flywheel system discharge sequence for serial flywheel configuration 38
Figure 19. Proposed flywheel configuration and discharge sequence for 10 minute 2.5 MWe case 38
Figure 20. Von Mises stresses in HIA rotor core due to 300 m/s centrifugal loading 41
Figure 21. Von Mises stresses in HIA rotor core due to 300 m/s centrifugal loading, detail lobe root 42
Figure 22. Concept flywheel package for standalone ship energy storage system 44
Figure 23. Schematic diagram of the basic MPM skid used for simulation studies 48
Figure 24. Overall system model 49
Figure 25. Turbine rpm vs. time under the load transitions 51
Figure 26. Turbine transient when the actual system is connected after the initial 5 s initialization 52
Figure 27. Detail of turbine transient under load reduction from 1.8 MW to 0.75 MW 52
Figure 28. Detail of turbine transient under load increase from 0.75 MW to 1.8 MW 53
Figure 29. Detail of turbine transient when the system load is raised from 1.8 to 4.2 MW 53
Figure 30. Detail of section with models of motor loads 1 (top) and 2 (bottom) 55
Figure 31. Detail of section with models of motor loads 3 with variable speed drive 55
Figure 32. Line-to-line voltage response to successive starts of two induction motors 56
Figure 33. Starting current profile of motor no. 1 57
Figure 34. Starting current profile for motor number 2 58
Figure 35. DC bus currents at the time of starting of motor number 1 59
Figure 36. DC bus currents at the time of starting of motor number 2 59

Figure 37. Transient response of line-to-line voltage and dc bus voltage after starting of motor number 3 60
Figure 37. Detail of waveforms 61
Figure 38. Icon, mask parameters, and first layer of improved model for the variable frequency drive 62
Figure 39. Extended time simulation with various loads - simulation was interrupted after 19.46 s for insufficient memory 63
Figure 40. Voltage loop flowchart – part 1. 65
Figure 41. Voltage loop flowchart – part 2. 66
Figure 42. Current loop flowchart. 67
Figure 43. Control action flowchart. 68
Figure 44. Parameter input screen for control block for flywheel generator field and active rectifier 69
Figure 45. New control block for flywheel generator field and active rectifier 70
Figure 46. First level of final control block for flywheel generator field and active rectifier 70
Figure 47. Detail of voltage loop sub-block 71
Figure 48. Detail of current loop sub-block 72
Figure 49. Initialization transient for the turbine rpm that is reflected in an unregulated voltage output from the permanent magnet turbine generator 73
Figure 50. Line-to-line voltage on the ac bus showing effect of control system 74
Figure 51. DC bus currents during initial transient 75
Figure 52. Line-to-line ac bus voltage as load current is stepped up from initial no-load 76
Figure 53. Fundamental current and total harmonic distortion (x100) during step load transients 77
Figure 54. Basic block diagram of demonstration system 80
Figure 55. Example composite rotor component for large energy storage flywheel 86

Executive Summary

Increasing demand for reliable, efficient electric power aboard ships coupled with rising fuel and logistics costs have increased interest in reducing fuel consumption throughout the US Navy. This contract addresses the use of energy storage and high speed power generation to reduce fuel consumption of DDG51 Arleigh Burke class destroyers. Electric energy storage can add significant value to the efficiency, operation, and reliability of naval ship power systems. The energy reserve can improve ship efficiency and reduce fuel consumption by acting as an uninterruptible power supply (UPS) and enabling single generator operations. This allows a single gas turbine to operate closer to its peak efficiency point rather than the current practice of running two generator sets at light load. In the event of turbine failure, the energy storage unit provides power for critical loads until a second generator set can be brought online.

Energy storage can also provide new operational capabilities to supply or absorb transient loads, such as pulsed energy weapon systems and underway replenishment systems, thus isolating the main generator from the duty cycle these dynamic loads impose. Beyond UPS mode, energy storage can be used to improve reliability and power quality by stabilizing the grid against voltage, frequency, and power factor variations. Energy storage, therefore, offers many advantages and will likely be a high priority addition to future naval ships as well as retrofits to existing platforms.

This contract, aimed at considering some of these issues, was awarded as a supplement to work done under ONR Grant N00014-06-01-0886 “A Megawatt Power Module for Ship Service”, whose effort it expands and completes. In the grant, it was shown that the preferred energy storage technology was by means of flywheels due to their relatively small size and high turnaround efficiency.

One critical benefit for retrofit integration of energy storage into the DDG-51 class ships is the ability to package the energy storage flywheel system in the current volume of modified AG9140 power systems. Space can be made available for this addition by removing the gear box and low speed generator, and replacing them with a compact, direct drive generator and 60 Hz inverters. These modifications free the needed volume to package the flywheels within the existing volume.

Under the present contract the following major activities were conducted:

a. identification and preliminary design of a suitable motor/generator for the flywheel storage
b. trade study to define optimal flywheel storage strategy and related technical issues
c. additional modeling and simulation to evaluate the technology demonstrator and completion of a high fidelity simulation model of the system
d. developed plans for a technology demonstrator leveraging experience and hardware from other programs
e. preliminary evaluation of retrofit issues and integration of the system into the DDG51 platform

Based on the system modeling, fuel savings projections, and the ship integration studies, the high speed generator and flywheel energy storage system are a viable approach to realizing significant fuel savings on the DDG51 ship service generation system. The flywheel energy storage system is effective at mitigating system transients and can provide the required 10 minute ride-through duration to enable multiple start attempts on a second gas turbine generator set. Solid models of the system show that the modified system can be installed with minimal extension beyond the footprint of the current AG9140 ship service generator sets. A ship installation study identified a procedure to enable retrofit of the new ship service generator system components while minimizing the need for hull penetrations. Using the fuel costs, load profile and duty cycle from BAA07-029, projected fuel savings are one the order of $1M per year per ship.

Program Overview

Background

Office of Naval Research Contract N00014-07-C-0361 was awarded on March 27, 2007 and received by UT-CEM on April 6, 2007. This report covers project activities until the end of the contract in September 2008. Activities under this contract have been conducted as a supplement to efforts under ONR Grant N00014-06-01-0886 "A Megawatt Power Module for Ship Service", therefore the reader is encouraged to consult also the final report of that grant for a complete overview of the project.

This program, under both grant and contract, addresses the use of energy storage and high speed power generation to reduce fuel consumption on military ships. To focus the analysis on a specific application, the DDG51 Arleigh Burke class ships was studied. Specifically, this program aims at improving efficiency and permitting safe operation of the ship on one gas turbine generator set running close to its rating, rather than the current practice of running constantly two generator sets at light load. In the event of turbine failure, the energy storage unit will provide power for critical loads until a second generator set can be brought online.

The basic concept for an advanced Megawatt Power Module (MPM), as discussed in detail in the grant's final report, is shown in figure 1. The major objective of the present contract was the abatement of technological risks inherent with the introduction of a new technology in a naval environment. To this end, the definition of a cost effective technology demonstrator that would represent adequately the notional system in figure 1, supported by suitable simulation studies, and the specification of critical components, supported by necessary trade studies, became central goals of the program.

This demonstrator would be designed to de-risk the follow-on ship-system specific production unit identifying and closing any system specific technology gaps. It would contain all the major components of the production system focusing on maturing the Technology Readiness Level (TRL) of an optimized power system including high speed generator topology, high-energy flywheel, power generation and power conversion technologies.

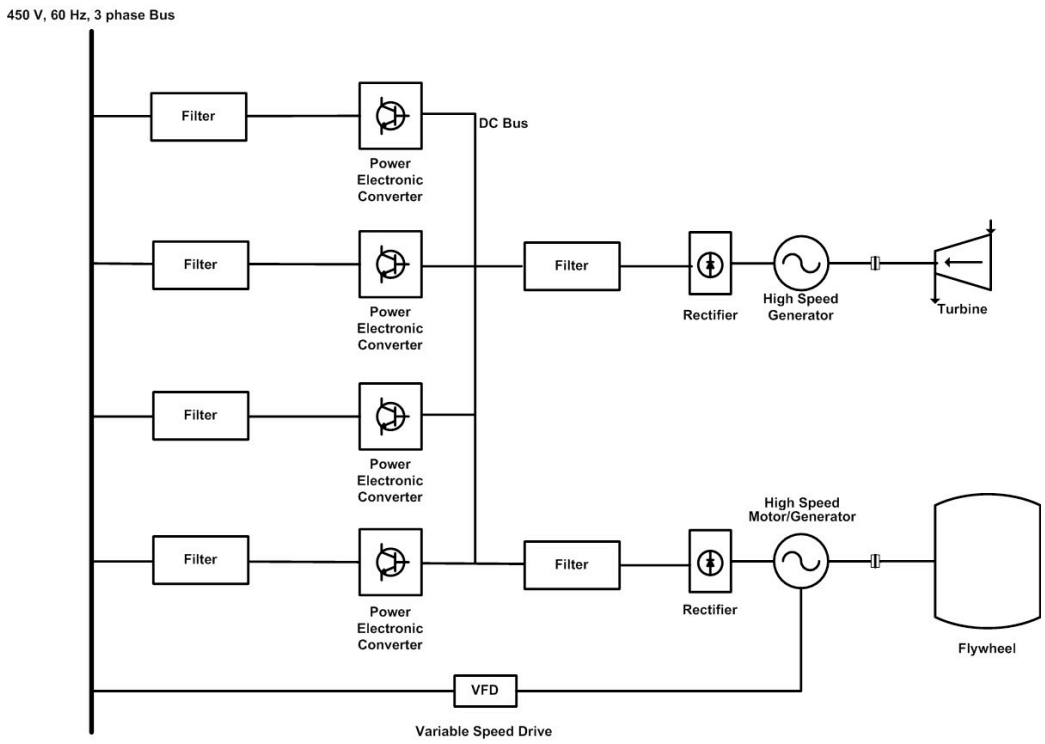

Figure 1. Notional megawatt power module

Prior to the undertaking of this project, the University of Texas at Austin Center for Electromechanics (UT-CEM) had just completed a program for a locomotive power system similar to the present project for class DDG51 destroyers. Under this program, known as the Advanced Locomotive Propulsion System (ALPS), key components of a 2 MW flywheel energy storage system were built and tested and became part of a laboratory demonstration system at UT-CEM. Consequently, it was possible to leverage the experience as well as the actual hardware developed under ALPS in the performance of the work under the present contract to reduce the cost of a planned demonstrator system. Therefore, an additional key task throughout the performance of this contract became the preliminary evaluation of the technologies and design criteria used in the ALPS energy storage system relative to the DDG51 marine application. Finally, issues related to integration of the proposed system as a retrofit in a DDG51 destroyer environment, its reliability, and the projected fuel savings accruing from its adoption were investigated.

Flywheel Motor/Generator

Trade Study

A full trade study among the different options for the flywheel motor/generator was conducted and is summarized herein. Concomitant with this work, simulation of the performance of the selected machine was done in large part under the companion grant (N00014-06-01-0886) from ONR and is reported in that final report.

The envisioned technology demonstration of uninterruptible power supply (UPS) functionality of the Megawatt Power Module (MPM) would employ the existing ALPS flywheel (FW) hardware where possible. A recognized limitation of the ALPS energy storage system for this application is the existing AC induction motor/generator (M/G) design. The AC induction machine requires external voltage and frequency excitation (supplied through an external power converter or motor drive) to function in generator mode. This issue highlights a key difference between the ALPS power system and ONR MPM: in the ALPS system, the flywheel's intended function was to deliver and recover energy from an ever-present DC bus through an active power converter which established the line voltage and frequency, not to generate into a dead bus during a fault of the primary power generation system, which is one of the requirements for the MPM.

Although a technical demonstration using the induction machine is possible, the existing induction M/G is not well suited to the technology demonstration or the target Engineering Development Model (EDM) system for the ONR MPM. Therefore, alternative motor/generator topologies were reviewed and evaluated for suitability relative to the energy storage system for the DDG51 power system application. The conclusion of this study recommends the selection of the "Homopolar Inductor Alternator" otherwise known as an "AC Homopolar" or "Synchronous Homopolar" machine for this application. The various motor/generator machine topology options are summarized in the following sections.

Existing AC Induction MG with Separate Excitation Circuit

This option considers the risks and benefits of using the existing ALPS induction machine with external circuitry for the system demonstrator. This option offers low hardware cost as this machine is currently built and operational, however it is not representative of an

EDM machine since the induction machine is ultimately a poor choice for the DDG51 ship service application. Additionally, there are substantial technical risks associated with this approach.

While an induction machine is inherently unable to generate output without excitation, it is nevertheless technically possible to supply temporary external AC excitation to activate or "boot strap" the machine to the point that the machine can generate net power, allowing the main inverter to then take over and regulate machine voltage and frequency. This "self excited induction generator" (SEIG) mode of operation is however very challenging due to the fact that machine output is a function of multiple variables: speed, electrical frequency, load, and power factor, over which the controller does not necessarily have independent control.

Literature shows that intensive modeling and simulation work can be performed to predict the performance envelope and design a controller for SEIG mode, however the system will remain sensitive to modeling error and there is therefore a risk that extensive debugging will be necessary during testing. The key risks of this approach occur in the test phase and include: 1) low output capability, 2) large output voltage and power swings, and 3) potential collapse of output. Without additional power conversion equipment, collapse of the induction machine output could result in a fully charged flywheel with no effective way to dissipate the stored energy. Given the goal of demonstrating reliable power with a tight power quality band, the high risk of this approach failing to meet the performance specifications is not worth the potential hardware savings costs. Additionally, this approach would demonstrate a machine that is substantially different from the target EDM configuration. For these reasons, the SEIG option is not recommended for the demonstrator machine.

Permanent Magnet M/G

This option considers building a replacement M/G as a conventional synchronous AC permanent magnet (PM) rotor design. This approach may allow use of portions of the existing MG housing as a cost savings measure.

The PM synchronous machine has a strong advantage in its ability to generate AC output into a dead bus. The PM design is very power dense, having the advantage of being potentially

the smallest design for the required power range. Further, this type of machine design is mature and therefore relatively straightforward to design with good predictability of output.

A critical disadvantage of the PM design as a flywheel M/G is that its output voltage is dependent on the operational speed. In a flywheel (FW) application in which speed varies over a 2:1 range in order to supply the required energy, the PM machine output voltage will also vary by this large range. When designed to meet rated voltage at the ½ speed point, the high machine voltage (~2 kV) at full speed will likely become problematic for the power electronics required to interface the flywheel energy storage system to the ship service ac bus.

Another negative attribute of the PM machine is its risk of uncontrolled discharge in a fault condition. In the event of a stator fault or system short circuit, the PM machine will continue to passively generate voltage as long as the flywheel is spinning, without the ability to switch it off, as the PM field on the rotor cannot be regulated. This risk of uncontrolled discharge (energy release) could further result in catastrophic mechanical failure or system damage. This issue is especially critical considering the large amount of energy storage required by the DDG51 ship power system application.

Mechanically, the design and fabrication of the PM rotor is also challenging for high speed applications. In particular, magnet retention at high tip speeds requires detailed stress analysis and potential fabrication and installation of composite retention bands, both of which add cost over some other design options.

Wound Field Synchronous M/G

This option considers building a replacement M/G as a conventional synchronous AC wound field (WF) rotor design. This approach may allow use of portions of the existing induction M/G housing as a cost savings measure.

Like the PM synchronous, the WF synchronous machine has a strong advantage in its ability to generate AC output into a dead bus. The WF is only a slightly less power dense machine than the PM machine, as it requires an exciter and rotating diode array on the rotor to inductively energize the field winding. The WF machine is a mature technology and relatively straightforward to design with good predictability of output.

The WF machine also has an advantage over the PM machine in its ability to be regulated through control of the field excitation. This overcomes both the voltage speed dependence problem and the uncontrolled discharge risk. The WF machine voltage can be adjusted as a function of speed and load, and can be "turned off" when not needed to reduce losses or prevent unintended discharge.

The main drawbacks of the WF machine relate to the fabrication complexity and reliability risks of insulated windings and diode rectifiers on a high speed rotor. For moderate speed applications, the wound field machine is very robust. However, in high speed applications, the increased centrifugal loading of the conductors can lead to relative motion and insulation damage. This situation can be exacerbated by the transient nature of the UPS application – stresses due to thermal gradients during high power transient discharges can increase the mechanical stresses on the critical field winding insulation system. Development of winding fabrication techniques and extensive prototype testing are required to ensure a reliable and robust design of a WF machine for high speed applications. These factors imply significant development costs and potential technical risks during testing.

Homopolar Inductor Alternator M/G

This option considers designing and building a replacement M/G design for the FW, in the topology of a "homopolar inductor alternator" (HIA). This approach may also allow use of portions of the existing M/G housing as a cost savings measure.

The homopolar inductor alternator, also known as "AC homopolar" or "synchronous homopolar" machine is one of the less common topologies that is recently finding renewed success as a FW M/G because of its particular suitability to the application. The HIA has a long history of use as a high frequency generator dating back to 1942; however in most conventional applications it has been superseded by WF or PM synchronous machines. Despite its modest commercial use, it is a strong candidate for a high speed FW M/G and is worth revisiting from this new perspective. As part of the technology assessment, an extensive literature search was conducted to explore prior and current work on this machine topology; the bibliography of the literature search is attached to this report as Appendix 1.

The general components of the HIA are shown in figure 2.

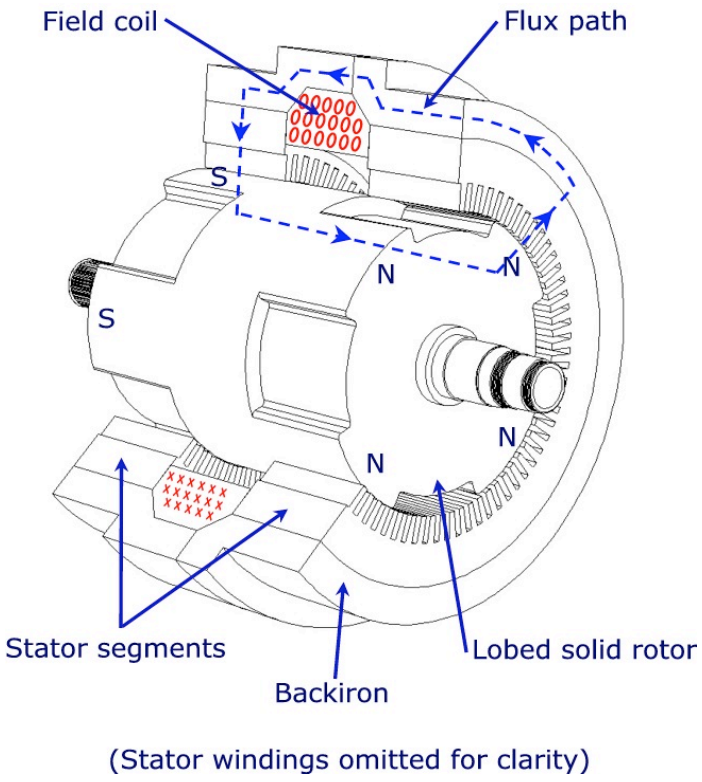

Figure 2. Section view of homopolar inductor alternator

The unique characteristics of an HIA machine for use in FW M/G applications are: solid robust rotor mechanical structure for reliability and long life at high operating speeds, external output control for regulation ability over a large speed range, low rotor losses–near zero in standby mode for easier thermal management (possibly within the vacuum housing), and terminal characteristics which mimic conventional synchronous ac machines allowing for the use of off-the-shelf motor drive technology.

The HIA is an externally excited synchronous machine with the field winding located on the stator side, with an otherwise conventional stator winding. The rotor is a solid steel construction bearing no electrical windings or magnets. The rotor is normally sectioned into two segments, with toothed lobes. The circumferentially wound field coil creates a flux which flows axially through the stator backiron, radially inward through one half of the rotor, axially down the rotor, and radially outward through the other rotor segment. All poles on each lobed rotor

segment are the same polarity (hence the name homopolar); one segment is all north poles, the other all south. These rotor lobes create permeance waves that generate the alternating MMF field.

The HIA combines the key functionality advantages of the other topologies, with some additional advantages as well. Like a PM machine, the HIA machine has the ability to generate output into a dead bus. Like a WF machine, the HIA machine has full field control to adjust for speed and load variations, and retains the ability to turn the machine "off" in standby mode or to prevent unintended discharge. Further, the HIA machine can provide all of these ideal functions without the need for permanent magnet retention or the risk of rotor winding insulation failure. Additionally, the HIA rotor magnetic losses can be designed to be extremely low, near zero in standby mode. This feature may allow the ultimate EDM machine to be integrated into the FW vacuum housing, providing a smaller overall package, and possibly eliminating the maintenance of vacuum seals and rolling element bearings altogether.

One potential negative aspect of the HIA design for this application is a lower power density than the other M/G technology options considered. The HIA machine output is in general lower than other machine topologies due to its low utilization of the magnetic circuit, resulting in a larger machine for the same power output. However, considering the possibility of integrating the EDM machine into the vacuum housing due to its low losses, the whole package with an HIA may in fact be smaller as the larger machine size may be outweighed by the elimination of a shaft coupling, vacuum seal, and mounting adaptor.

Another potential negative trait of the HIA machine is the windage loss and noise caused by the large teeth or lobes on the surface of the rotor. One potential solution for this is to fill the gaps between the teeth with a lightweight non-magnetic material restrained by a retention banding, adhesive bonding, engagement features, or a combination. The use of a retention banding increases the magnetic air gap and therefore compromises the magnetic design, so this should be avoided if possible. If the designed losses are sufficiently low, the machine may be integrated into the vacuum housing for the EDM flywheel battery, and windage would therefore not be an issue.

Another potential drawback of the HIA design is the relatively intense design work required to accurately predict the performance and losses of the machine. A 1 MW, turbine-

driven generator of this topology was built and tested by Schneider Electric France in the 1980's, but otherwise no published machines of this scale can be used as reference points. Since this machine is not very widely used, there are few established design guidelines and no turn-key design codes for optimizing the sizing. Further, the design is not conducive to 2-dimensional or axisymmetric analysis, so more labor intensive 3-D analysis must be performed. For this reason, the performance of the concept HIA would require more thorough analysis than conventional electric machine geometries. However, the design work fundamentally employs very predictable electromagnetic theory and does not require any new development per se.

Based on the strong technical merits of the HIA machine for this application and the potential advantage of integration into the flywheel housing for a smaller overall package in the EDM machine, strong consideration of the HIA machine is warranted.

Motor/Generator Technology Comparison

A detailed quantitative comparison of the machine types was performed based on both technical and overall considerations, and prepared in chart form in order to assist in the topology selection. In both technical and overall considerations, the homopolar inductor alternator was the strongest candidate. These charts are presented below as tables 1 and 2.

Table 1. Evaluation of MG topologies based on technical risk issues

	New design wound field synchronous	New design PM rotor synchronous	New design AC homopolar MG	Modify existing induction MG
Electrical Design	High	Low	Med	High *
Mechanical Design	High	Med	Med	Low
Voltage Speed Dependence	Low	High	Low	High *
Voltage Load Dependence	Low	Med	Low	High
Risk of Output Loss	Low	Low	Low	High *
Uncontrolled Discharge Risk	Low	High	Low	Low
Rotor Cooling	High	Low	Low	Low
Rotor Insulation Failure Risk	Med	Low	Low	Low

*Rating based on effort to achieve reliable self excitation of induction machine

Table 2. Evaluation of MG topologies based on overall assessment

	New design wound field synchronous	New design PM rotor synchronous	New design AC homopolar MG	Modify existing induction MG
Engineering Effort	High	Med	High	High *
Fabrication Effort	High	Med	Med	Low
Technical Risk	High	Low	Low	High *
Demonstrator Cost	High	High	Med	Low
Demonstrator Volume	Low	Low	Med	Med
Time to Complete	High	High	Med	Low
Risk of Demo Power Compromise	Low	Low	Med	High *
Safety Risk	Low	High	Low	Low
Difficulty for EDM	Med	High	Low	High

*Rating based on effort to achieve reliable self excitation of induction machine

HIA Machine Concept Integration

In order to evaluate the performance and output of the candidate HIA machine topology for adaptation to the ALPS flywheel system, the first step was to configure a machine to fit within the constraints of the existing induction machine geometry as a point of reference. This approach used the existing housing structure for the new design, simplifying fabrication and reducing costs for the technology demonstrator and leveraged the existing bearing systems, squeeze film dampers, lubrication, and sealing components—all of which are time consuming aspects of design and fabrication of a new high speed rotating machine prototype.

This process allowed the estimation of the important geometric parameters of the HIA used to evaluate its performance, including: rotor active length, rotor diameter, field coil area, end turn length, and air gap. Further, this process revealed key mechanical parameters for initial analysis such as rotor stresses and rotor dynamic loads. Assumptions were made in the preliminary sizing of the HIA including: machine pole count will be higher than the ALPS

machine, providing shorter end turns (which allows the HIA rotor to grow in length) and less stator yoke (allowing the HIA rotor to grow in diameter). The added length increases the output torque linearly, and the added diameter increases the output power with the square of the diameter increase. The field coil active length was set at 1/3 of the rotor core length which appears to be common in HIA machines. The stator slots were sized to occupy approximately 50% of the stator bore periphery, and their depth was set to 4x the width. The conductor coil size was reduced to reflect the difference between this machine's 1 MW intermittent duty requirement, and the induction motor's 2 MW continuous duty rating. The rotor air gap was reduced for the HIA as it was no longer required as a cooling channel for large rotor losses on the induction machine. The rotor lobe dimension was set using a common ratio approximately 10:1 between lobe and slot air gap. The stator back iron thickness was selected somewhat arbitrarily. It should be reiterated that these values are rough conceptual dimensions used in order to obtain approximate power output ratings, and that a detailed design process will have to be undertaken to optimize each parameter to ensure maximum power and efficiency.

A 3D solid model of the concept HIA machine was developed based on the ALPS induction motor model, and the two are shown in section for comparison in figure 3.

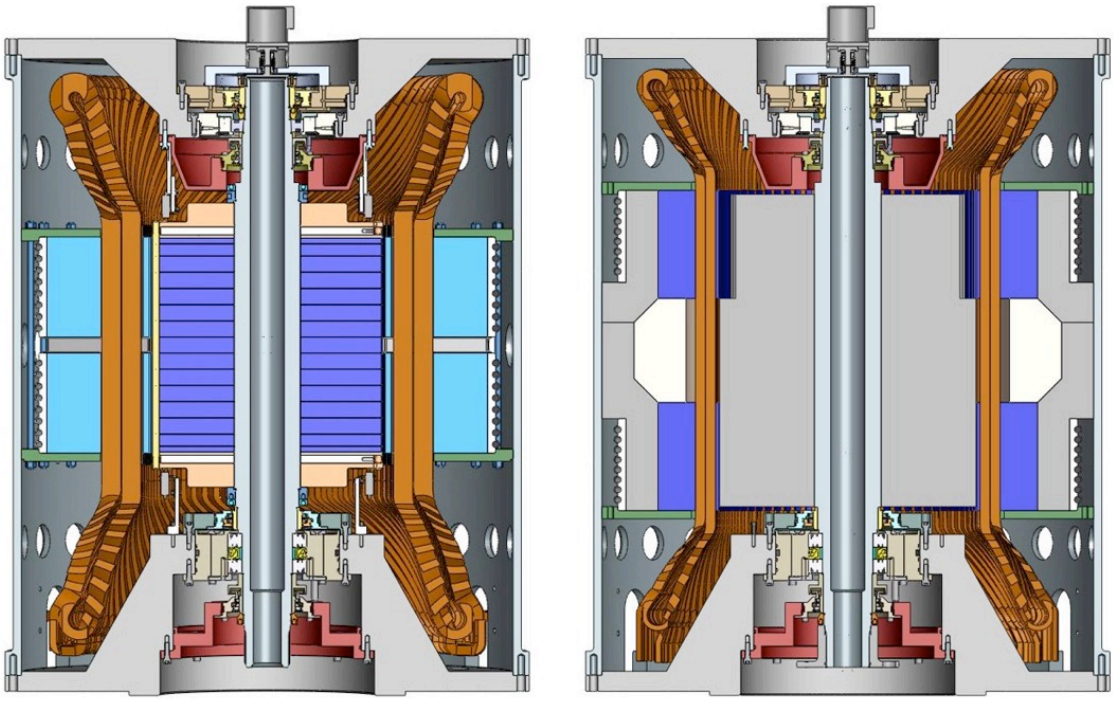

Figure 3. Comparison of induction (left) and HIA (right) geometry

The rotor diameter of 16 in. was an initial selection that required a mechanical feasibility check since the spin stresses in this part are ultimately a limiting factor. The rotor was analyzed for operation at 15,400 rpm which is the nominal overspeed of the ALPS flywheel. At this diameter and speed, the tangential velocity (tip speed) of the steel rotor would be 328 m/s, or 300 m/s at 14,000 rpm.

The analysis assumed an interference fit was required between a hollow rotor core and the shaft. Analysis results showed that the maximum stresses in the rotor core due to centrifugal loading and the interference fit at the overspeed condition were 100 ksi. This value would provide a very long fatigue life for heat treated, aircraft grade AISI 4340 steel which may have an ultimate strength >250 ksi. The conclusion of this preliminary analysis showed that the 16" diameter assumption for 15,400 rpm operation is feasible in a toothed solid HIA rotor, and could possibly be increased to provide more power if the flywheel testing employs a lower limit speed such as 14,000 rpm as predicted.

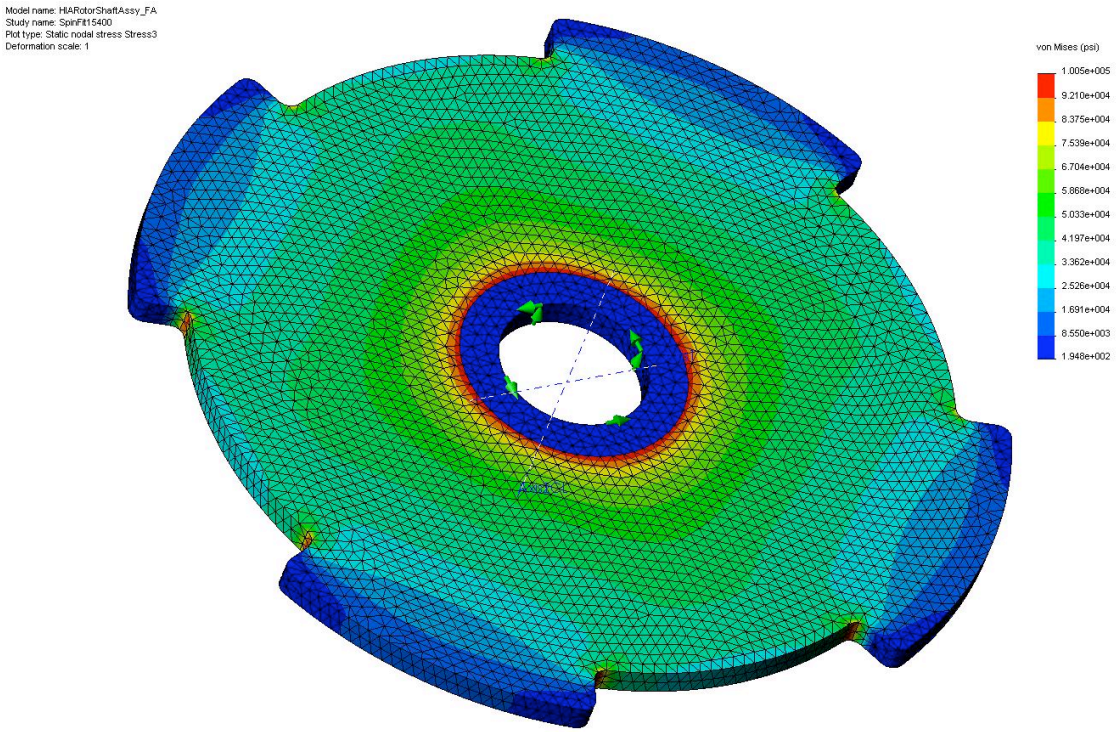

Figure 4. Results of preliminary stress analysis to determine feasibility of assumed HIA rotor geometry

Preliminary 1 MW HIA Performance Analysis

A baseline HIA machine design was developed and detailed closed-form calculations were performed to predict the power rating of the machine for the flywheel motor/generator application. The preliminary target for the HIA power rating was 1 MW to support a technology demonstration program using existing elements of the UT-CEM flywheel motor/generator. The 1 MW power rating was chosen so as to establish a good benchmark for the HIA while a detailed study of the system topology was being conducted: once the feasibility of this benchmark rating had been established, it would be relatively easy to adjust the design to satisfy the final requirements. This indeed was the case, as will be seen in later sections of this report.

Numerous mathematical treatments of the electro-mechanics of the HIA were reviewed in the literature to develop the basis for performance predictions. In particular, the works by Msekela[1], Jain[2], and Walker[3] provided the most thorough and applicable information. These closed form solutions (shown below) were implemented and then compared to two published machine designs for validation. Where necessary, parameters that were not included in the example designs had to be assumed for comparison. The results of the comparison between the predictions and the published performance of design cases showed excellent agreement, validating this approach. This method of predicting the HIA machine performance using closed form expressions was then applied to HIA machine designs of the scale needed in megawatt level flywheel motor/generators. For the detailed HIA machine design required for prototype fabrication, full physics based, 3-D finite element analysis would be performed to confirm the performance predictions with greater detail and fidelity.

The following closed form calculations were evaluated:

$$S_s = C_m \cdot D^2 \cdot L \cdot n$$

$$C_m = \frac{\pi^2}{60} 10^{-7} \cdot \alpha_i \cdot A_s \cdot B_\delta \cdot k_B \cdot k_{w1}$$

$$P_s = \eta \cdot \cos\varphi \cdot S_s$$

[1] Msekela, J.A.N., "A feasibility study of a high speed homopolar machine", PhD Thesis, 1995, KTH Royal Institute of Technology, Stockholm Sweden.

[2] Jain, G.C., “Design Aspects of a Homopolar Inductor Alternator”, IEEE Transactions on Power Apparatus and Systems, Vol. 83, pp. 1009-1015, October 1964.

[3] Walker, J.H., “The theory of the inductor alternator”, Proc. IEE Vol 89, 1942, pp 227-241.

where,

S_n = Apparent power of machine (VA)

C_m = Machine constant

P_n = Real power of machine (W)

D = Stator inner diameter (mm)

L = Active length of single rotor segment (mm)

n = Shaft speed (rpm)

A_1 = Stator current loading (A/cm)

B_δ = Peak air gap flux density (T)

k_B = EMF form factor

k_{w1} = Stator winding factor

η = Machine efficiency

$\cos \varphi$ = Load power factor

The HIA point design evaluated with this approach was a 1 MW motor/generator for a 15,000 rpm flywheel and the envelope of the UT-CEM induction motor/generator was used to define the overall extents of the geometry. This approach would enable the use of elements of the existing UT-CEM machine to reduce costs of a demonstration of this technology with the UT-CEM energy storage flywheel. While the maximum outer diameter and length of the machine were constrained, the rotor dimensions were not constrained to the existing values. The HIA machine's solid rotor allows it to operate at a larger diameter (and tip speed) due to the stronger construction than a squirrel cage induction rotor. Further, the HIA machine would be a higher pole count (four or greater) allowing a reduction of the stator yoke (permitting the same stator overall OD despite the larger ID and the addition of the field coil back iron) and reduced end turn length (permitting a longer rotor), thereby allowing more active length and diameter within the same overall dimensions, as shown in figure 5. The dimensions of the design case are listed in table 3.

Table 3. HIA motor generator design example dimensions

Stator overall OD (including backiron & cooling jacket)	30.68 in.
Stator ID	16.10 in.
Air gap	0.05 in.
Rotor core length	19.50 in.
Active length per segment	7.80 in.
Field coil axial length (between segments)	3.90 in.
Stator core overall length (end turn to end turn w/ connections)	33.60 in.

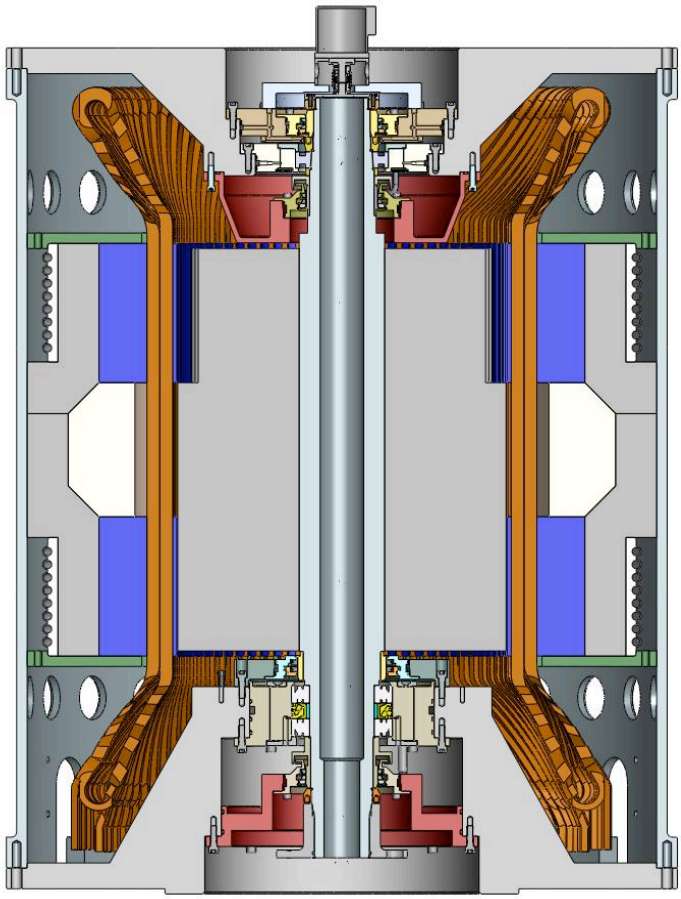

Figure 5. HIA motor generator section

The design example dimensions and the appropriate electrical parameters were analyzed with the HIA performance equations to estimate the output capability of this size machine. The parameters used in the HIA performance calculations are summarized in table 4.

The selected speed for the analysis was 7,500 rpm, corresponding to the half speed point of a 15,000 rpm flywheel. Due to the squared relationship between rotor speed and stored energy, the flywheel will deliver 75% of its peak stored energy at half speed. This design point was chosen since it is the most challenging condition (highest torque) when constant power is required over the 2:1 speed range.

The results show that this initial design example is capable of delivering 0.9 MW of real power into a 0.90 power factor rectifier load, which is near the 1 MW design goal.

Table 4. HIA motor generator design example performance predictions

C_m	4.42e-6	Machine constant
D	406	Stator inner diameter (mm)
L	198	Active length of single rotor segment (mm)
n	7500	Shaft speed (rpm)
α_δ	0.63662	Pole span factor
A_1	400	Stator current loading (A/cm)
B_δ	1.0	Peak air gap flux density (T)
k_B	1.1107	EMF form factor
k_{w1}	0.95	Stator winding factor
η	0.93	Machine efficiency
cos φ	0.90	Load power factor
S_n	1,081,901	Apparent power of machine (VA)
P_n	905,551	Real power of machine (W)

With further iteration the desired 1 MW performance should be achieved within the existing space envelope. With an approximately 10% increase to the stator current loading or air gap flux density, this machine design will produce the nominal 1.0 MW rating at the most challenging half speed point. At higher speeds, the power capability of the machine increases, therefore the field coil excitation can be regulated to provide constant power and constant voltage. This established the feasibility of the HIA design and any further detail was deferred to a later time when the final actual design rating would be decided.

Field Coil Design Check

One of the most unique aspects of the HIA machine is the axial flux field coil located on the stator. This component is not found in convention synchronous or induction machines, and therefore was worthy of a preliminary design check when implemented at the 1 MW scale.

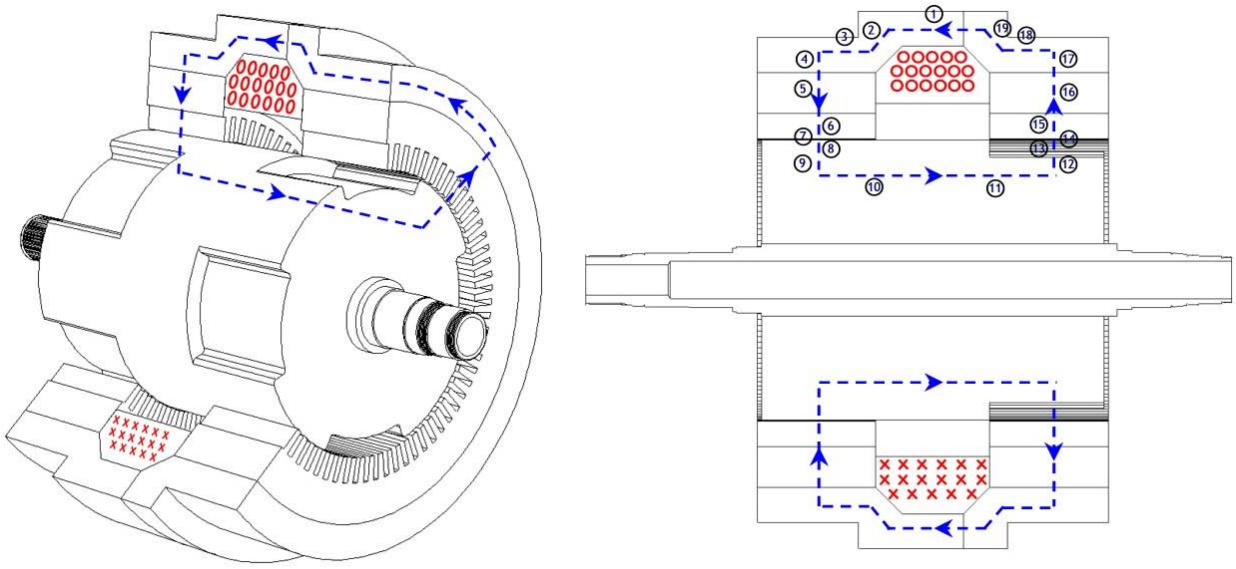

Figure 6. HIA motor generator flux path and magnetic circuit model

For this analysis, a magnetic circuit calculation was performed using the design example geometry (fig. 6). As an initial assumption, the field coil axial length was set to equal the length of one of the two rotor active segment lengths (6.5 in.), based on examples seen in smaller scale

designs in the literature. The magnetic circuit was decomposed into individual elements of simple geometry to compute the reluctance of the path. A magnetomotive force (mmf) was then applied to this circuit and varied to provide the desired 1.0 T peak air gap flux. Table 5 summarizes the HIA motor/generator field coil magnetic circuit calculations. Based on these calculations, the necessary mmf was 2950 A-t.

Table 5. HIA motor generator field coil magnetic circuit calculations

Computes Flux Path Elemental Values								
Description	*Mean Path Length [m]*	*Mean Path Area [m^2]*	*Path Relative Permeability []*	[R=l/(u*A)] *Path Reluctance [A-t / Wb]*	[B=Phi/A] *Path Mean Flux Density [T]*	[H=B/u] *Path Mean Magnetic Field [A/m]*	[mmf=H*l] *Path Mean Magnetizing MMF [A-t]*	[%=mmf/n*i] *Path Mean [% of MMF]*
Axial backiron	0.1524	0.11625896	500	2086	0.46	731	111	3.8
Backiron bend	0.053848	0.10004432	500	857	0.53	850	46	1.6
Axial backiron	0.085725	0.10004432	500	1364	0.53	850	73	2.5
Radial backiron	0.0254	0.15598483	500	259	0.34	545	14	0.5
Radial lams	0.059436	0.14057079	1000	336	0.38	302	18	0.6
Radial stator teeth	0.03683	0.02876932	1000	1019	1.86	1477	54	1.8
Air gap	0.00127	0.05286226	1	19118	1.01	804049	1021	34.6
Radial rotor teeth	0.0254	0.04940398	500	818	1.08	1721	44	1.5
Radial rotor	0.0381	0.07245917	500	837	0.74	1173	45	1.5
Axial rotor	0.08255	0.06688539	500	1964	0.80	1271	105	3.6
Axial rotor	0.08255	0.06688539	500	1964	0.80	1271	105	3.6
Radial rotor	0.0381	0.07245917	500	837	0.74	1173	45	1.5
Radial rotor teeth	0.0254	0.04940398	500	818	1.08	1721	44	1.5
Air gap	0.00127	0.05286226	1	19118	1.01	804049	1021	34.6
Radial teeth	0.03683	0.02876932	1000	1019	1.86	1477	54	1.8
Radial lams	0.059436	0.14057079	1000	336	0.38	302	18	0.6
Radial backiron	0.0254	0.15598483	500	259	0.34	545	14	0.5
Axial backiron	0.085725	0.10004432	500	1364	0.53	850	73	2.5
Backiron bend	0.053848	0.10004432	500	857	0.53	850	46	1.6

Field Coil Magnetic Structure Outputs

Total reluctance of structure	55231	(A-t/Wb) [Rt=R1+R2+…]
Total flux in structure	0.0534	(Wb) [Phi=mmf/Rt]
Flux linkage of structure	15.76	(Wb-t) [Lambda=n*Phi]
Inductance of structure	1.5757	(H) [L=Lambd <-- NOTE: only holds for one single coil winding (not parallel coils)

The calculated mmf was then applied to a realistic coil design to verify that the space allocated for the field coil is reasonable and to estimate the voltage, current, and resistive losses associated with operating the field coil in this 1 MW design example. The results of this analysis (table 6) showed that the field coil necessary to generate the required mmf could be 295 turns at 10 A, with a resistance of 1.88 Ohms. For this case, the field coil power supply could operate at 18.8 V, and generate only 188 W of losses. These values are very reasonable, and could be

easily contained in the allotted volume. In fact, the 1.54 A/mm^2 current density and 0.157 space utilization value were so conservatively low that the field coil space was reduced to 3.9 in. length for a second design iteration. The machine performance parameters presented earlier were generated using this updated 3.9 in. coil length.

Table 6. HIA motor generator field coil sizing

Field coil length, current density analysis	
Field coil current (A)	10
Number of turns of field coil (n)	295
Average coil radius (m)	0.3
Coil total length (m) [len=pi*Dmean*n]	556.06
Conductor area (m^2)	6.50E-06
Resistivity (Ohm-m) for hot Cu	2.20E-08
Resistance (Ohm) [R=rho*len/A]	1.88E+00
Current density (A/m^2) [J=i/A]	1.54E+06
I^2R loss (W) [P=i^2*R]	188.2
Coil voltage (V) [V=i*R]	18.8
Field coil cross sectional area (m^2)	1.918E-03
Design available field coil area (m^2)	1.218E-02
Ratio of calculated to available area	0.157

Based on these calculations, the selected HIA design it appears possible to implement a 1.0 MW HIA design using the geometry constraints of the existing ALPS induction motor/generator. More detailed design would be conducted as part of a prototype development activity for this machine.

Flywheel Energy Storage

Flywheel Rotordynamic Analysis

Installing or retrofitting energy storage flywheels into an existing Navy ship may require modifications to the ship for access, as a flywheel can be a relatively large component relative to the small access ways through the ship. A Rolls Royce study of DDG51 retrofit issues is presented in Volume 3 of this report. For example, the existing UT-CEM laboratory flywheel is approximately 65 in. in overall diameter and is designed to deliver 370 MJ. The ONR application initially was thought to require a total of 630 MJ of delivered energy based on 2.1 MW of power for 5 minutes, but as the program evolved, the baseline power level and required discharge duration times were extended to 2.5 MW with a 10 minute discharge duration. In order to eliminate or minimize the need for hull penetrations for the flywheel installation, the design of the flywheel had to be adjusted. If the flywheel overall diameter is designed appropriately, the units may be installed into the ship via existing passages, for example through an escape trunk. These considerations suggest that an ideal flywheel may be relatively small diameter and long length, and that multiple smaller flywheels may be used to meet the total energy storage requirements. A design goal is to provide all required energy storage and delivery from the energy storage flywheels located on only two of the three ship service generator sets, allowing one unit to be offline for maintenance or repairs.

Long, small diameter flywheels present technical challenges. The first design issue is the storage capacity -- flywheel energy grows with the cube of diameter (while holding tip speed constant), but only linearly with length. Reducing the flywheel diameter therefore strongly influences the stored energy density. Another challenge of high L/D flywheels is the impact on rotor dynamics. The maximum speed of all rotating machines is fundamentally limited by resonance – as a machine's operating speed approaches the frequency of a rotor flexible mode, resonance will occur and operation can become rough in the best case or unstable in the worst. Holding all other parameters the same, as a rotor gets longer, its flexible vibration mode frequencies decrease and the maximum speed must drop to avoid resonance.

Most rotating machines are designed to operate at a speed at least 20% below the first bending mode of the rotor to minimize response and avoid the risk of running through a

resonance. The UT-CEM flywheel is such a design, and its resulting composite length over diameter ratio (L/D) is 0.68. In order to design a smaller diameter flywheel, an L/D ratio closer to 2 would be desired. However, the implication is that the machine would need to run through the first flexible mode and operate above this critical frequency. This is in fact possible (and used in other machines) using active magnetic bearings located properly on the rotor with a compensator algorithm providing the system sufficient damping to minimize response of the flexible mode. The goal for this sizing analysis is therefore to operate above the first flexible mode, but with a minimum of 20% margin below the 2nd flexible mode.

To evaluate the practical limitations of length and diameter for flywheels in the size class demanded by the ONR application, a design sheet was developed. This process identified candidate designs over a range of L/D from 0.5 to 2.5; however, more detailed analysis was required to find the actual maximum length for a given diameter. The candidate flywheels of the design sheet were translated to 3-D solid models, and finite element frequency analysis was performed to identify the mode margins.

The first analysis case was for an overall diameter access limit of 41.5 in., with parameters listed in table 7. CosmosWorks frequency analysis was performed on many configurations of L/D at this diameter, and the results revealed that a reasonable upper limit of L/D for this case was 1.75, enabling four flywheels to provide the total energy storage requirement. Modal frequency results and the operating speeds are compared in table 8. A 20% mode margin between the rotor maximum speed (383 Hz) and the 2nd flexible mode (461 Hz) was achieved as desired. Figure 7 shows the exaggerated deflection shape of the 2nd flexible mode. Ideally, the 1st mode would be below the ½ speed operating point, however for this design it was slightly above the ½ speed frequency. These values are acceptable for a first pass design check and further design work would be performed to adjust the exact location of the modes in both the rotor and magnetic bearing compensator designs.

Additional rotordynamic analysis was performed in order to evaluate the effect of rotation on the location of the flexible modes using XLRotor software. This approach takes into consideration the gyroscopic stiffening effect which has a tendency to increase the frequency of modes at higher speeds. These results showed that the mode margins increased to the degree that the rotor could feasibly be lengthened (model and results shown in figures 8 and 9), allowing the

diameter to drop further. Additionally, this analysis revealed a very strong sensitivity to the size of the axial magnetic bearing, suggesting that the 3 g axial load capacity of the thrust bearing should be reconsidered. If a 1 g rated axial bearing would meet the needs of the application, the L/D ratio could be increased further, allowing easier installation into the ship.

Table 7. Long flywheel design parameters

Parameter	Value
Composite body L/D	1.75
Composite rotor OD (in.)	32.4
Composite rotor length (in.)	56.7
Overall OD (in.)	41.5
Composite mass (lbm)	2449
Rotor length overall (in.)	90
Shaft speed (rpm)	19146
Energy stored (total / deliverable) (MJ)	210 / 158
Motor generator power, parallel discharge (kW)	525
Motor generator peak torque @ ½ speed (N-m)	524

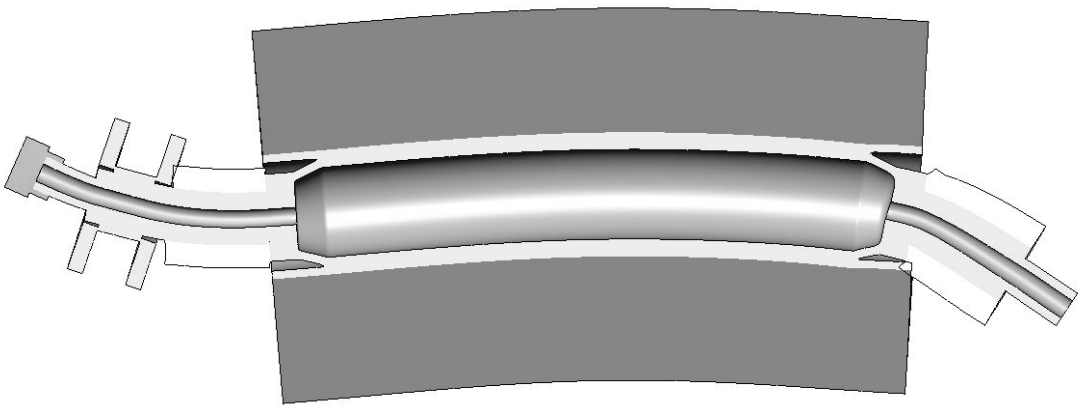

Figure 7. Deflected mode shape results for 2nd flexible mode of rotor (free-free)

Table 8. Flywheel operating speeds vs. flexible mode results

FW operating speeds	Rotor flexible modes
192 cps (½ speed = 9573 rpm)	206 Hz (1st)
383 cps (max speed = 19146 rpm)	n/a
460 cps (max speed + 20%)	461 Hz (2nd)

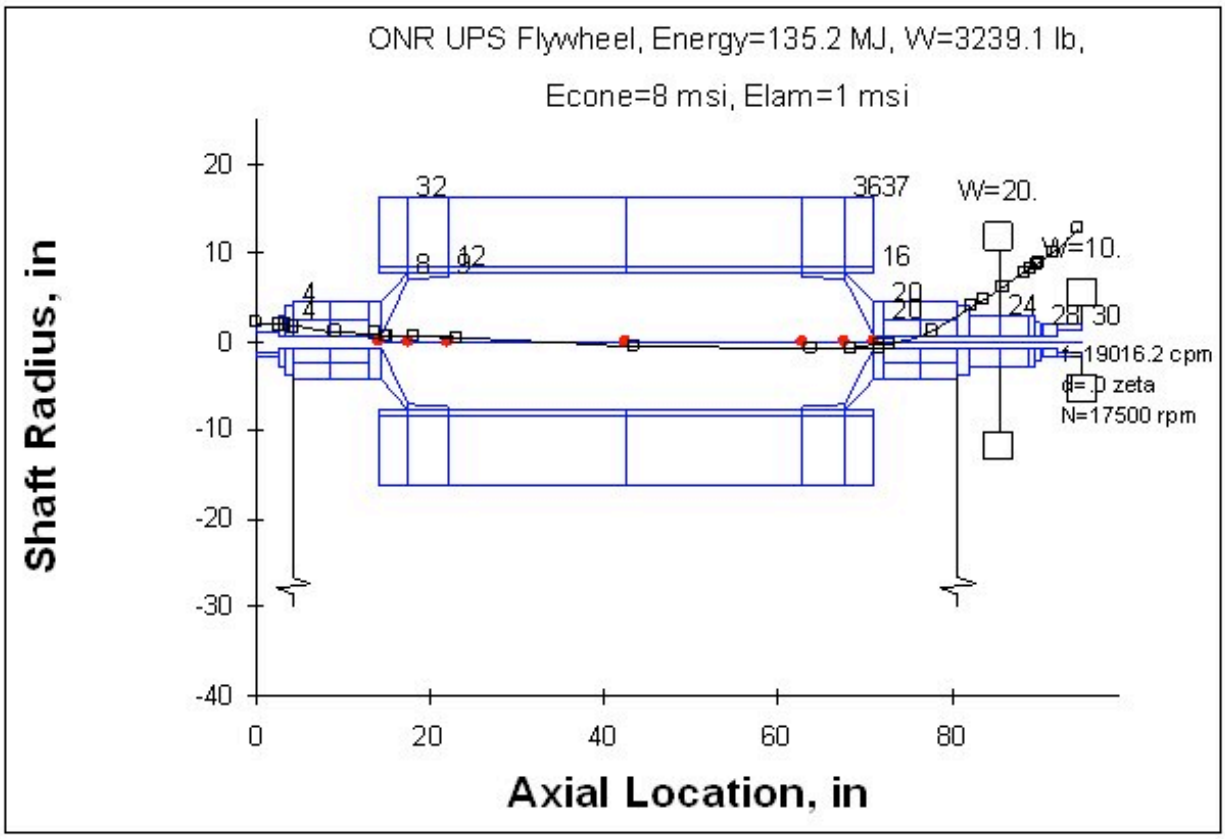

Figure 8. XLRotor model of rotor for rotor dynamic analysis

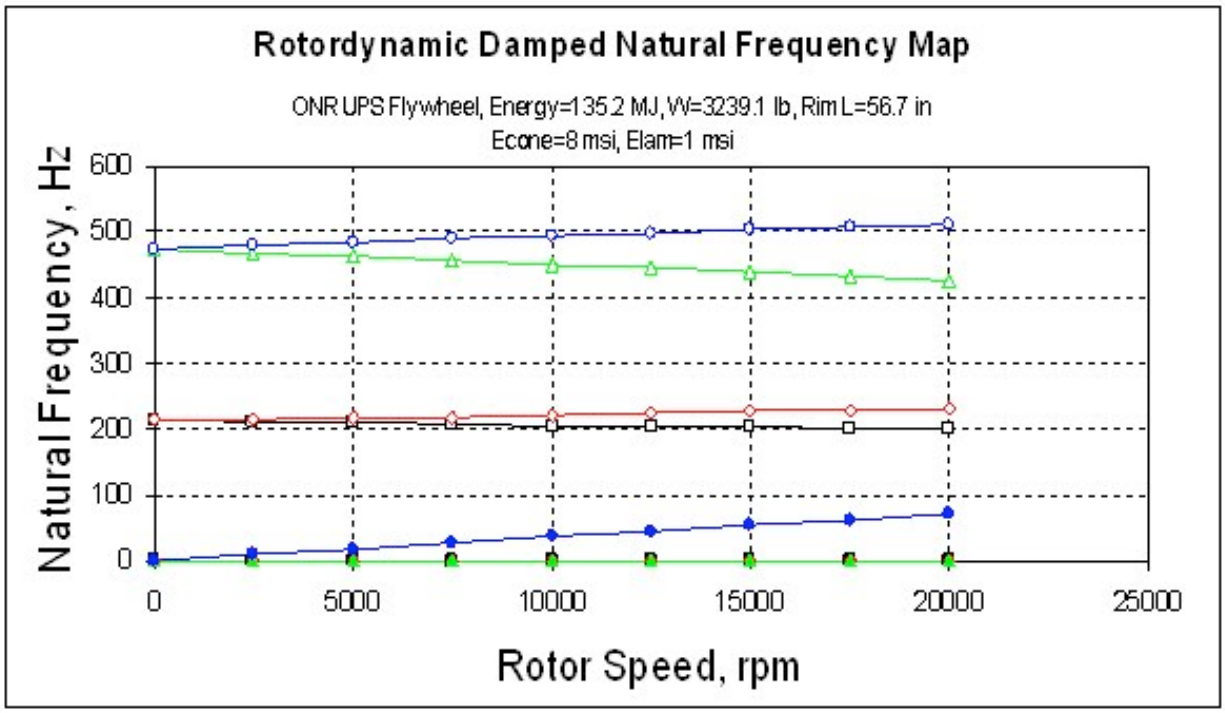

Figure 9. Variation of rotor modes with operating speed

FW Point Design Options for Ship Integration

The rotor design exercises yielded preliminary point designs of flywheels to evaluate the integration into a naval ship. Two sizes were configured: 4 FW (two per ship service generator skid) and 8 FW (four per ship service generator skid) to supply the ship energy requirements of 630 MJ delivered, based on 5 minutes of operation at 2.1 MW. The flywheel designs included a preliminary composite body design, steel stub shafts, magnetic radial and thrust bearings, and coupling connection. The details of these two designs are presented in table 9. The relative size of the flywheel rotors for these two cases can be seen in figure 10.

Table 9. Flywheel point designs for multi unit installations

Parameter	4 FW Case	8 FW Case
Energy per FW (total / del.) (MJ)	210 / 158	106 / 80
Total mass per FW (lb)	15,400	7,700
Overall length (in.)	90	72
Overall diameter (in.)	41.5	33.3
Rotor OD (in.)	32.4	25.8
Max shaft speed (rpm)	19146	24044
Composite mass (lb)	2450	1236
Power per MG (kW)	525	265

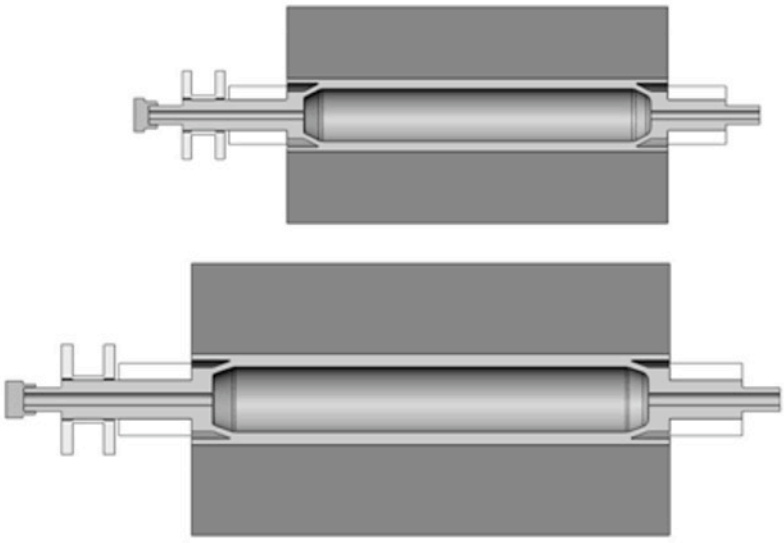

Figure 10. Comparison of rotor sizes for 4 FW and 8 FW installation cases

The rotor dynamics evaluation continued with a thorough reconsideration of the magnetic bearing sizing requirements. The DDG51 application does not demand the 3 gee's capacity for thrust that was assumed originally. Instead, a 1 gee capacity thrust bearing was assigned for this analysis, providing generous capacity for the combined loading of a ship propulsive thrust, and thrust load component due to pitch angle. This value is likely very conservative as well, and may be further reduced in the future when detailed dynamic requirements are established, however 1 gee offers a more realistic design assumption for initial consideration. (It should be noted that the magnetic thrust bearing does not need to bear transient shock loads as much of this will be transmitted to the auxiliary rolling element bearings.) Resizing the thrust bearing reduced the weight of this assembly from 88 lb to approximately 20 lb. This has the effect of increasing the frequency of the first bending mode of the shaft since the bearing is a large mass located on the flexible stub shaft extension. An image of the rotor section with the reduced thrust bearing is shown in figure 11. The rotor portion of the magnetic thrust bearing is shown in green, radial bearings in blue.

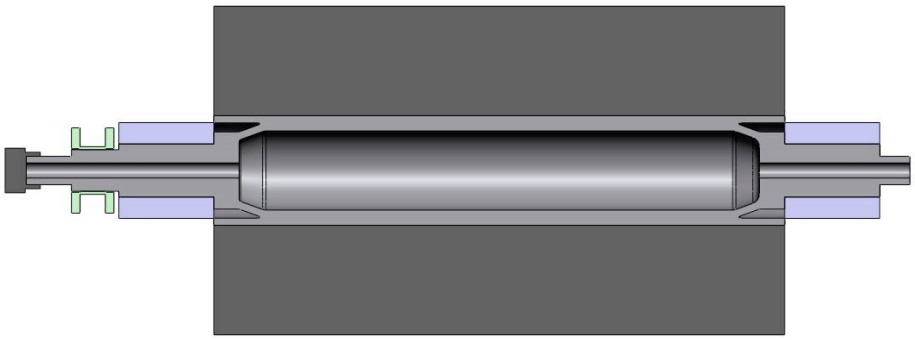

Figure 11. Section of 210 MJ flywheel rotor model showing reduced thrust bearing

The results documented here are for the 210 MJ flywheel, which corresponds to a 4 flywheel system with 630 MJ of delivered energy. The flywheel outer diameter was selected to be 32.4 inches based on shipboard space constraints. A flywheel peak tip speed of 825 m/s was selected based on desired factors of safety for the composite material. The flywheel operating speed range was selected to range from 50% speed to full speed, so that 75% of its peak stored energy is utilized. The inner diameter of the composite flywheel was selected to be 1/3 of the

outer diameter (based on UT-CEM's previous design experience). Given these selections, peak speed is then 19,146 rpm. The length of the composite flywheel will be 58.6 inches, but could potentially be shortened a small amount due to energy stored in the shaft. This results in a flywheel length close to 55.6 inches. As sized, the flywheel rotor weighs 3400 lb, and stores 210 MJ at 19,146 rpm.

The radial magnetic bearings were sized as follows, based on previous design experience:

- F_{rb} = ½*3*rotor weight (each of two bearings)
- Projected loading pressure at capacity of 53.7 psi
- L/D = 1 (this allows axial space for sensors and retaining plate)
- The lamination tip speed is also limited to 220 m/s. When this comes into play, the capacity will be slightly less than 1.5 g's per bearing.
- OD/ID_{lams} = 1.8
- OD/ID_{shaft} = 4.4, but must also be small enough to give a minimum of ½ inch wall thickness under the backup bearings.

The double acting axial bearing was sized using relationships derived from a previous sizing study done in 1995 for the ALPS bearings.

- F_{ab} = 1*rotor weight
- ID = $0.17387*(F_{ab})^{0.39133}$ (ID of thrust runner)
- OD = $0.25235*(F_{ab})^{0.43453}$ (OD of thrust runner)
- L = $0.12471*(F_{ab})^{0.43635}$
- W = $0.00018172*(F_{ab})^{1.4376}$
- Thrust runner tip speed also must not exceed 330 m/s
- L/D approximately 0.49
- Loading pressure approx 88 psi (using thrust runner area).

Mechanical backup bearings to support the flywheel at speeds up to 19,146 rpm will have 70 mm bore size ($1.34*10^6$ DN). In contrast to the vertical ALPS flywheel, a single duplex pair will be adequate at each end of the shaft. A Barden 1914H bearing has 7751 lb dynamic load capacity. This is more than 9 times the nominal radial load per bearing, so the 1914H should be

adequate. It has a maximum speed rating of 19,300 rpm for continuous operation when oil lubricated. The ALPS bearings were size 118H (90 mm) with a maximum speed rating of 15,000 rpm.

A conceptual flywheel housing design was developed incorporating the magnetic bearing sizing to provide overall scale for the energy storage flywheel. The housing model includes radial and thrust magnetic bearing stators, a composite containment liner, and structural stainless steel vacuum enclosure, shown in figure 12. Overall dimensions and weights were compiled for the concept of both the 4 FW and 8 FW configurations, and are listed in table 9 above. It should be noted that the dimensions include only the flywheel component and do not include the separately mounted motor generator. The generator power is presented assuming parallel discharging of flywheels from two skids (4 FW or 8 FW), although other discharge configurations are possible as well.

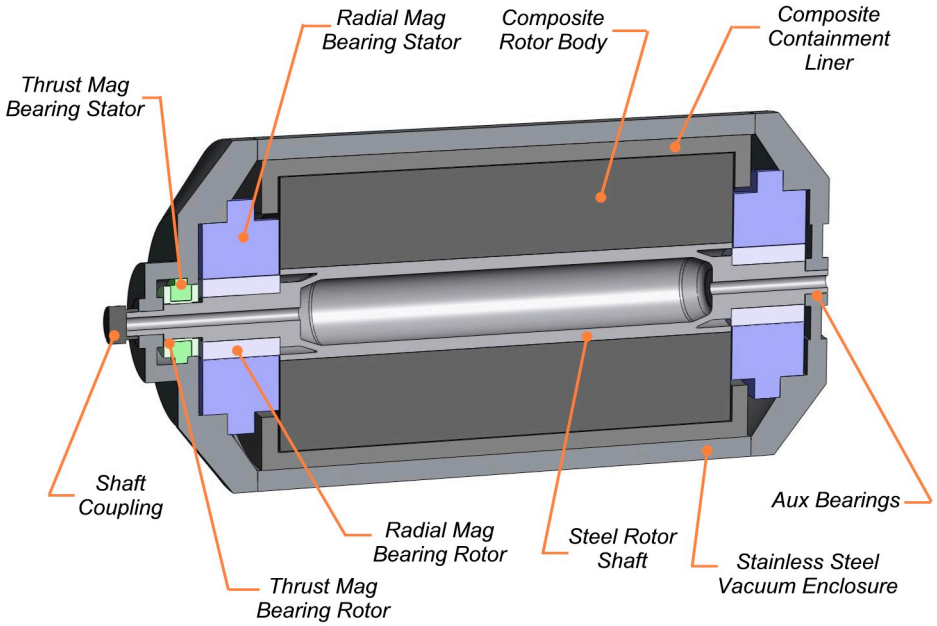

Figure 12. Section of flywheel including all main internal components

Preliminary Evaluation of FW and Motor Generator Integration

The motor generator design process was applied to the appropriate electrical and physical size for the objective 4 FW and 8 FW design cases. The parameters of the concept HIA motor

generators for the candidate flywheel sizes are presented in table 10. Again note that the generator power is presented assuming parallel discharging of flywheels from two skids (4 FW or 8 FW), although other discharge configurations are possible.

Table 10. Motor generator physical and electrical parameters

4 FW, 525 kW MG	8 FW, 263 kW MG	FW Case, MG Rating
19146	24044	Maximum speed [rpm]
9573	12022	Minimum shaft speed [rpm]
313	229.39	stator lamination ID [mm]
152	111.87	active length of stack [mm]
400	400	stator loading [A/cm]
1	1	peak gap flux density [T]
0.636619772	0.636619772	pole span factor
1.1107	1.1107	EMF form factor
0.95	0.95	stator winding factor
0.93	0.93	assumed machine efficiency
0.9	0.9	assumed power factor
76	55.935	axial field coil length [mm]
4.41986E-06	4.41986E-06	machine constant
0.485623003	0.487684729	single stack L/D ratio
2	2	stack length / field coil ratio
156.8884668	144.3942261	rotor tip speed (m/s)
14.96062992	11.01082677	total stator length [in]
630	313	apparent power [kVA]
527	262	real power output [kW]
31.3	23.0	Length overall [in]
24.4	17.9	Overall diameter [in]

The detailed component models of the flywheel and motor generators were used to generate an integrated flywheel energy storage system model. The purpose of this model is to visualize the completed flywheel assembly and evaluate potential mounting locations in a representative power system layout. The integrated flywheel-motor generator assembly for the 4 FW case is shown in figure 13, including mounting pedestals, and electrical cable terminations. The flywheel system was then packaged into a representative integrated power system, including a direct drive turbo-alternator, power electronics, and enclosure platform, shown in figure 14.

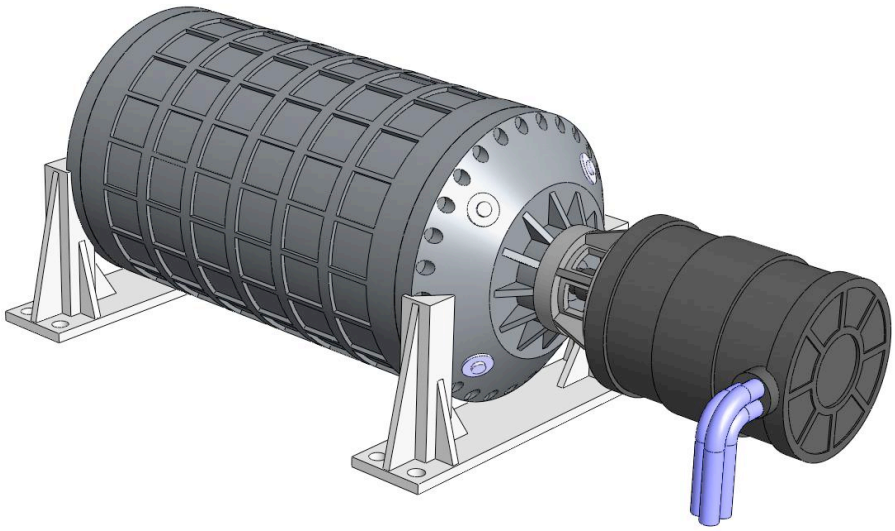

Figure 13. Integrated 210 MJ flywheel and 525 kW HIA motor generator package

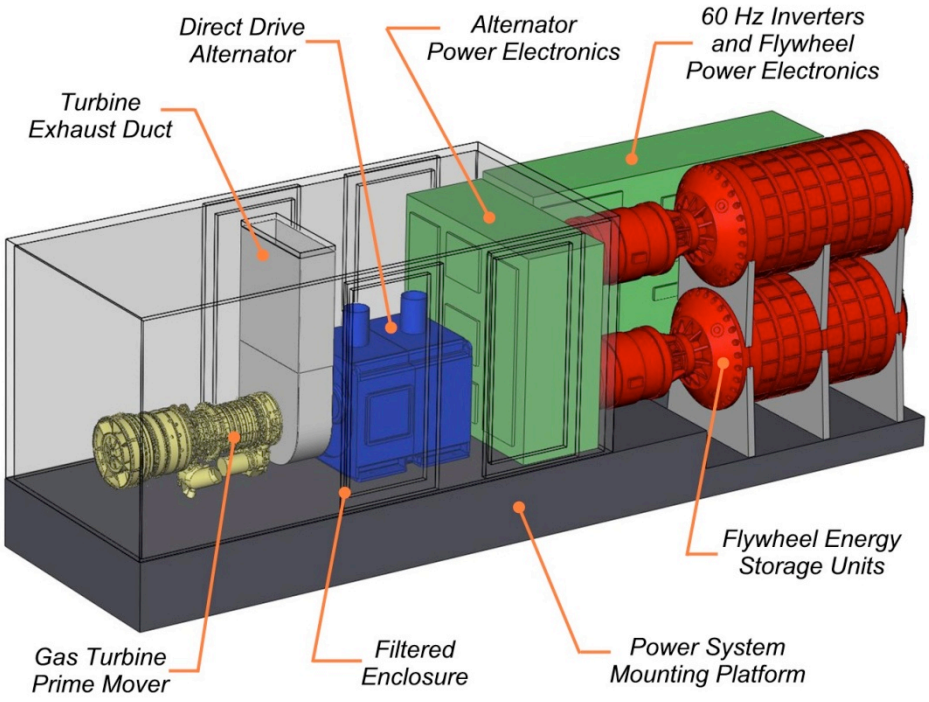

Figure 14. Flywheel system depicted in representative integrated electric power system

Flywheel Bearing Loads due to Ship Motion

An evaluation of the effect of ship motion on flywheel bearing loads to quantify required bearing capacities was conducted. While at sea, the motion of the ship produces loads on both the radial and axial bearings which are not present when the ship is motionless. Strictly speaking these are dynamically produced loads, but they act in a quasi static sense because they vary with time at relatively slow rates. The NAVY standards document DOD-STD-1399-301A, dated July 21, 1986, presents expressions to use for calculating some of these components, along with appropriate ship parameters for a typical destroyer. The formulas used here are given in figure 15, along with the flywheel parameters and assumed ship motion input parameters. Conservative estimations were made for unknown parameters; these calculations can be refined as more accurate information is developed.

The two aspects of ship motion that affect most significantly the radial bearing forces are the “sea state” rating and the maximum turning rate of the ship. These values translate into the dynamic motions of pitch, roll, yaw, heave, and surge. Because the flywheels are designed with their rotational axes aligned with the ship longitudinal axis, the roll mode is effectively isolated from creating gyroscopic forces, causing only lateral dynamic forces on the bearings. This flywheel mounting orientation is preferred as the roll rate is the highest of all motion contributions - approximately 4 times the peak pitch rates. Bearing forces contributions due to ship motion at Sea States 4 and 7 have been computed, and are shown in table 11. The turning rate assumed for this calculation was a full 360 degrees in 90 s – this value was selected to provide an extremely conservative benchmark for the preliminary calculations until more accurate turning rate data can be obtained.

Interpretation of the results show that for a severe case of sea state 7 motion combined with a high turn rate maneuver, the peak radial bearing loads increase 90%, effectively doubling the load requirement of the bearings. The design capacity used for the concept flywheel magnetic radial bearings was 3 gees, implying a margin of over 50% with respect to the worst case dynamic loading. In the case of transient shock loads that exceed this radial capacity, the rolling element auxiliary bearings will safely restrain the flywheel.

Table 11. Radial and axial bearing reaction forces for several sea state conditions

	Radial		Axial		Mount Moment
	% of nominal	lb	fraction of rotor W	lb	ft-lb
Calm seas w/o turning	100%	1800	0	0	9600
SS 4 w/o turning	117%	2106	0.07	252	11232
SS 4 w/turning	128%	2304	0.07	252	12288
SS 7 w/o turning	176%	3168	0.282	1015	16896
SS 7 w/turning	190%	3420	0.282	1015	18240

Regarding the axial bearing results, the sea state 7 motion conditions resulted in a peak axial load of 1015 lb. (In calm seas, there is nominally no axial load). The design capacity used for the concept flywheel magnetic axial bearings was 1 gee, implying a margin of 72%. As with the radial bearings, in the case of transient shock loads that exceed this axial capacity, the rolling element auxiliary bearings will safely restrain the flywheel.

The reaction moments that the spinning flywheel exerts on the ship at the mounting location as a result of ship motion were computed by this analysis as well. In the severe case of sea state 7 motion combined with a high turn rate maneuver, the peak reaction moment was 18,240 ft-lb per flywheel. This value is very reasonable considering the size of the equipment, requiring no special considerations. These modest gyroscopic forces will not have any appreciable effect on the ship structure or handling.

In conclusion, the ship motion analysis demonstrated that the bearing capacities assumed during the flywheel preliminary concept design are appropriate, and that the flywheel gyroscopic forces due to ship motion will not have any adverse impact to the ship structure or handling.

Bearing loads for a longitudinally mounted flywheel on a ship.

Typical destroyer per example case in DOD-STD-1399 Section 301A, 21 July 1986

$\Omega := 1914\text{rpm}$	$\Omega = 2004.964\frac{1}{s}$	rotor speed	
$M := 3600\text{lb}$	$M = 1632.933\text{kg}$	rotor mass	
$Ip := 35715\text{lb}\cdot\text{in}^2$	$Ip = 10.452\text{m}^2\cdot\text{kg}$	rotor polar inertia	
$It := 1704632\text{lb}\cdot\text{in}^2$	$It = 498.843\text{m}^2\cdot\text{kg}$	rotor transverse inertia	
$b := 64\text{in}$	$b = 1.626\text{m}$	bearing span	
$Tr := 10\text{s}$	$Tr = 10\,\text{s}$	period of roll	
$Tp := 7\text{s}$	$Tp = 7\,\text{s}$	period of pitch	
$\phi := 24\text{deg}$	$\phi = 0.419$	maximum roll angle	
$\theta := 4\text{deg}$	$\theta = 0.07$	maximum pitch angle	
$\theta' := \theta\cdot\frac{2\pi}{Tp}$	$\theta' = 0.063\frac{1}{s}$	peak pitch rate	$\theta' = 3.59\frac{\text{deg}}{s}$
$H := 0.2\text{g}$	$H = 1.961\frac{\text{m}}{s^2}$	Heave	
$S := 0.15\text{g}$	$S = 1.471\frac{\text{m}}{s^2}$	Surge	
$\psi' := 360\frac{\text{deg}}{90\text{sec}}$	$\psi' = 0.07\frac{1}{s}$	max turning rate, sustainied not too important (5%)	$\psi' = 4\frac{\text{deg}}{s}$

Draght is 31 ft, vertical distance from waterline to underside of hull.

$X := 150\text{ft}$	$X = 45.72\text{m}$	this input value is somewhat important (16%)
$Y := 20\text{ft}$	$Y = 6.096\text{m}$	this input value is not too important (6%)
$Z := 25\text{ft}$	$Z = 7.62\text{m}$	this input value is not important (3%)

$$Ax := g\cdot\sin(\theta) + S + \frac{4\pi^2}{Tp^2}\cdot\left(\theta^2\cdot X + \theta\cdot Z\right) \qquad Ax = 0.282\text{g}$$

$$Ay := g\cdot\sin(\phi) + \frac{1}{2}\cdot\frac{4\pi^2}{Tp^2}\cdot\theta\cdot X + \frac{4\pi^2}{Tr^2}\cdot\left(\phi^2\cdot Y + \phi\cdot Z\right) \qquad Ay = 0.709\text{g}$$

$$Az := g + \left(H + \frac{4\pi^2}{Tp^2}\cdot\theta\cdot X + \frac{4\pi^2}{Tr^2}\cdot\phi\cdot Y\right) \qquad Az = 1.565\text{g}$$

$Fgyropitch := \frac{Ip\cdot\Omega\cdot(\theta')}{b}$ $\quad Fgyropitch = 807.785\text{N}$ this radial force acts in lateral, Y, axis

$Fgyroyaw := \frac{Ip\cdot\Omega\cdot(\psi')}{b}$ $\quad Fgyroyaw = 899.941\text{N}$ this radial force acts in vertical, Z, axis

$$Fradial := \sqrt{\left(\frac{1}{2}Ay\cdot M + Fgyropitch\right)^2 + \left[\frac{1}{2}Az\cdot M + \frac{It}{b}\cdot\left(\frac{2\pi}{Tp}\right)^2\theta + Fgyroyaw\right]^2} \qquad Fradial = 14931.264\text{N}$$

$Faxial := Ax\cdot M$ $\quad Faxial = 4512.138\text{N}$

Figure 15. Mathcad document for calculating bearing reaction forces

Flywheel Discharge Sequence Option Evaluation

This section evaluates the options for discharge of multiple flywheels to supply the total power and energy requirements for the megawatt power module, and identifies the preferred topology. There are three basic approaches to the discharge sequence of multiple flywheels in UPS mode: A) parallel discharge, B) parallel / serial discharge, and C) serial discharge. The pros and cons of all three options were compared to identify the preferred configuration for the objective system. The total power and energy requirements assumed for this analysis correspond to 5 minutes of electrical support at 2.5 MWe, supplied by 4 flywheels. However, the same methodology applies equally to the 10 minute, 8 FW configuration. As the following table shows, the flywheels are sized equally in all three cases, but the motor generators and power electronics change rating and size accordingly.

Table 12. Nominal flywheel ratings for discharge sequence options (4 FW, 5 min. discharge at 2.5 MW)

	Parallel	Parallel / Serial	Serial
Total Flywheel Energy (kWh)	208	208	208
Total Flywheel Power (kW)	2500	2500	2500
Energy per Flywheel (kWh)	52	52	52
Power per Flywheel (kW)	625	1250	2500

Option A): Parallel Discharge of Four Flywheels

In the parallel discharge option (fig. 16), all four flywheels discharge concurrently for the full duration of the 5 minute UPS support, each at the 625 kW power level. Assuming two flywheels per skid with two active skids, this approach requires a total of 1.25 MW of active power conversion for each skid. This option requires all four operational flywheels to support the full 2.5 MWe load; if any one flywheel does not discharge properly, then the UPS system can't manage full load power for even a portion of the 5 minute duration.

Parallel Discharge

Pros:

- Minimum size and rating motor generator
- Minimum size and rating FW power electronics
- Lowest cost and volume

Cons:

- Least fault tolerant configuration

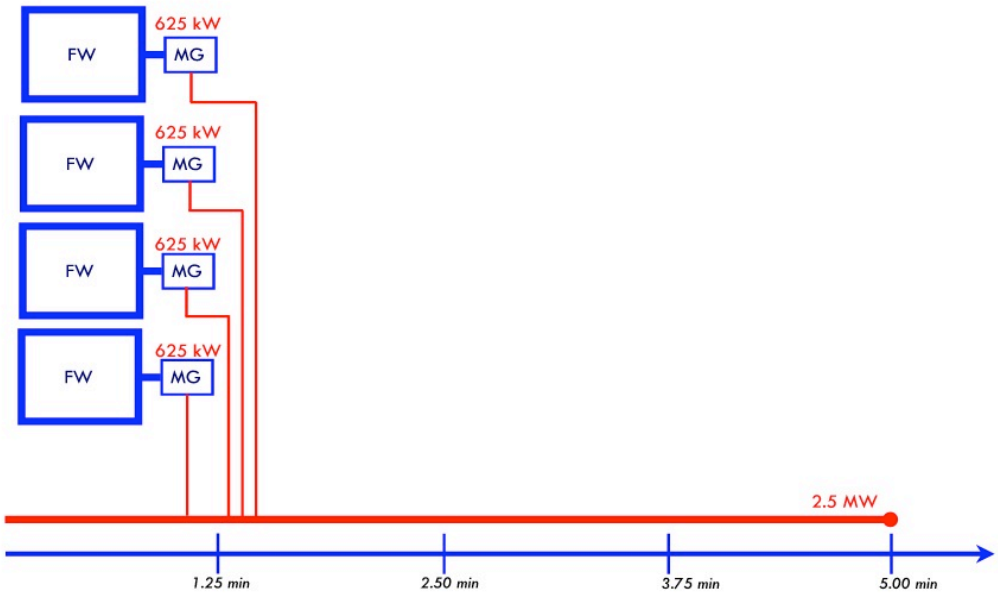

Figure 16. Flywheel system discharge sequence for parallel flywheel configuration

Option B): Parallel / Serial Discharge of 4 Flywheels

In the parallel / serial discharge option (fig. 17), a group of two flywheels (one skid) discharges in parallel, followed in series with a second group of two flywheels (second skid). Each skid generates full ship service power for half of the required UPS duration. This approach requires a total of 2.5 MW of active power conversion for each skid and a 1.25 MW motor/generator on each flywheel. In the event of a fault of any one flywheel, this option allows one remaining skid to support the full 2.5 MWe load, for at least 2.5 minutes.

Parallel / Serial Discharge

Pros:

- Increased reliability by requiring only two flywheels to manage full load (with reduced duration).
- Simpler controls-- during a main generator trip, transition to UPS is handled by “local” flywheels on that skid.
- Medium cost and volume of power electronics
- May allow reduction of total number of flywheels if energy requirements drop

Cons:

- Increases the size and rating of motor generator
- Doubles the cost and size of flywheel power electronics over parallel option

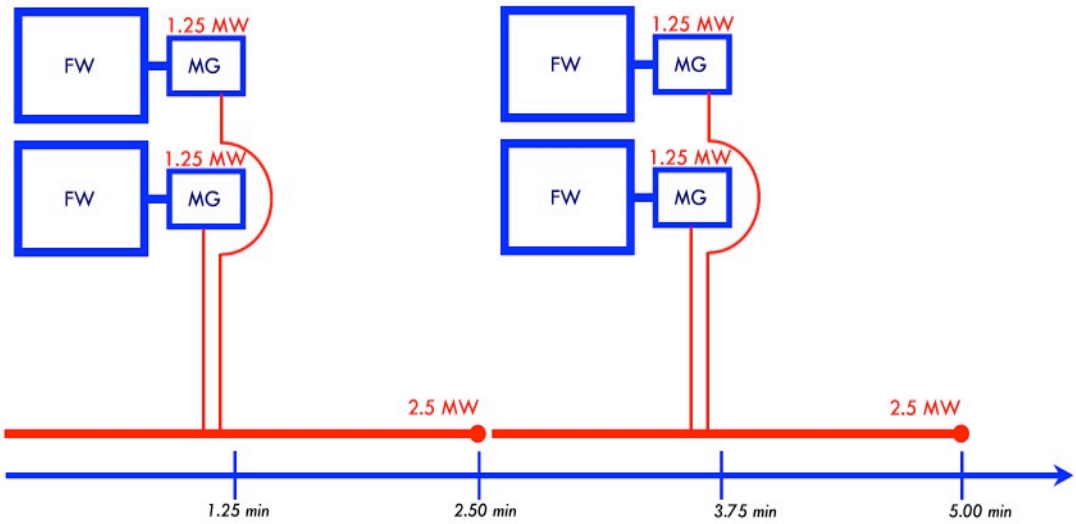

Figure 17. Flywheel system discharge sequence for parallel / series flywheel configuration

Option C): Serial Discharge of 4 Flywheels

In the serial discharge approach (fig. 18), the 4 total flywheels among both skids discharge independently and sequentially to provide 2.5 MW for 5 minutes. This approach requires 2.5 MW of active power conversion per flywheel (5 MW per skid) as well as a full 2.5 MW motor/generator on each flywheel. In the event of a fault of any one flywheel, this option allows the remaining flywheels to support the full 2.5 MWe load for at least 3.75 minutes.

Serial Discharge
Pros:

- Highest reliability as any single flywheel can provide full power for 1.25 minutes
- Transition to UPS is handled by “local” flywheels, simplifying communication and control of the remote skid
- Allows reduction of total number of flywheels if energy requirements drop

Cons:

- Largest size and rating motor generators
- Highest cost and volume power electronics (5 MW flywheel PEs per skid-- may be not feasible)

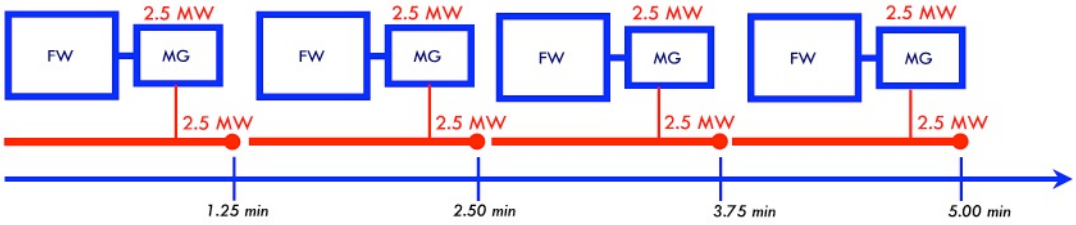

Figure 18. Flywheel system discharge sequence for serial flywheel configuration

Qualitatively comparing these options, it becomes clear that option C, serial discharge offers the greatest reliability and redundancy, at the expense of the largest volume (power electronics, motor generators, and auxiliaries), and highest cost. Option A, parallel discharge is the most compact (by sharing load and auxiliaries), at the expense of fault tolerance. Considering the fact that installed volume is a particularly challenging requirement in this application, option B parallel / serial discharge configuration offers the best combination of adequate redundancy and reasonable installed volume.

In conclusion, the parallel / serial discharge approach with flywheels grouped functionally according to their installed skid location is the recommended configuration for both the 5 and 10 minute UPS requirement systems. The schematic of the flywheel discharge sequence for the 10 minute system is shown in Figure 19.

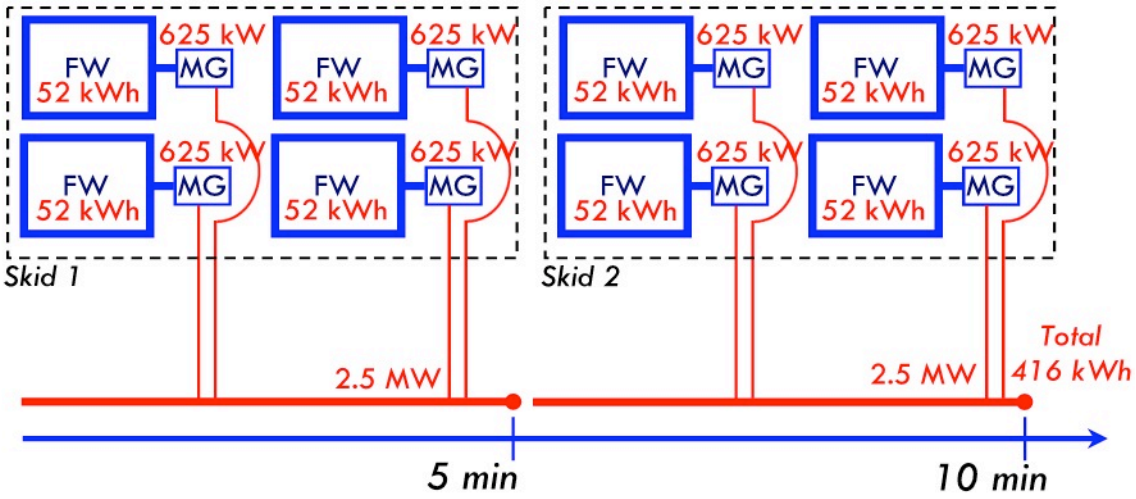

Figure 19. Proposed flywheel configuration and discharge sequence for 10 minute 2.5 MWe case

Baseline 1.25 MW Flywheel Motor Generator and Power Electronics

1.25 MW HIA Design

As the laboratory demonstration plans were being updated to increase the flywheel discharge power from 1.0 to 1.25 MW in order to better represent one flywheel of the EDM system (see section above on flywheel discharging), accordingly, the design of the motor generator was revised, with the intent remaining to constrain its overall size to the housing of the existing flywheel induction motor/generator. Sufficient margin existed in the original homopolar inductor alternator (HIA) concept design to allow for this change with minimal adjustment, involving increased peak flux density and pole span. The new design values can be seen in table 13.

Table 13. Motor generator physical and electrical parameters

Nominal 1.25 MW , 7,500 – 12,500 rpm operation	
12,500	Maximum speed [rpm]
7,500	Minimum shaft speed [rpm]
406	stator lamination ID [mm]
198	active length of single lam stack [mm]
400	stator loading [A/cm]
1.25	peak gap flux density [T]
0.80	pole span factor
1.1107	EMF form factor
0.95	stator winding factor
0.93	assumed machine efficiency
0.9	assumed power factor
99	axial field coil length [mm]
6.94 E-06	machine constant
0.487	single stack L/D ratio
2	stack length / field coil ratio
265	rotor tip speed at 12,500 rpm (m/s)
159	rotor tip speed at 7,500 rpm (m/s)
19.5	total stator length [in]
1699	apparent power [kVA]
1422	real power output [kW]

1.25 MW Power Electronic Modules

The increased power from the flywheel motor/generator also required a review of the ratings of the American Superconductor power electronics modules which link the motor/generator to the common dc bus. Although each of the two parallel flywheel power converter modules are nominally rated for 1 MW at unity power factor and 60 Hz, the higher frequency of the flywheel motor/generator will increase the switching losses in the converter IGBT's. American Superconductor was asked to assess the impact of the increased power at the higher frequency of the 4 pole flywheel motor/generator. The initial review of the flywheel power converter modules indicated that the additional switching losses could be accommodated, although slightly increased harmonic losses might be reflected into the motor/generator windings.

Flywheel Motor Generator Rotor Stress Analysis

The castellated profile of the HIA rotor results in stress concentrations at the outer diameter of the steel rotor core. This geometry is not typical of conventional electric machines, and, therefore, a preliminary analysis was conducted to evaluate whether it may be a limitation to high speed operation.

To calculate stresses in this region, finite element stress analysis was performed on the proposed rotor profile, and the stresses were evaluated with centrifugal loading of a 300 m/s tip speed (regarded as the upper limit of the range of design speeds under consideration). The subject model is a 16 in. OD steel rotor core, with two lobes per segment (effectively a 4 pole electric machine). The minor diameter between the lobes is 15 in. with a 0.25 in. radius fillet at the step. The test speed was 14,000 rpm to result in the 300 m/s peripheral velocity. The analyzed rotor core geometry has a bore assuming the rotor core is interference fit onto a separate shaft. However in practice, the rotor core may be a solid forging which would further reduce the stresses in this region. An internal pressure of 500 psi was applied to the bore of the rotor model to reflect the residual (at-speed) interface pressure from the shaft to core shrink fit. The final design of the shaft to core fit will be developed based on more detailed evaluations of the fit requirements and fatigue considerations. Finite element analysis results show that the peak Von Mises stress in the part is at the inner diameter, as expected. The peak stress in this region is very reasonable at approximately 85 ksi as shown in figure 20.

The peak Von Mises stress at the lobe root was calculated using a refined mesh in this area. Von Mises stresses in this region are predicted to be approximately 65 ksi, as shown in figure 21. This value is very reasonable and approximately 40 ksi higher than the VM stresses elsewhere at the OD face, indicating a stress concentration factor of approximately 2.8. In conclusion, the stress concentration effect of the castellated HIA rotor has been shown to be insignificant, and not a limiting factor, even up to 300 m/s tip speeds in a solid core rotor.

Further design refinements in this region are expected to incorporate features to support lightweight spacers to smooth the rotor profile and reduce windage losses.

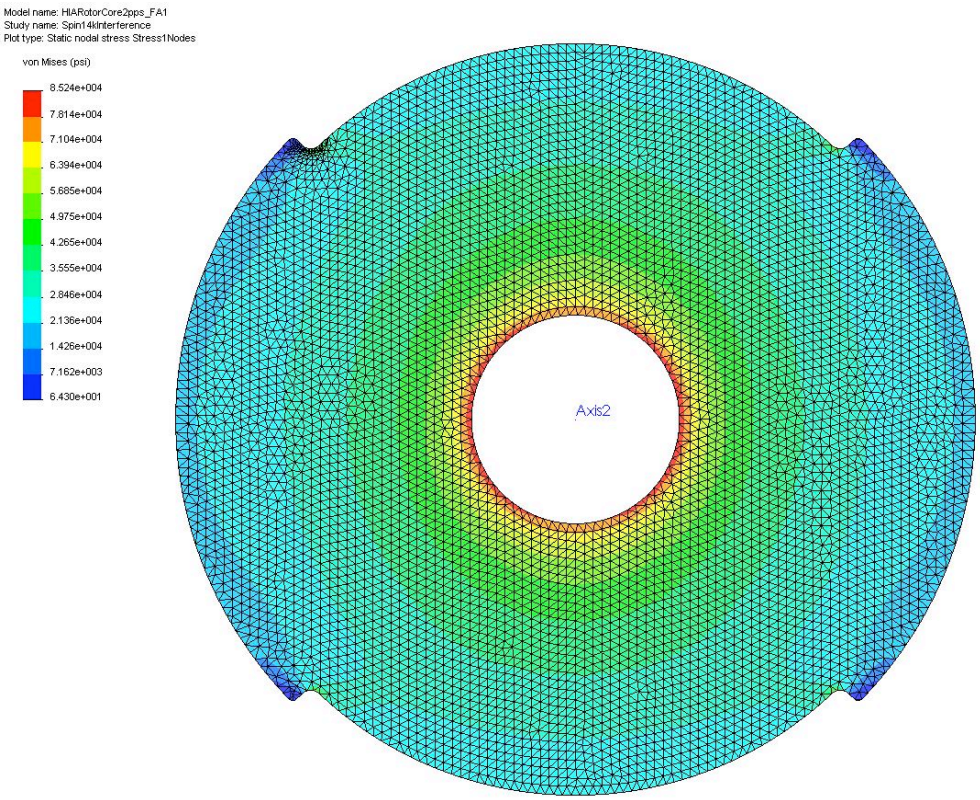

Figure 20. Von Mises stresses in HIA rotor core due to 300 m/s centrifugal loading

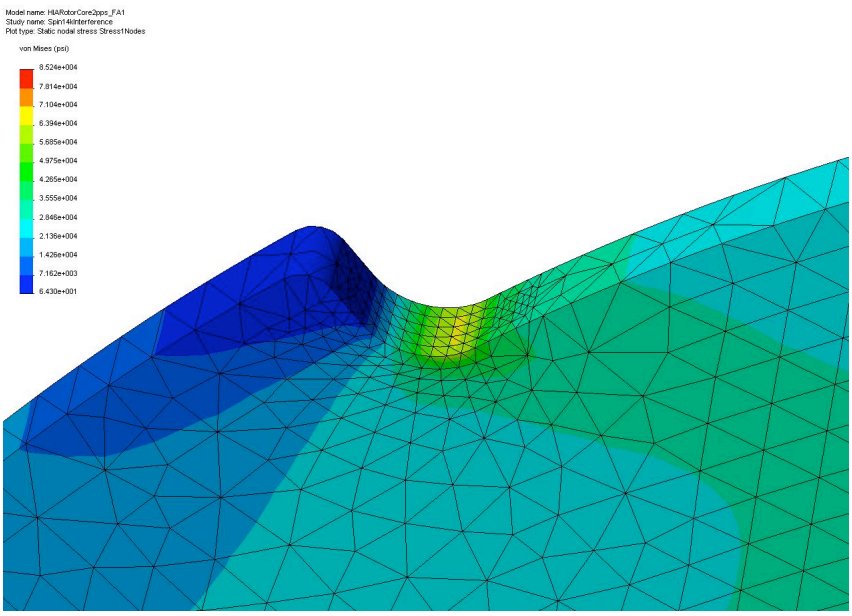

Figure 21. Von Mises stresses in HIA rotor core due to 300 m/s centrifugal loading, detail lobe root

Number of Flywheels and System Package Modeling

This section presents a discussion about the choice of the number of flywheels and an example of packaging and integrating a stand-alone flywheel energy storage system into a naval ship.

Electric energy storage can add significant value to the efficiency, operation, and reliability of naval ship power systems. The energy reserve can serve to improve ship efficiency and reduce fuel consumption by acting as an uninterruptible power supply (in the event of a main generator fault) enabling single generator operations and thereby allowing a single gas turbine to operate closer to its peak efficiency point. Energy storage can also provide new operational capabilities to supply or absorb transient loads, such as pulsed energy weapon systems and underway replenishment systems, thus isolating the main generator from the duty cycle these dynamic loads impose. Beyond UPS mode, energy storage can be used to improve reliability and power quality by stabilizing the grid voltage, frequency, and power factor. Energy storage therefore offers many advantages and will likely be a high priority addition to future naval ships as well as retrofits.

One critical benefit for retrofit integration of energy storage into the DDG-51 class ships is the ability to package the energy storage flywheel system in the current volume of modified AG9140 power systems. Space can be made available for this addition by removing the gear box and low speed generator, and replacing them with a compact, direct drive generator and 60 Hz inverters. These modifications free the needed volume to package the flywheels within the existing volume.

Another option for adding energy storage to naval ships, without the need to upgrade the main generators, is to integrate independent energy storage modules into the existing power system. This approach would use modular, standalone flywheel packages to facilitate integration into the ship platform. Such packages could include the energy storage flywheel, a direct coupled motor generator, auxiliaries, and power electronics required to interconnect the electrical output of the flywheel transparently to the 450 V, 60 Hz service grid.

Standalone flywheel energy storage can be implemented in a variety of scales- from one large flywheel, to many small power system modules distributed throughout the ship, all interconnected by the service grid. Previous flywheel design studies for comparable MW-level energy storage applications conducted by UT-CEM indicated that the most economical approach is to minimize the number of units and maximize scale. On the other hand, distributing multiple flywheels increases fault tolerance and redundancy, and may offer distinct integration advantages for retrofits applications which may not have large unoccupied volumes.

For a retrofit application, our recommendation is to balance these considerations by selecting the largest flywheel unit size which can be installed without major impact to ship structure, and using multiple flywheels of this scale to meet the total energy need, providing a favorable combination of flywheel capital costs, ship integration costs, performance, and reliability/redundancy.

To quantify the baseline flywheel sizing, a preliminary evaluation of the installation of a flywheel was conducted, considering the maximum flywheel size that can be feasibly installed with minimal impact to the ship structure during retrofit. For the study, the team assumed that the major pieces of the flywheel system (flywheel, motor / generator, power electronics) would be individually brought into the ship, and assembled in place. This study found that a flywheel unit size of approximately 90 in. length x 41 in. outer diameter (corresponding to a system of 4

flywheels to supply the total energy for a 5 minute discharge, 8 flywheels for a 10 minute discharge) could be installed with minimal impact to the ship structure, while flywheels larger than this may require more significant ship modifications. The flywheel unit size was therefore selected around this criterion, and a system package concept for single flywheel unit was developed. Depending on the final locations selected for integration of the energy storage components, the flywheel packages could be expanded to 2, 3, or 4 flywheel modules.

The concept standalone flywheel energy storage system package includes the flywheel and direct coupled motor generator, lubrication, vacuum, and controls auxiliary modules, and power electronics and switchgear to connect the flywheel's output to the 450 V, 60 Hz, three phase ship service grid. This equipment is mounted in an enclosure with a shock isolated base. For the five minute discharge system, four of these modules would be distributed through the ship, as space allows, to supply the energy and power demands. For the 10 minute discharge system, eight flywheels of this size would be needed. In each case, one backup unit may be desired for redundancy so one unit may be taken out of service at any time for maintenance. The nominal dimensions of this concept for a single flywheel energy storage module are shown in figure 22.

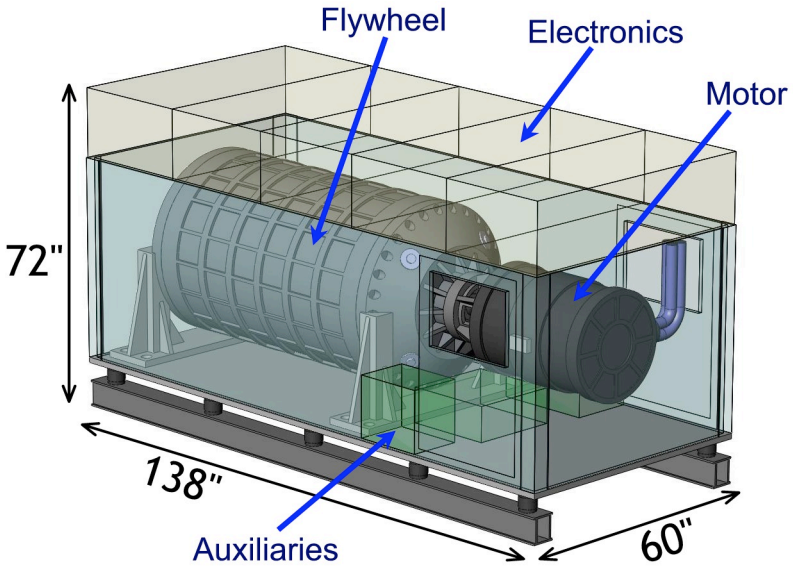

Figure 22. Concept flywheel package for standalone ship energy storage system

Flywheel System Component Technical Specifications

The significant physical parameters of the flywheel energy storage system are discussed in this section, including the dimensions, weight, center of gravity, electrical input and output, cooling requirements, and ship interface. The parameters are presented in tables 14 and 15, itemized separately for the flywheel and the motor generator.

Table 14. Physical characteristics for 2.5 MW, 10 minute UPS energy storage system

Component Physical Characteristics	Flywheel	Flywheel M/G
Salient Characteristics:		
Length, Width, Height	90"L, 41.5"W, 41.5"H	33.1"L,25.8"W,25.8"H
Maintenance Envelope (LxWxH)	130"L,81.5"W,81.5"H	73.1"L,65.8"W,65.8"H
Weight, Center of Gravity	14715 lb, COG*: 45.75"x, 0"y, 0"z	2368 lb, COG*: 16"x, 0"y, 0"z
Speed (rpm)	9573 - 19146 rpm	9573 - 19146 rpm
Equipment Rating:	52 kWh / FW deliverable (208 kWh per skid)	625 kW / MG (2.5 MW per skid)
Thermal – Cooling Required:		
Fluid – Type, Volume, Pressure	water, 10 gpm, 60 psi / skid	water, 28 gpm, 60 psi / skid
Thermal Discharge:		
Fluid – Type, BTUs, Vol, Press, Temp	water, 20 kW (1137 BTU/m), 10 gpm, 60 psi, 42°C outlet / skid	water, 56 kW (3185 BTU/m), 28 gpm, 60 psi, 42°C outlet / skid
Expected Mounting Location of Components – include Type of Mount	Pedestal mounted to modified AG9140 skid, shock isolated	Flange mounted to FW on modified AG9140 skid
Number of Units	4 FWs per skid	4 MGs per skid

* Origin is on rotational centerline at mating end of shaft

Table 15. Electrical characteristics for 2.5 MW, 10 minute UPS energy storage system

Component Electrical Characteristics	Flywheel	Flywheel M/G
Time to Full Power:		
From Standby	500 ms	500 ms
From Secured	1245 s (21 min)	1245 s (21 min)
Noise: Frequency(ies) and Level (dB)	160-319 Hz, 75dB (est)	160-638 Hz, 85 dB (est)
Operating Temp Range: Internal & External	100°C int. / 49°C ext.	140°C int / 49°C ext.
System Interface Requirements:		
Electrical Power: (Input)	up to 10 kW control power & auxiliaries	up to 19 kW charge maintenance / 5 kW excitation, & auxiliaries
Input Volts,Amps, Phases, Freq	220 V, 45.5 A, 1 ph, 60 Hz	460 V, 23.8 A, 3 ph, 60 Hz / 220 V, 22.7 A, 1 ph, 60 Hz
Input Harmonic Limits	MIL-1399	MIL-1399
Backup Source	Battery UPS for controls and bearings	Battery UPS for field excitation
Electrical Power: (Output)	N/A	625 kW / MG (2.5 MW per skid)
Voltage, Amperage, Frequency, Ph	N/A	600 Vl-lrms, 1402 Arms, 0-638 Hz, 3 ph
Output Harmonics	N/A	MIL-1399 Compliant at 60 Hz bus
Backup Source	N/A	N/A
Applicable Spec or MILSTD	N/A	MIL-1399

System Modeling with Simulink

Background

The preferred system configuration was studied as part of the companion grant (N00014-06-01-0886) and the result of the various trade studies are reported in that final report. In the present contract the simulation studies were carried further especially in regard to improving the energy storage control system and to making the physical behavior of the various components more realistic.

A basic functional diagram of the system used in the simulation studies is reported in figure 23. As can be seen, it contains the basic elements of the proposed power generation and energy storage skid: a turbine generator, two flywheel storage units, a common dc bus, four converters supplying the output ac line, means to recharge the flywheels, and a control system. The simulation of the performance of the system under different conditions was done with Simulink and was started under the companion grant and finished under the present contract. Therefore, since the simulation study was for some time concomitant for both grant and contract, the reader is encouraged to read both final reports for a complete summary of the modeling effort. The final configuration of the model as well as the user's manual are contained in this report. The paragraphs below summarize the main developments with the system simulation carried out under the present contract.

Rationalization of the Model

In order to make the simulation tool easier to use, the system's line diagram has been simplified considerably with respect to the one used in the simulations of the companion grant, without loss of capability or generality. The new line diagram is shown in figure 24. Essentially all items germane to a particular function have been combined into one Simulink block with input items pertaining to that block listed in a pop-up dialog box. All details about the construction of the block are still available by examining the lower levels within each block.

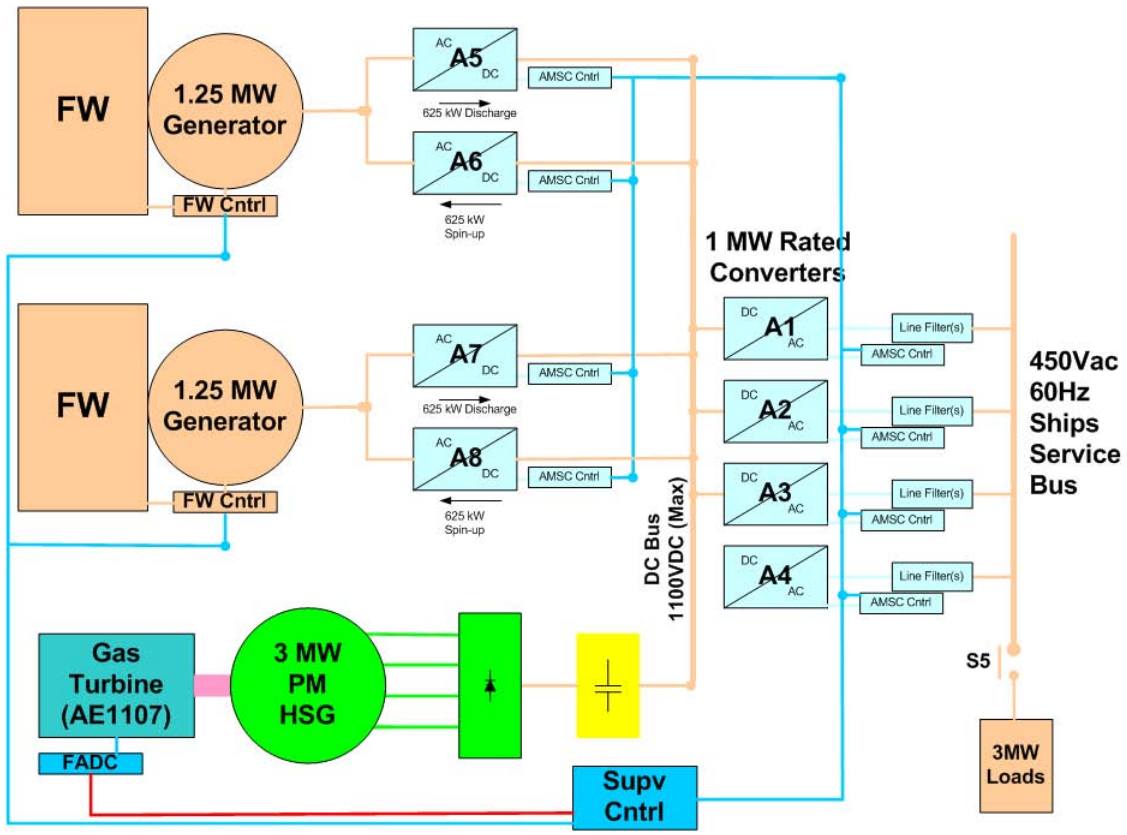

Figure 23. Schematic diagram of the basic MPM skid used for simulation studies

The dc and ac buses have also been given more prominence in the layout for easier identification, since they are key points in the logical construction of the system and locations where it is most likely that additional elements may be connected for future expansion.

Additional simplification of the circuit has also been achieved by using a small quantity of "GoTo/From" blocks for some signals. While these blocks simplify visually the circuital connections, they also make the circuit less immediately intelligible, if used extensively. Thus their use has been limited to few obvious instances.

Complete documentation on all parts of the system and full details for the use of the simulation tool are included in Volume 2 of this final report.

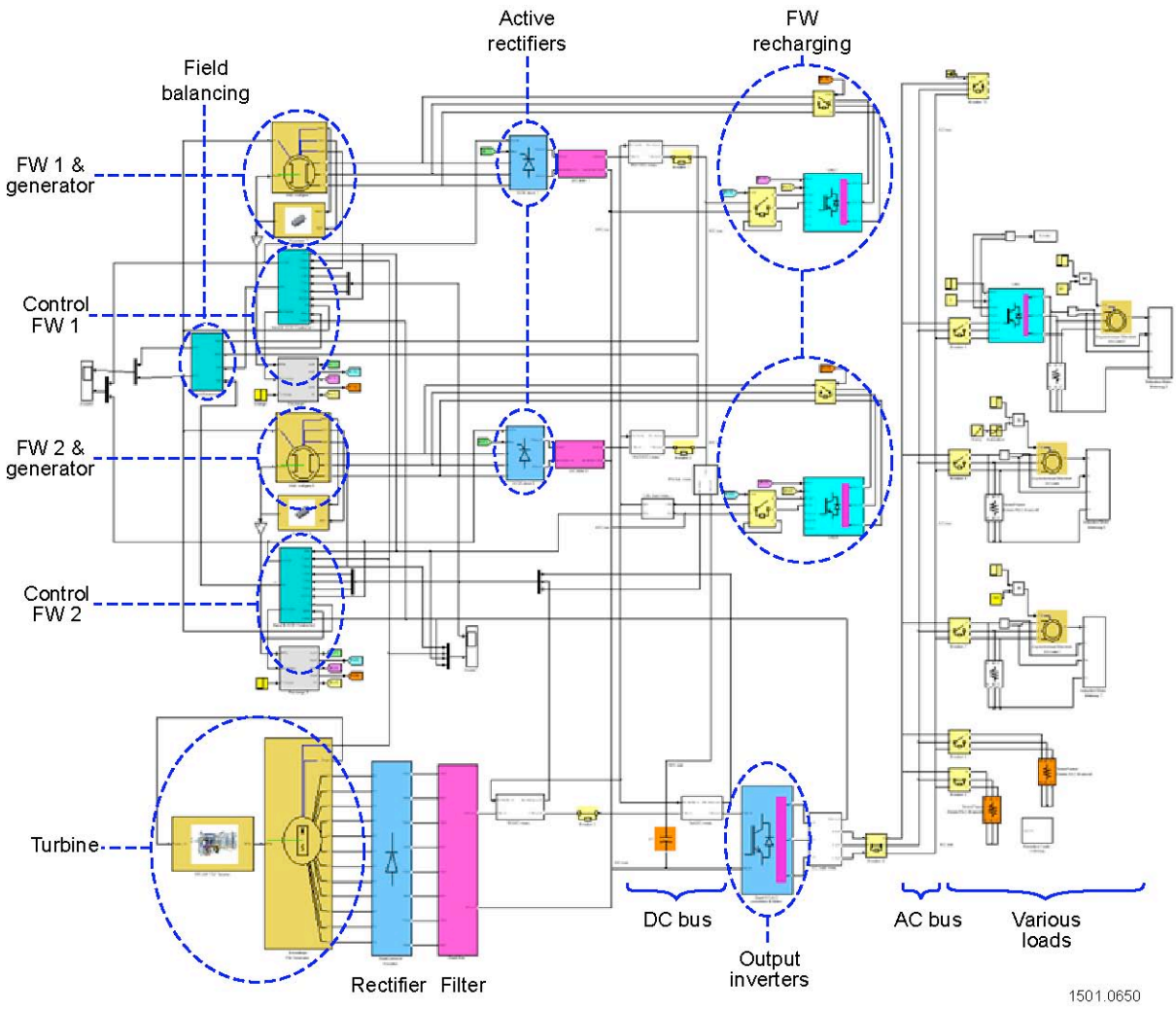

Figure 24. Overall system model

Blocks in figure 24 are color coded as follows:

a. Dark yellow	Rotating machines
b. Blue	Solid state devices
c. Light blue	VSD
d. Cyan	Control systems
e. Pink	Filter sections
f. Light green	Switching sections
g. Light yellow	Items with input control
h. Orange	Passive components
i. White	Data, metering, and miscellaneous blocks
j. Dark green	Metering and display blocks

The main substantive upgrades in the simulation since the end of the work done under the companion grant are discussed in the following sections.

High Fidelity Turbine Model

Rolls-Royce provided a new high fidelity model for the AE1107 turbine which was incorporated in the model and found to give improved results relative to the low fidelity model. Simulations with the high fidelity turbine model provided results more in line with expectations under transient conditions. The only drawback with this new model is that it needs to be initialized by at least a 5 s simulation run before steady state is attained. In fact, the initialization time could be even longer but it was kept to 5 s to avoid taking up too much useful simulation time. During the initialization time the turbine has to be kept under a fictitious load in order to complete the initialization successfully. Some typical results with the new turbine model are shown in figures 25 through 29; the results are based on the simulation scenario shown in table 16.

Table 16. Representative simulation scenario for system modeling

Time	Turbine load	Condition
0 – 5 s	2.25 MW	Initialization time with mock load on turbine
5 – 7.5 s	1.8 MW	Actual load switched in
7.5 – 10.5 s	0.75 MW	Turbine disconnected from actual load and applied to minimum mock load to keep turbine stable. Actual load is supplied by flywheel generators.
10.5 – 13.5 s	1.8 Mw	Turbine generator is re-connected to actual load
13.5 – 15 s	4.2 MW	Actual load increased

Figure 25 shows the turbine rpm versus time under the load transitions presented in table 16. The steady state turbine rpm is 14,500. The first 5 s are for the initialization of the turbine under a mock load of 2.25 MW with the system disconnected and, therefore these results should be ignored. Additional details of all transients after the completion of the initialization are given in figures 26 through 29.

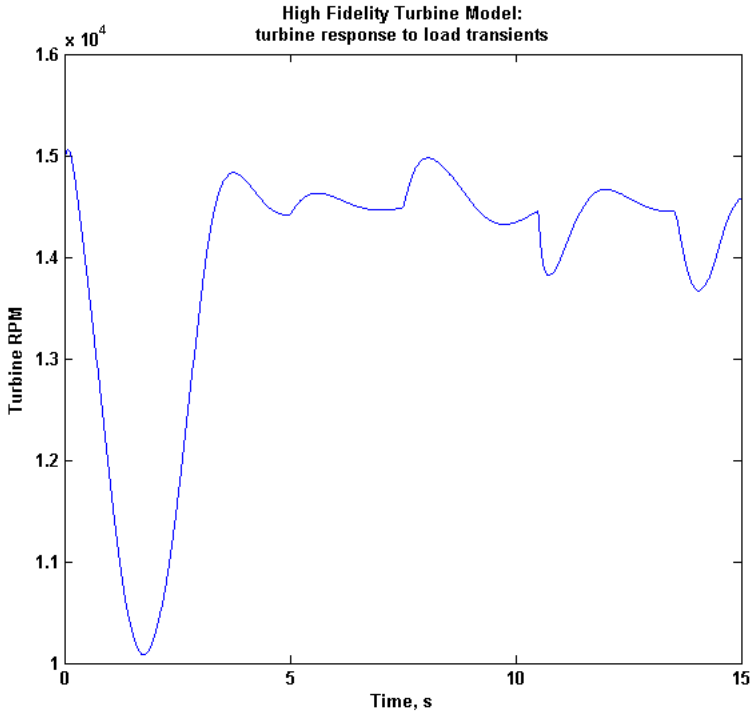

Figure 25. Turbine rpm vs. time under the load transitions

Figure 26 presents detail of turbine transient when the system is connected to the turbine after the initial 5 s of initialization. The initial mock load was 2.25 MW and the simulated load is 1.8 MW, so the turbine accelerates in response to the reduced load. Figure 27 shows the detail of turbine transient when the turbine is disconnected again from the system at a 1.8 MW load and continues separately under a 0.75 MW mock load, therefore the initial response for the turbine is to speed up. During this time the system load is carried by the flywheel generators. Figure 28 shows the transient response when the turbine load increases from 0.75 MW to 1.8 MW; as expected, the turbine speed initially decreases and then recovers to the target of 14,500 rpm. Figure 29 shows the transient response when the systems load is increased from 1.8 MW to 4.2 MW; again the turbine speed initially decreases and then recovers to the target speed of 14, 500 rpm.

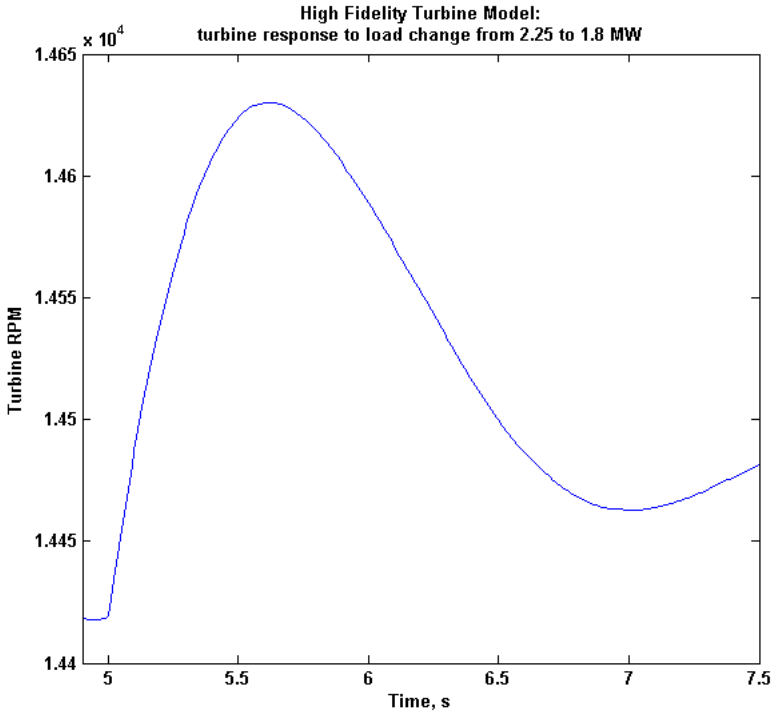

Figure 26. Turbine transient when the actual system is connected after the initial 5 s initialization

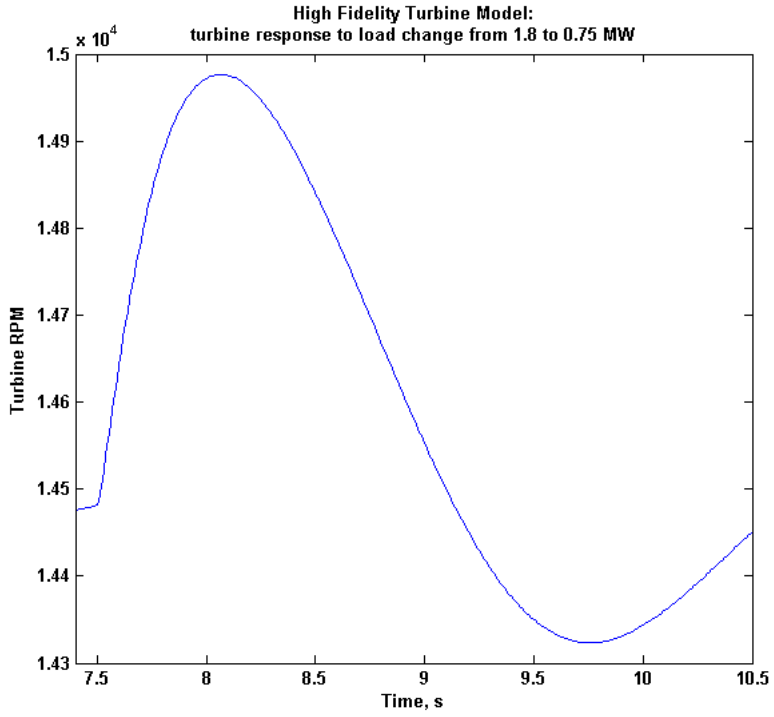

Figure 27. Detail of turbine transient under load reduction from 1.8 MW to 0.75 MW

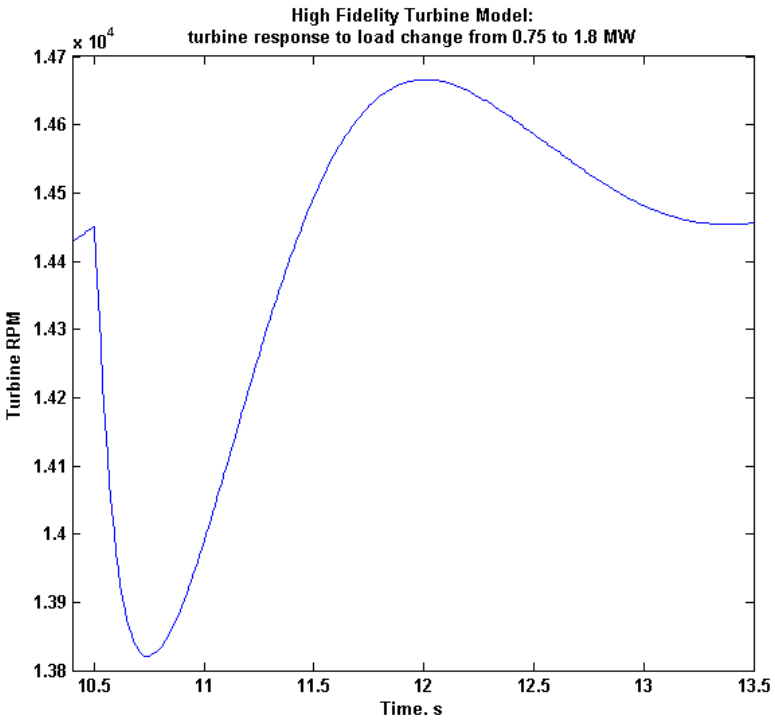

Figure 28. Detail of turbine transient under load increase from 0.75 MW to 1.8 MW

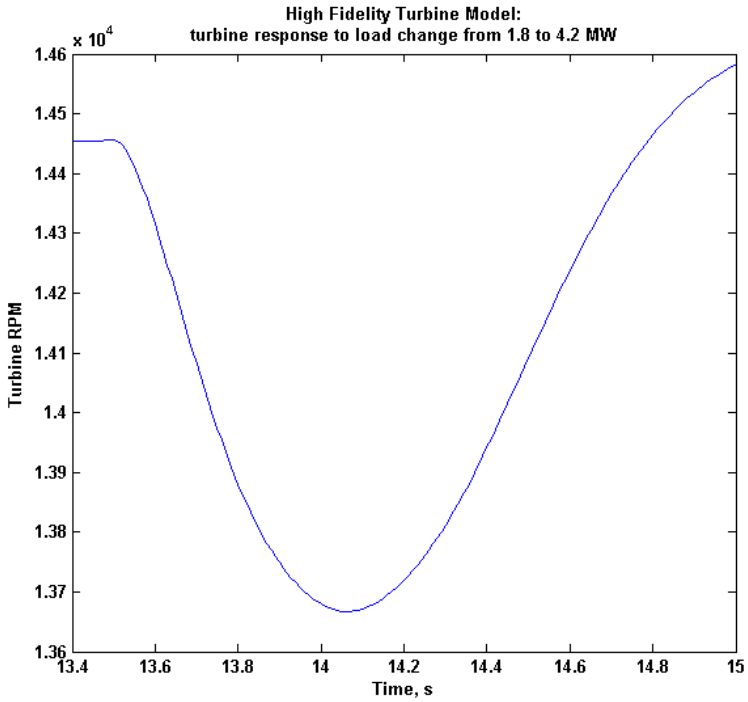

Figure 29. Detail of turbine transient when the system load is raised from 1.8 to 4.2 MW

It is clear from the examination of figures 25 through 29 that the high fidelity turbine model provides a realistic response of the turbine to transients both in terms of speed excursion and of time constant for the response. The low fidelity model (see the final report of the companion grant) was responding too quickly and with a very tight rpm variation that was believed to be inaccurate.

Realistic Load Models

In the companion grant, the various load scenarios had been implemented with simple lumped parameter equivalent circuits, which, although effective in their circuital representation, did not model the actual load characteristics in any physical detail. Therefore, attention turned to incorporating more realistic load models on the ac distribution grid.

The total load on the ac three-phase bus was now represented by a constant resistive load of 1 MW (e.g. lighting, heating, etc.), an intermittent resistive load of 1 MW, and three intermittent rotating loads as follows:

1. Motor load number 1 is a 200 HP, 460 V, 60 Hz, 1780 rpm induction motor started across the line and connected to a shaft load with a torque increasing linearly with speed (e.g. soft start)
2. Motor load number 2 is a 100 HP, 460 V, 60 Hz, 1780 rpm induction motor started across the line and connected to a shaft load with constant torque equal to full load torque (e.g. positive displacement pump)
3. Motor load number 3 is a 200 HP, 460 V, 60 Hz, 1780 rpm induction motor connected to a shaft load with a parabolic torque profile (e.g. centrifugal pump) but started via a variable speed drive

Figure 30 shows the Simulink models of the rotating machine loads for cases 1 and 2; figure 31 shows the Simulink model of the rotating machine load with a variable speed drive.

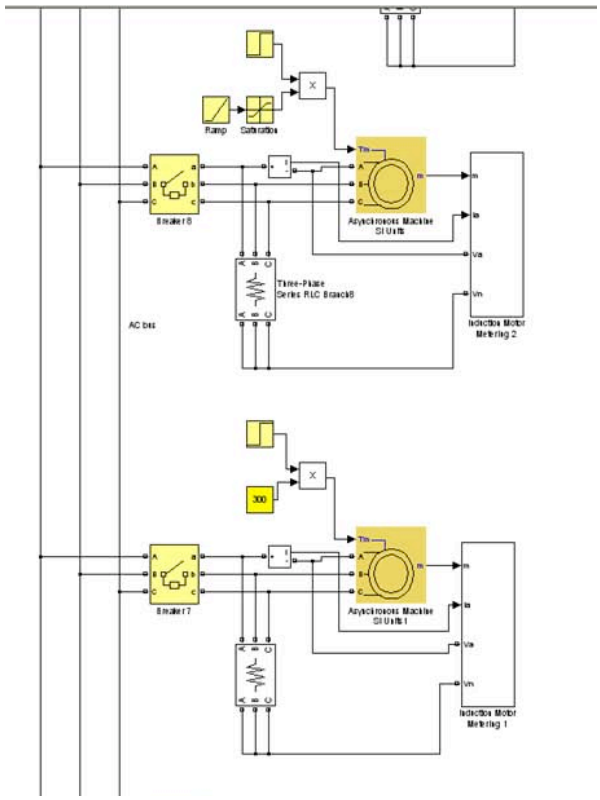

Figure 30. Detail of section with models of motor loads 1 (top) and 2 (bottom)

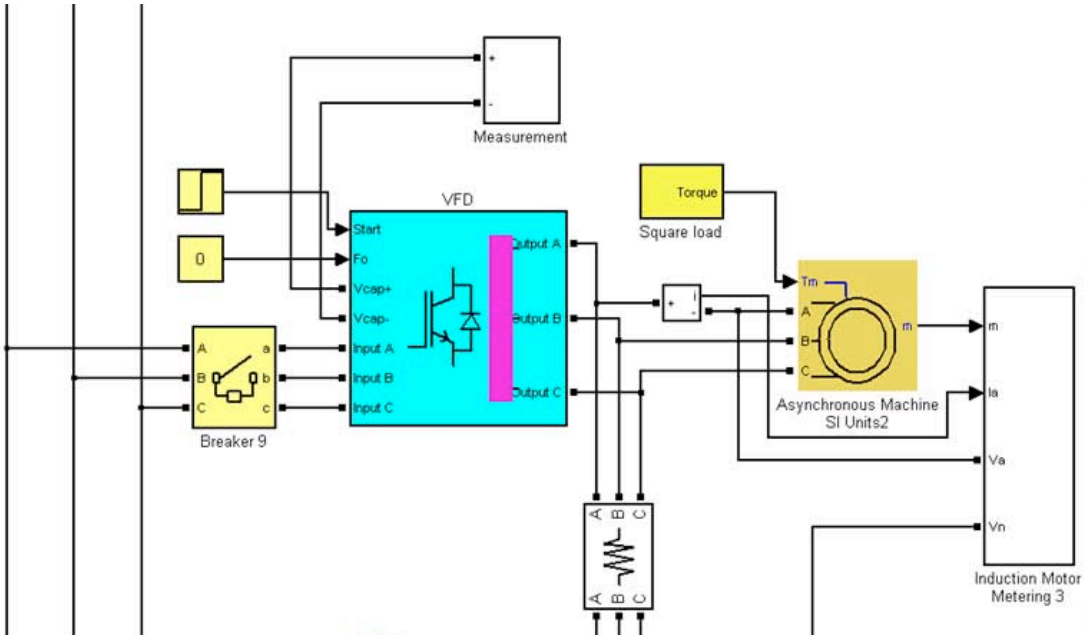

Figure 31. Detail of section with models of motor loads 3 with variable speed drive

The motors were actually modeled with their dynamic characteristics to provide a realistic representation of the transients on the power system. The simulation cases reported herein reflect a constant resistive load of 1 MW and examine the system response to the addition of the motor loads described above. It should be noted that, as far as current load is concerned, the effect of starting across the line a 200 HP motor is equivalent to a block load about 6 to 8 times its nominal rating during the motor acceleration period. Furthermore, the dynamic response of the machine and its low power factor during start-up give rise to transient current oscillations. Thus, starting two large motors in quick succession on the system already loaded to 1 MW, as was done in this simulation, is a rather severe test.

Figures 32 through 34 show the transients following the starting across the line of motor load number 1 followed in short succession by motor load number 2. Figure 32 shows the line-to-line voltage from an across the line start of two induction motors. The first motor is a 200 hp 1,780 rpm motor with a linear speed/torque profile and the second is a 100 hp induction motor with a constant full load torque profile. The ac voltage dips slightly in response to the first motor start event, but the transient response is more pronounced when the second motor starts while the first motor is still accelerating.

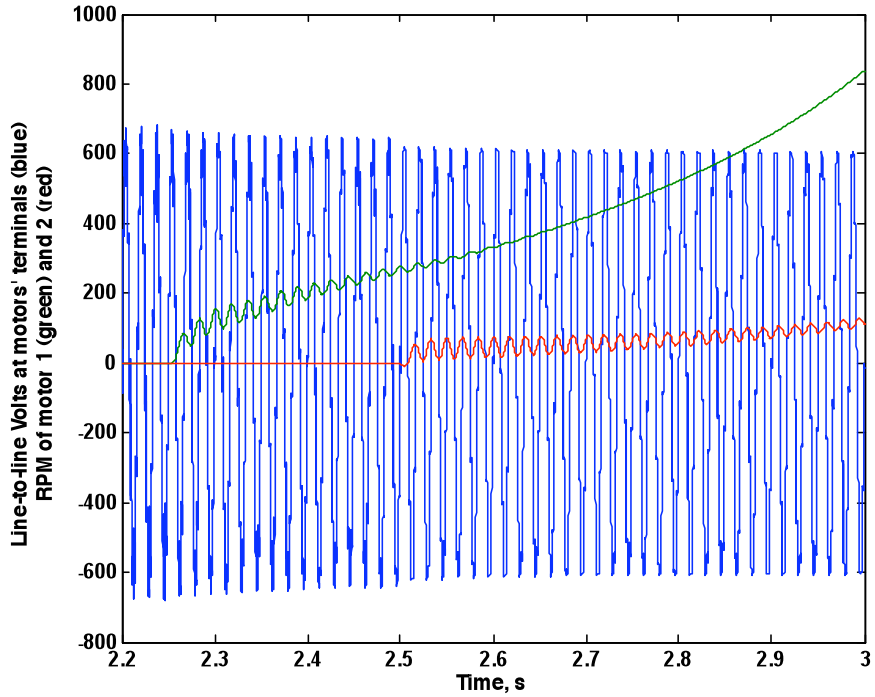

Figure 32. Line-to-line voltage response to successive starts of two induction motors

Figure 33 shows the transient current profile of motor number 1 (linear speed/torque profile) during the initial phase of the start sequence. Figure 34 shows the transient current profile of motor number 2 (constant full load torque). Note the slight oscillations in motor current just after starting – these oscillations are typical for motors of this size.

This study pointed out the need to revisit the issue of balancing the stiffness of the ac bus with the filtering requirements on one hand and cost and size of the system components on the other when the actual demonstrator will be built. Power quality limits on total harmonic distortion and the eventual implications of size and cost of the filter components will have to be considered in the design.

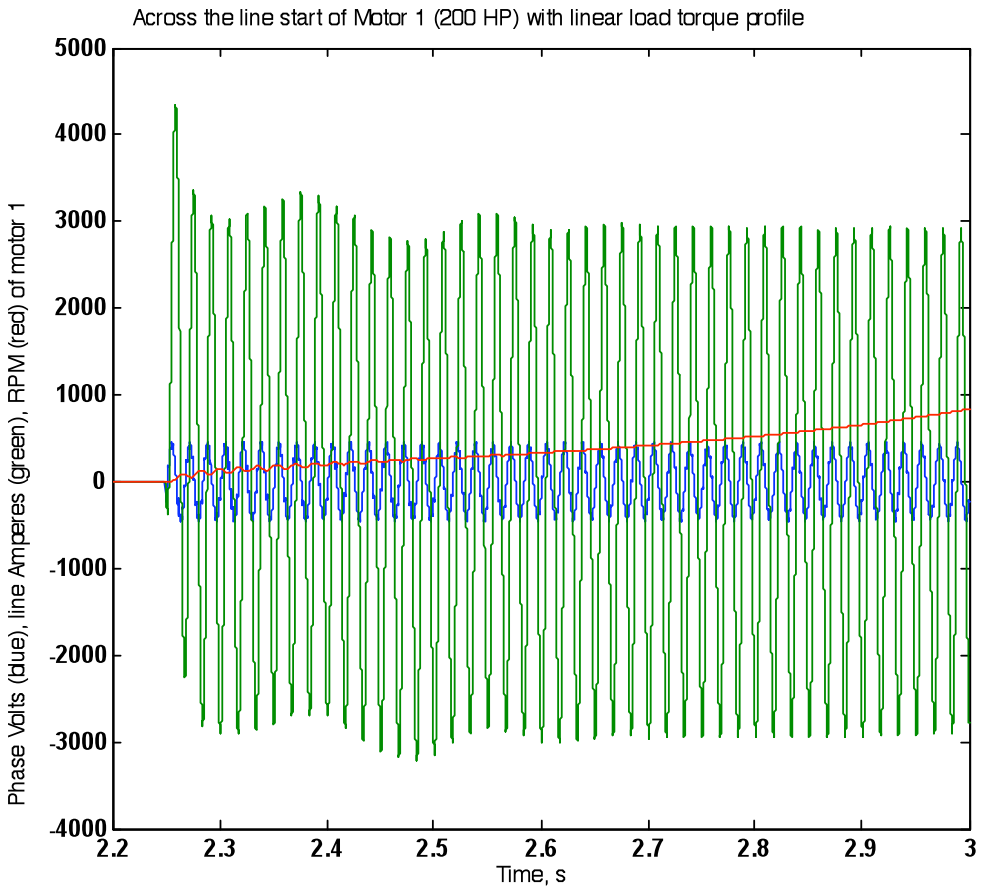

Figure 33. Starting current profile of motor no. 1

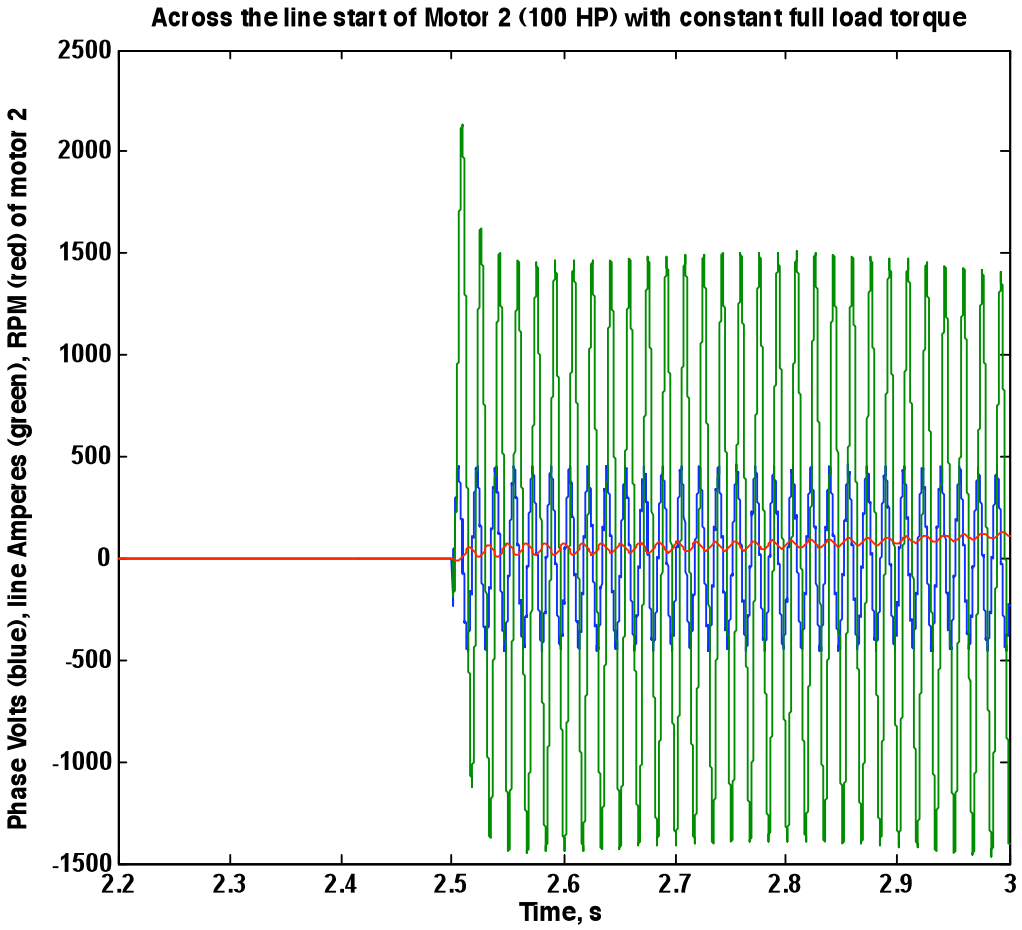

Figure 34. Starting current profile for motor number 2

Although there are no specifications attached with the dc bus per se, it is prudent to consider the operation of the system at that level as well, since it is an excellent way to assess the system reserves, potential under-designed/over-designed elements, and is an early indicator of possible system stability issues. Thus, it is also instructive to see the system's behavior at the level of the dc bus as shown in figures 35 and 36. Figure 35 shows the currents on the dc bus from the flywheel generators (blue and green traces overlay), the turbine generator (red), and the total dc bus current (cyan). Note the transient response of the flywheels in response to the start of motor number 1 – load leveling by the flywheels reduces the transient load seen by the turbine generator. Figure 36 shows the comparable dc bus currents in response to the start of motor number 2.

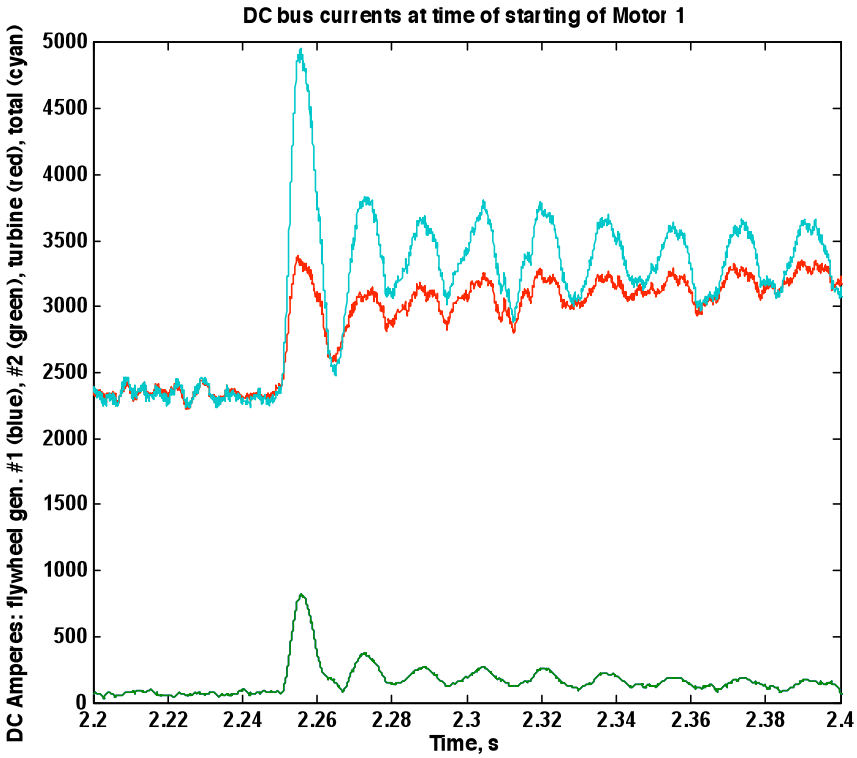

Figure 35. DC bus currents at the time of starting of motor number 1

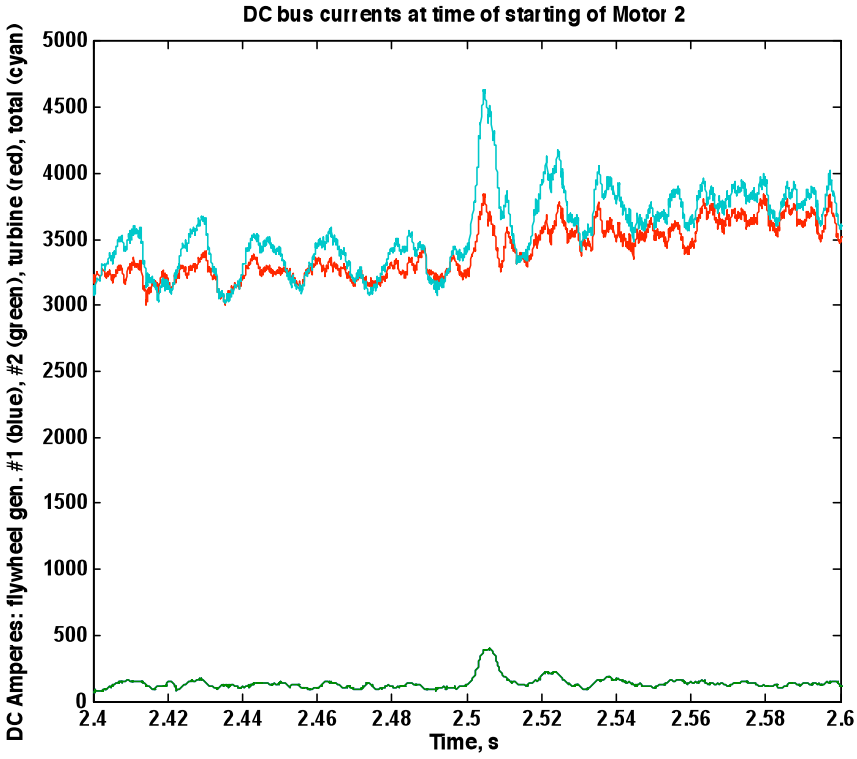

Figure 36. DC bus currents at the time of starting of motor number 2

Figure 37 shows the line-to-line voltage (green) and dc bus voltage (blue) transients in response to starting motor number 3 at t = 5 s. Figure 38 shows additional detail of the voltage waveforms after the motor has reached full speed at time t = 7 s. In this case the load torque is proportional to the square of the speed as might be seen in a centrifugal pump or blower. The variable frequency drive simulation was programmed for an acceleration time of 2 s. It can be seen that the ac bus is virtually unaffected by the addition of load no. 3 but that the dc bus undergoes some small but perceptible oscillations (~8%). Again this is probably an indication that the dc bus capacitive support should be stiffened, although the possibility that it may be the result of some numerical instability in the software cannot be dismissed: these interactions often occur when power converters drive other power converters, as is the case here.

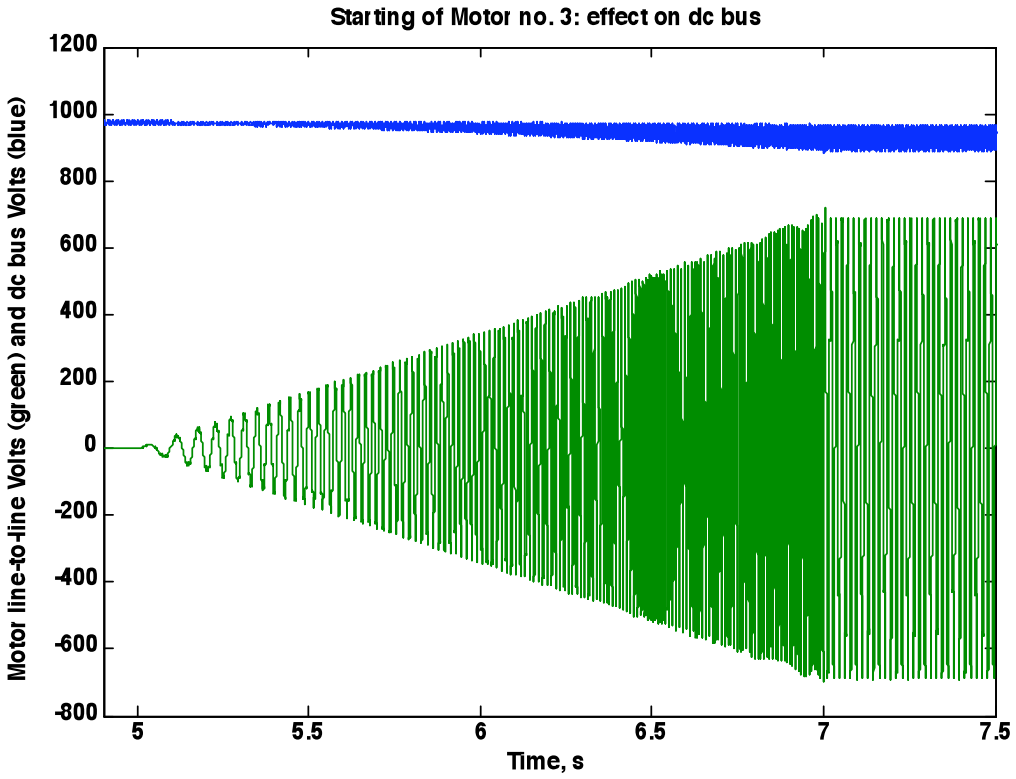

Figure 37. Transient response of line-to-line voltage and dc bus voltage after starting of motor number 3

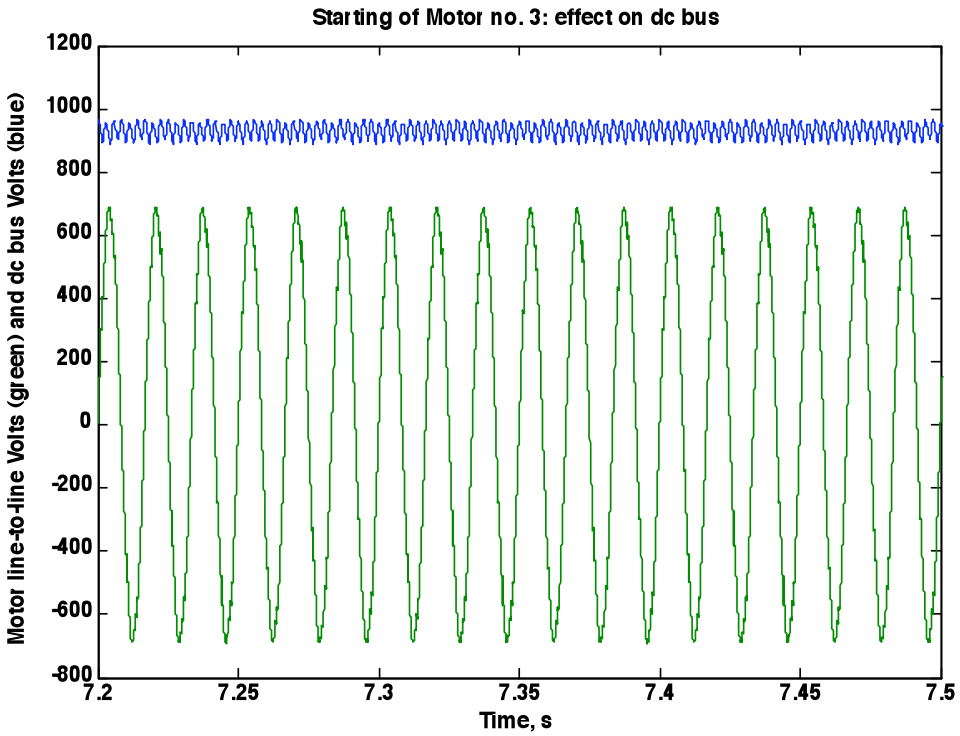

Figure 37. Detail of waveforms

Improved VFD Model

With the ultimate goal of moving closer to the objective system, it was decided to improve the model used for variable speed drives. Figure 38 shows the new system icon and mask parameters for the variable frequency drives used in the system model as well as the first layer beneath the mask. The icon has the three-phase ac inputs and outputs, some control inputs, plus an opportunity to connect to the drive's dc bus capacitor terminals. The icon masks several layers of representation for the variable frequency drive. The mask parameters are arranged in such a way as to resemble the most common inputs required in actual commercial drive packages. This is a step forward in the direction of actual implementation in a demonstrator test system.

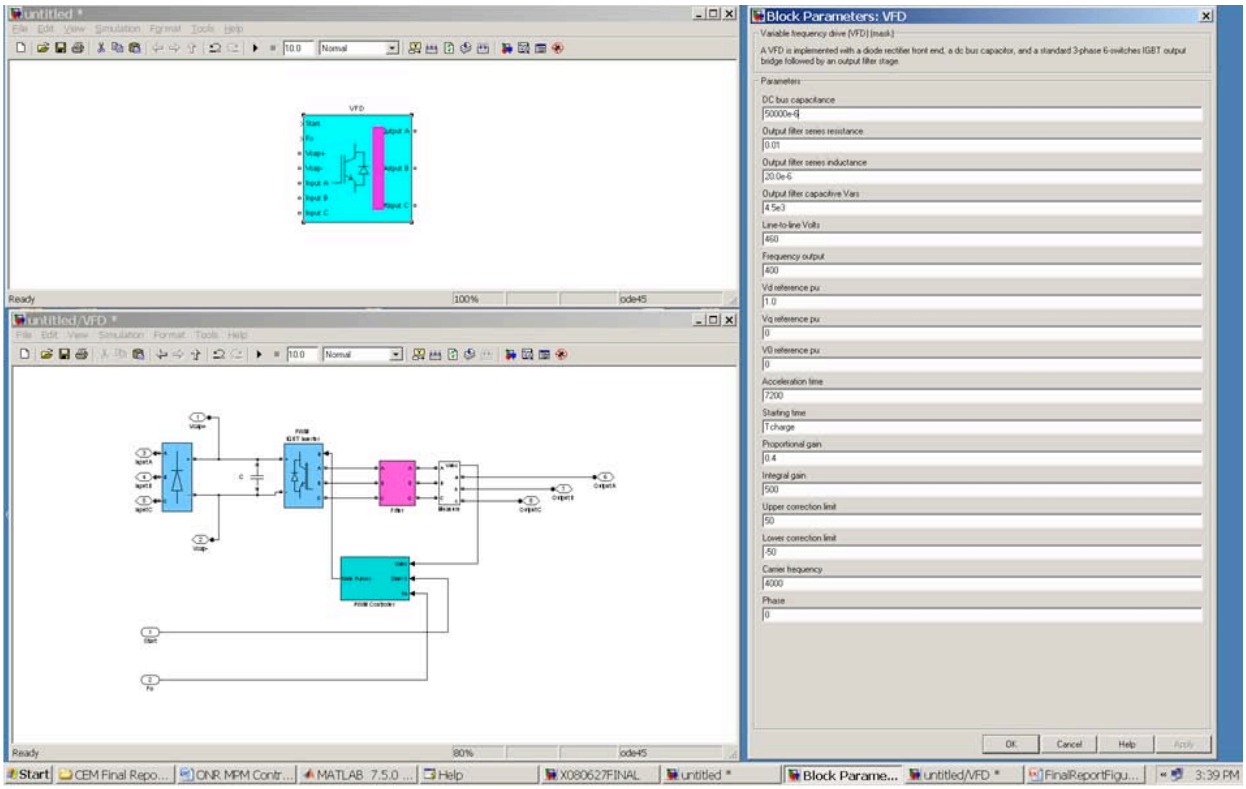

Figure 38. Icon, mask parameters, and first layer of improved model for the variable frequency drive

Extended System Simulations

Experience with several simulation runs revealed that simulation times much longer than 10 s can exceed the memory limitations of the typical desk-top or lap-top computer. The possible simulation length on these hardware platforms depends on the complexity chosen for the model (load combinations, switching cycles and time allowed for stabilization, whether flywheel re-charging is permitted, etc.). Meaningful simulations usually run between 10 and 20 s before experiencing platform memory limits and longer ones are possible only with models incorporating some significant level of simplification. Figure 39 shows a typical full system model simulation that ran for 19.46 s before terminating due to lack of memory.

In this simulation the low fidelity turbine model was used in order not to incur the 5 s initialization penalty intrinsic to the high fidelity model. Various loads were switched on and off as shown in table 17.

Table 17. Load profiles for extended duration simulation.

Time, s	**Description**
t< 0.5 s	Initialization (ignore)
t = 0 – 5 s	2.5 MW resistive load
t = 5 s	added 1 MW resistive load
t = 5 s	added 100 HP motor load, constant torque (motor load 1)
t = 10	added 200 HP motor load, torque ramp (motor load 2)
t = 14 s	added 200 HP motor load with 4 s acceleration (motor load 3)
t = 15 s	removed 1 MW resistive load and motor loads; started re-charging flywheels

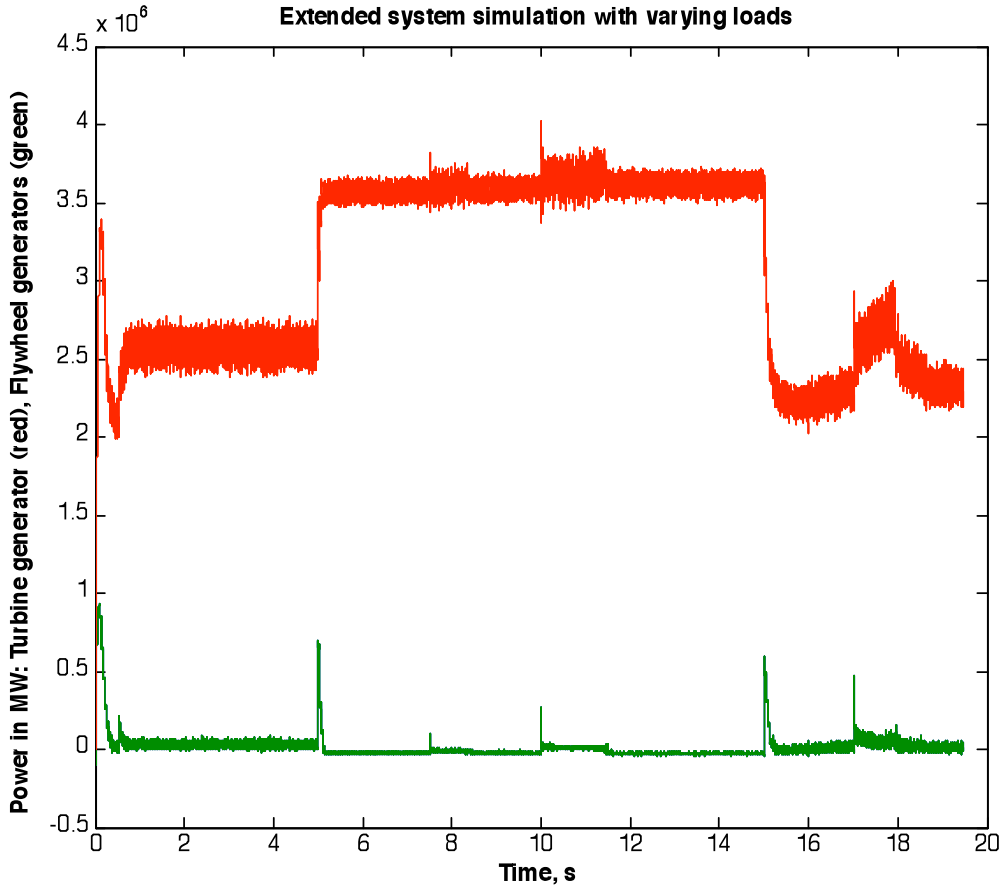

Figure 39. Extended time simulation with various loads - simulation was interrupted after 19.46 s for insufficient memory

Obviously, the use of the high fidelity turbine model would have limited the usable simulation time even further. It is clear that more extensive simulations will have to be run on more powerful hardware platforms than the standard desktop or laptop computer.

Control System Upgrade

The controllers of the flywheel generators/active rectifiers were completely redesigned over the course of the model rationalization. The overall architecture can be described as the combination of a current loop within a voltage loop. First, the controller checks that the dc bus voltage, the dc bus voltage rate of change in time, the turbine generator voltage, and the flywheel generator voltage are within pre-established bounds (voltage loop). If they are, the controller proceeds to check that the load current, the turbine generator current, and the flywheel current are within pre-established bounds (current loop). If any of the bounds are exceeded, corrective action is taken based on both voltage and current status (control actions). This strategy is more comprehensive than the one originally used in the companion grant and is believed to be a good basis for the implementation in hardware of the actual controller during a demonstration test.

Figures 40 through 43 show the equivalent flow chart of the new flywheel controller's voltage loop (part 1 and part 2), current loop, and control actions, respectively. The flow charts are extensively labeled so as to be self-contained and self-explanatory. The corresponding Simulink controller diagrams are shown in figures 44 through 49.

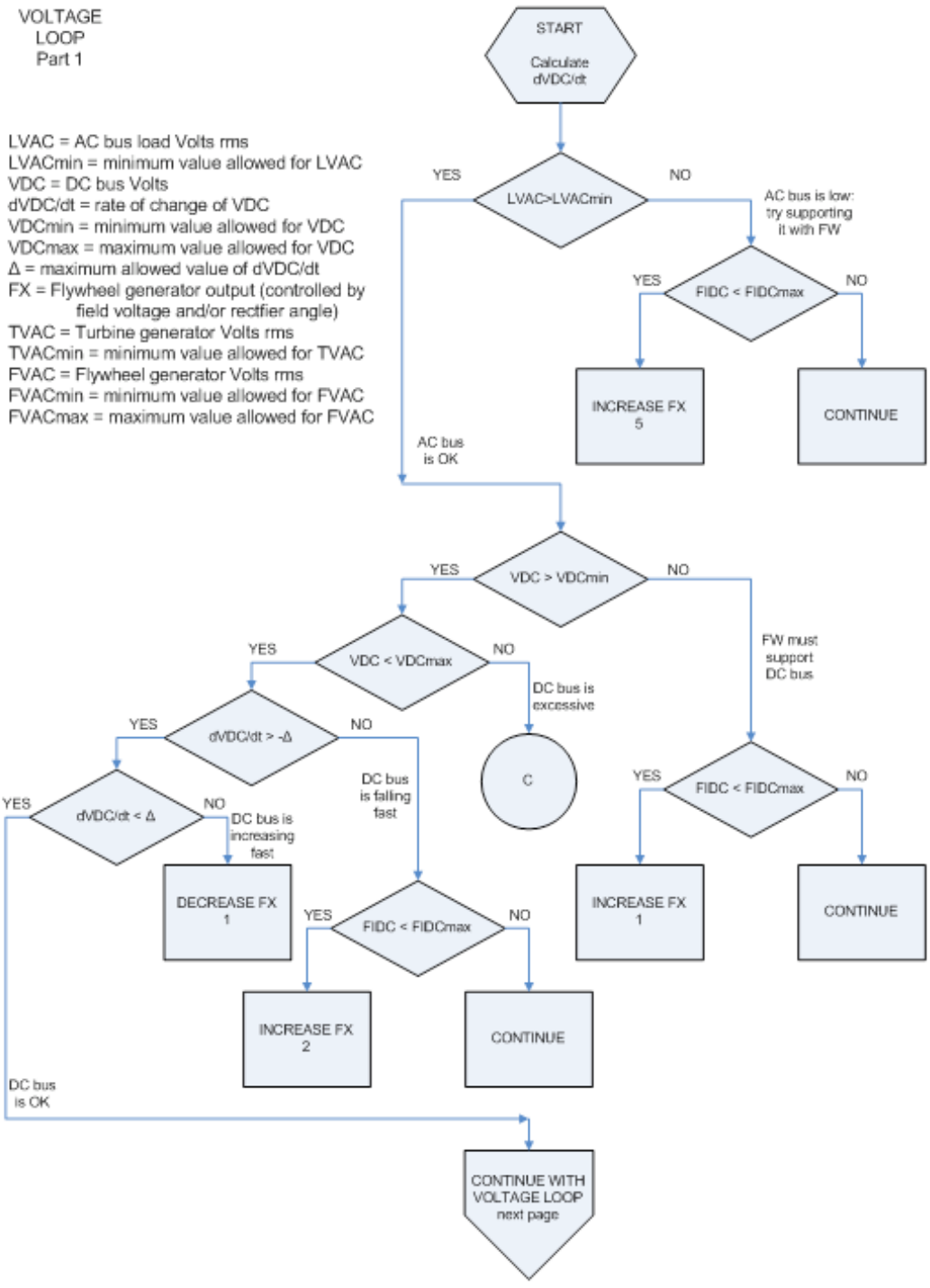

Figure 40. Voltage loop flowchart – part 1.

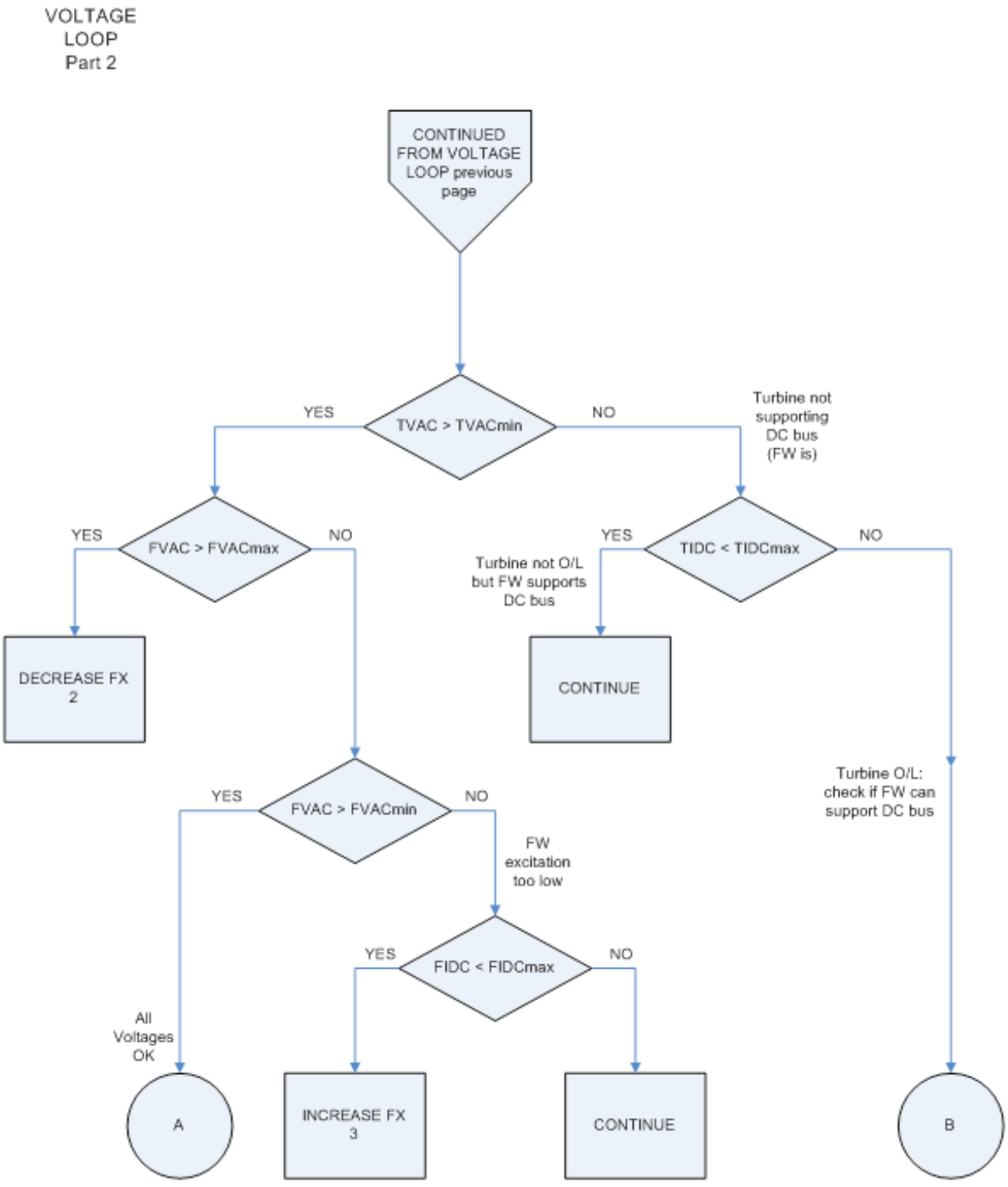

Figure 41. Voltage loop flowchart – part 2.

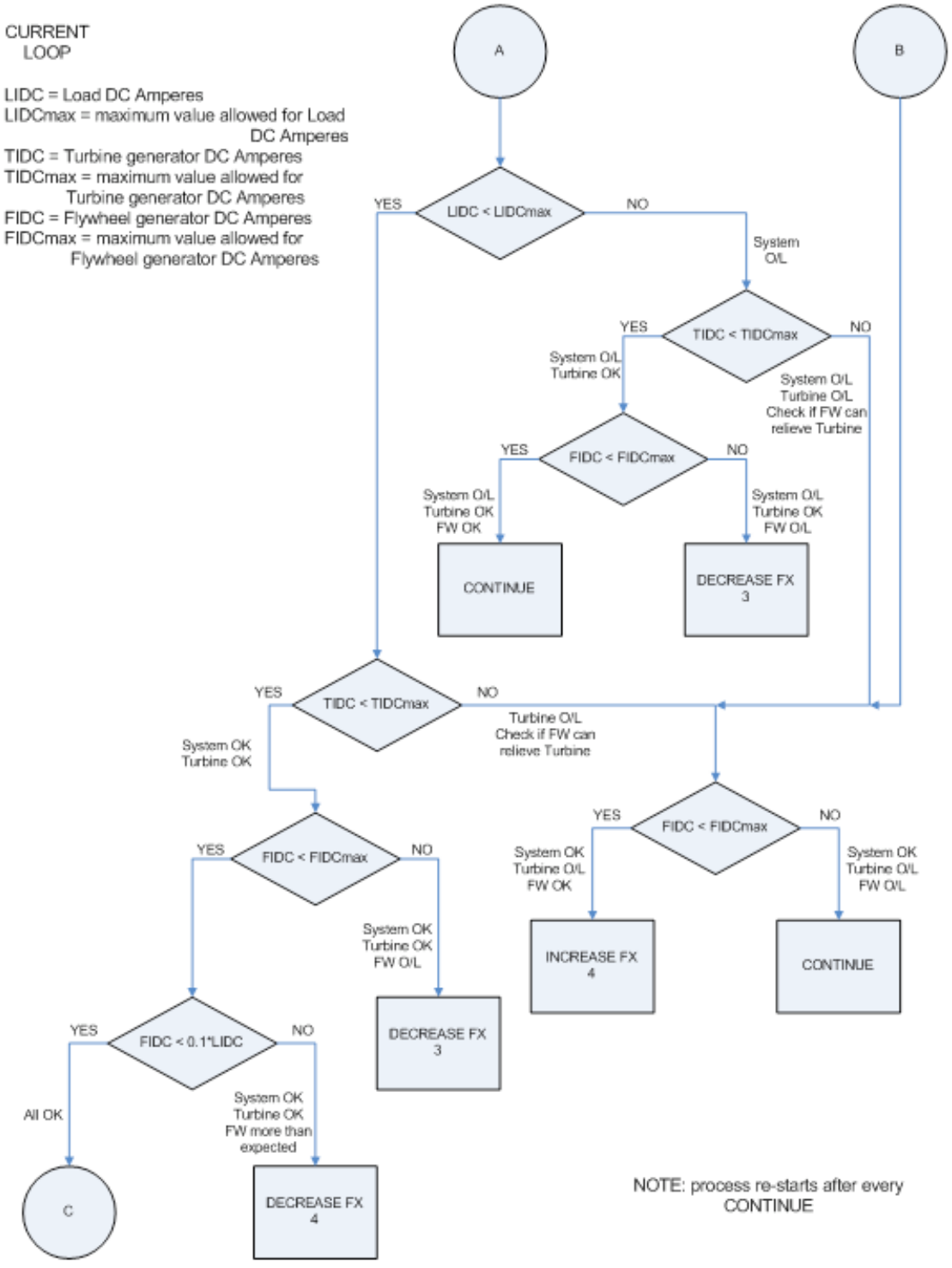

Figure 42. Current loop flowchart.

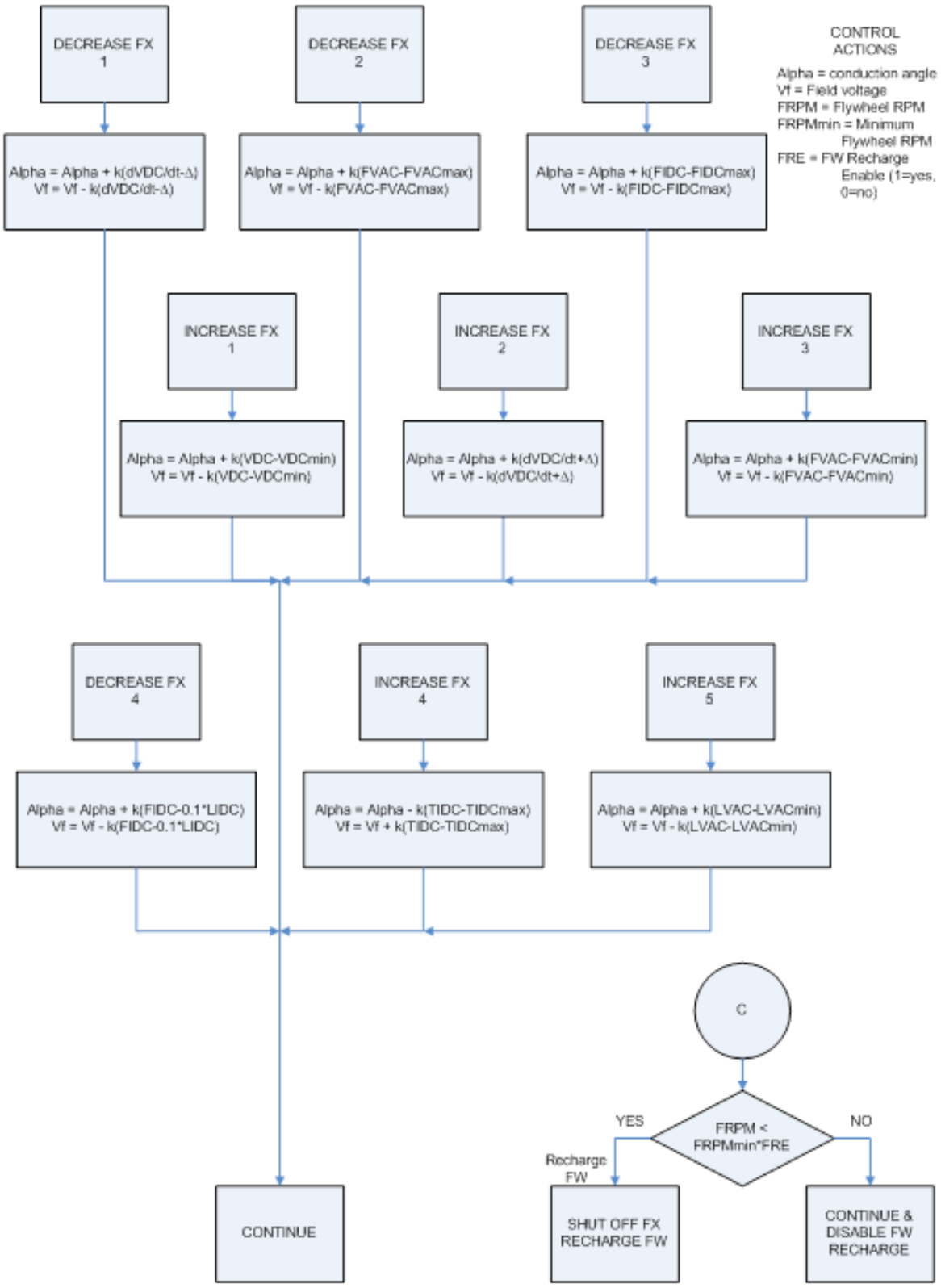

Figure 43. Control action flowchart.

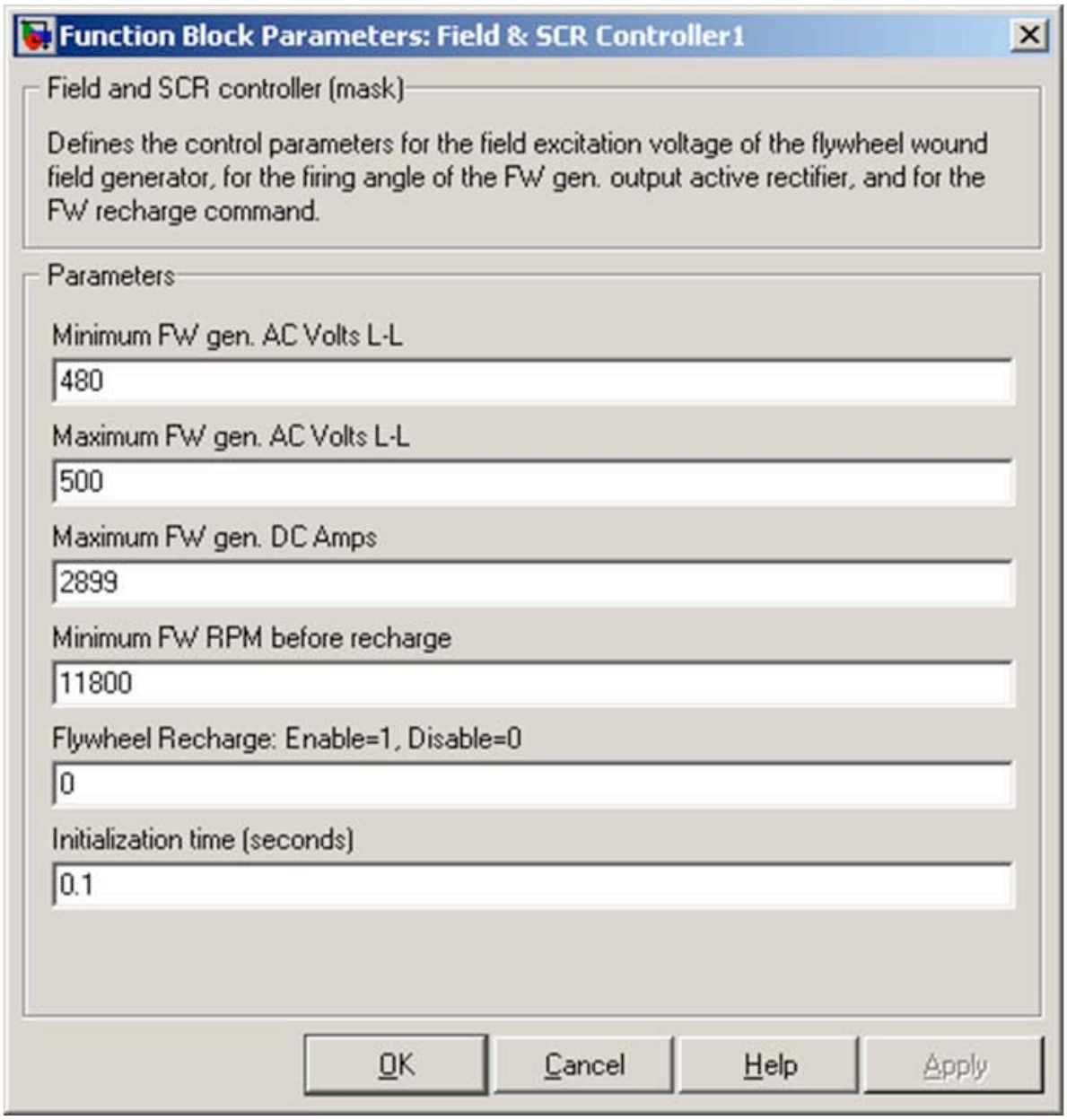

Figure 44. Parameter input screen for control block for flywheel generator field and active rectifier

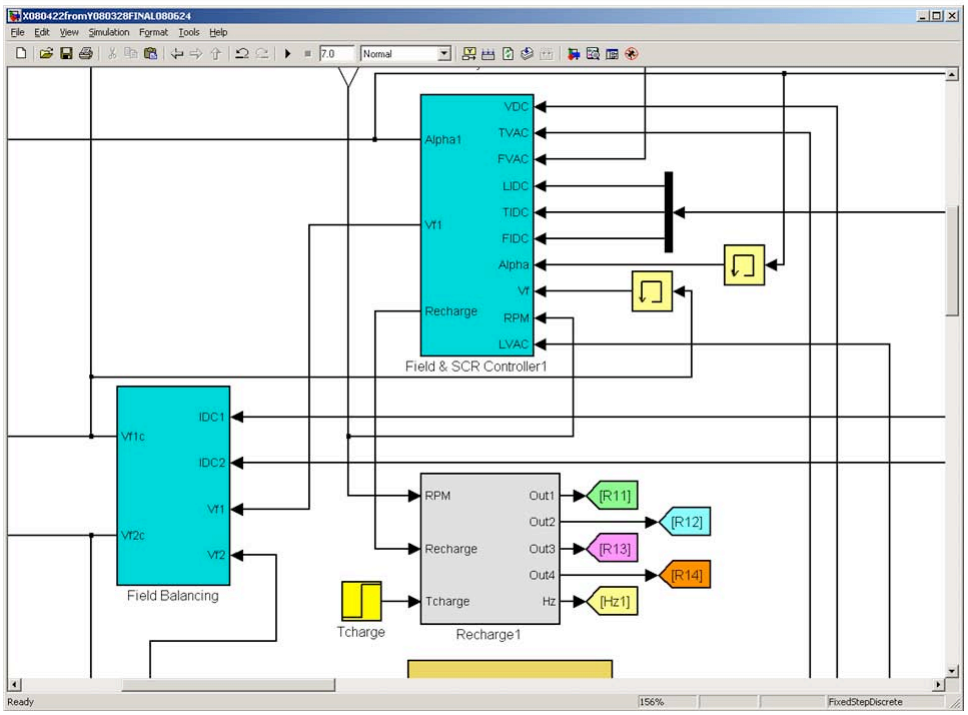

Figure 45. New control block for flywheel generator field and active rectifier

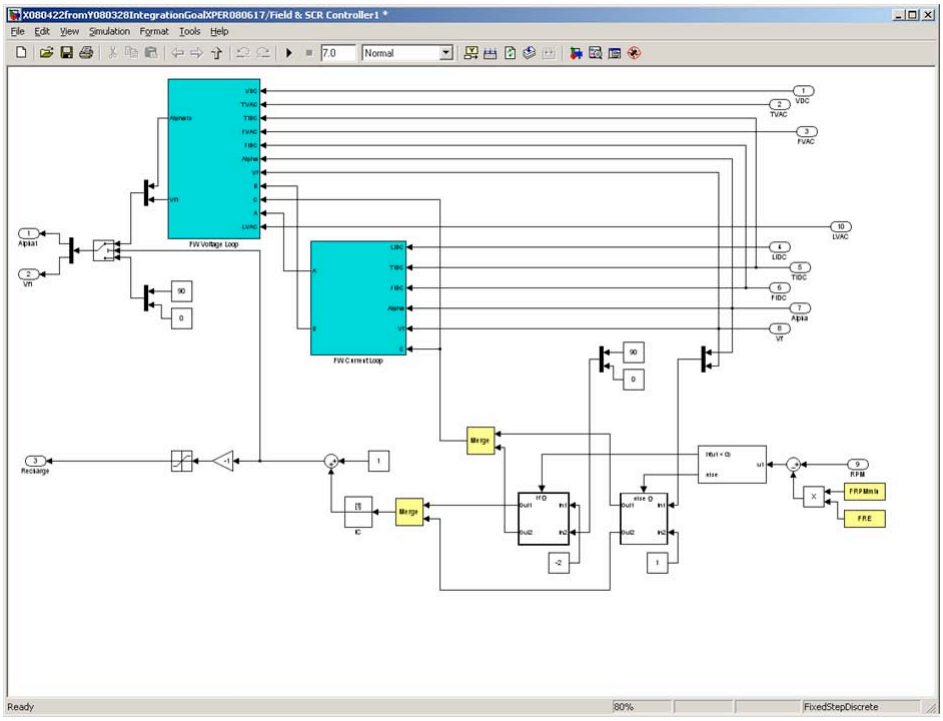

Figure 46. First level of final control block for flywheel generator field and active rectifier

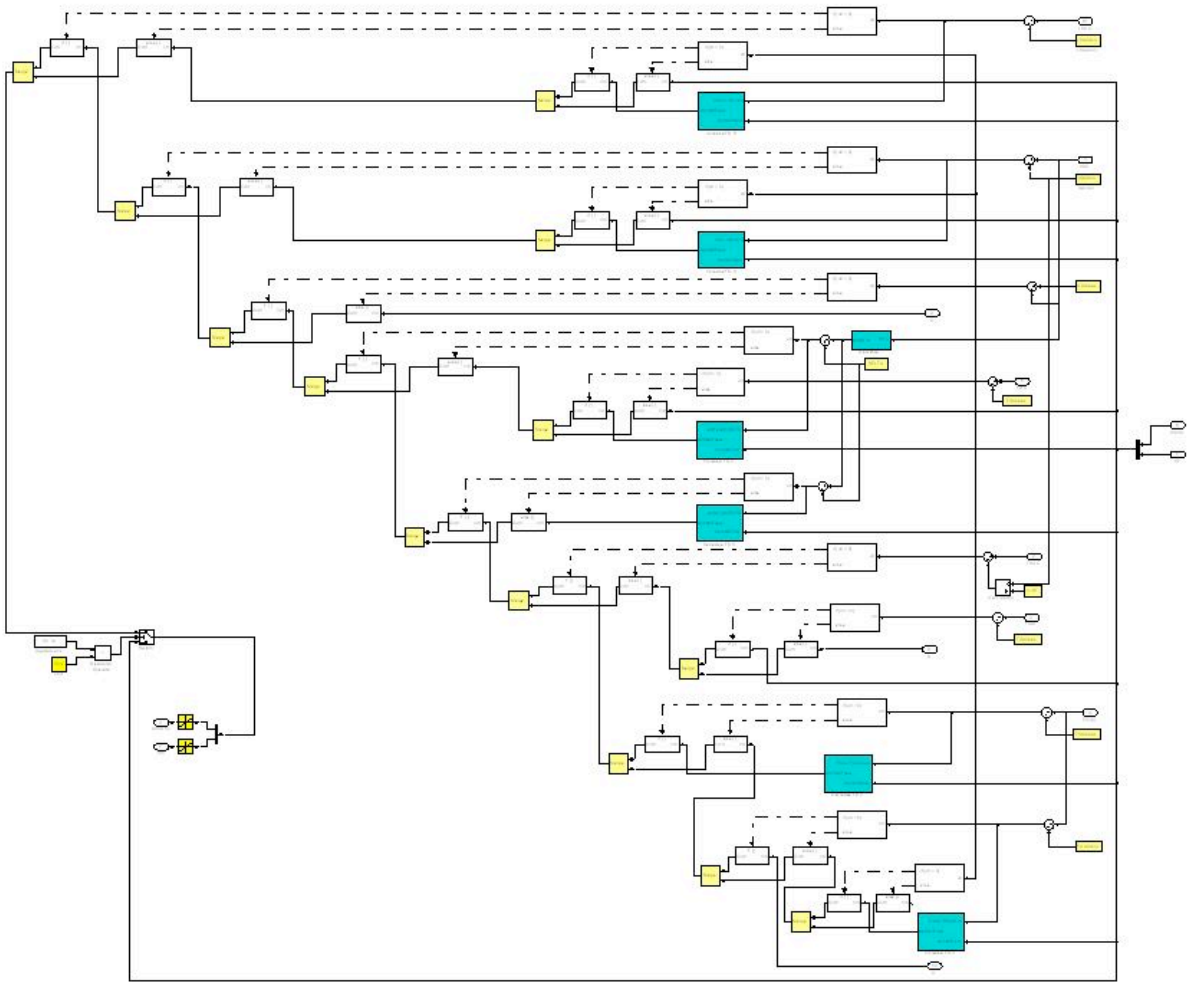

Figure 47. Detail of voltage loop sub-block

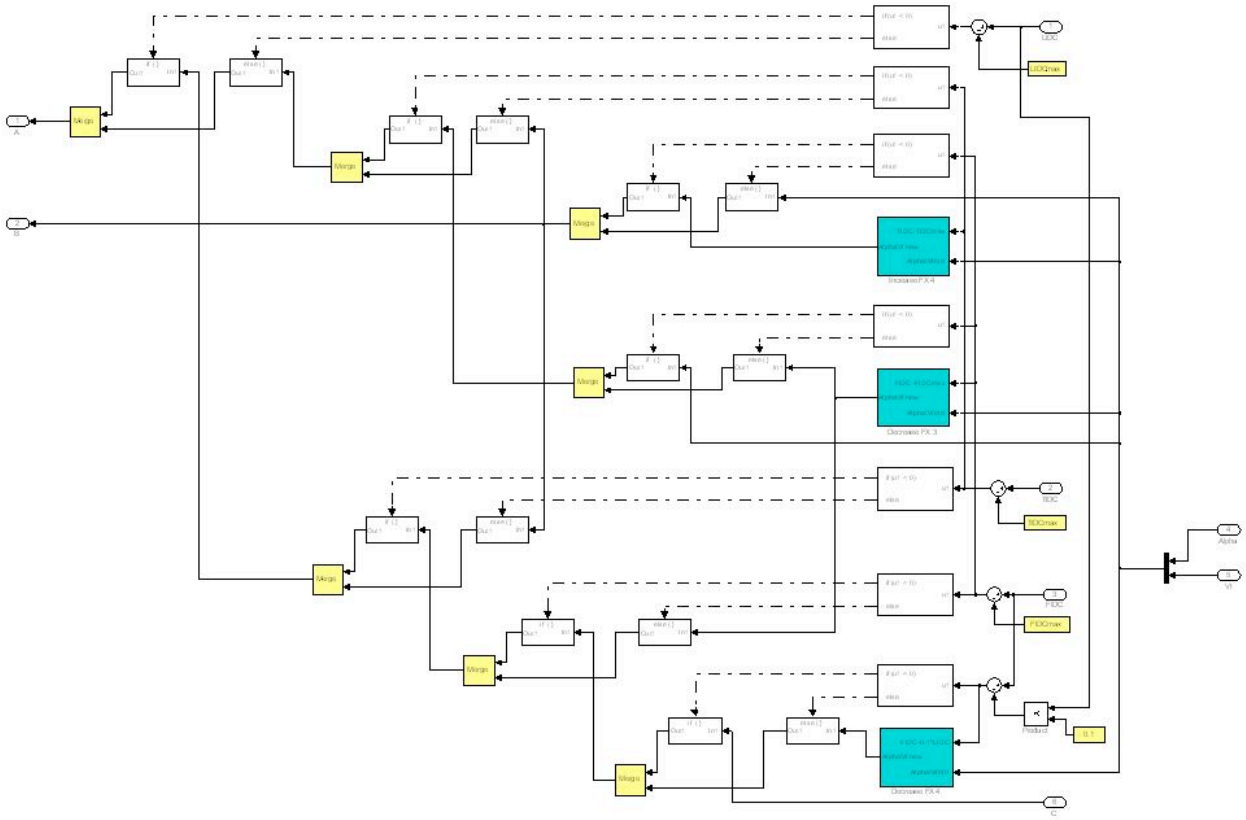

Figure 48. Detail of current loop sub-block

An example of the performance of the control system developed can be seen in figures 49 through 52. It has been mentioned previously that the high fidelity turbine model requires a 5 s minimum initial settling time in order to get through its proper initialization process. It has also been shown above that during this initial period the turbine speed undergoes rather wide excursions resulting in corresponding swings of the voltage generated by the permanent magnet turbine generator. These transients, although the result of the software implementation of the turbine model and, thus, not to be taken as necessarily real, are rather severe but the control system reacts to them as if they were true physical transients excited in the system.

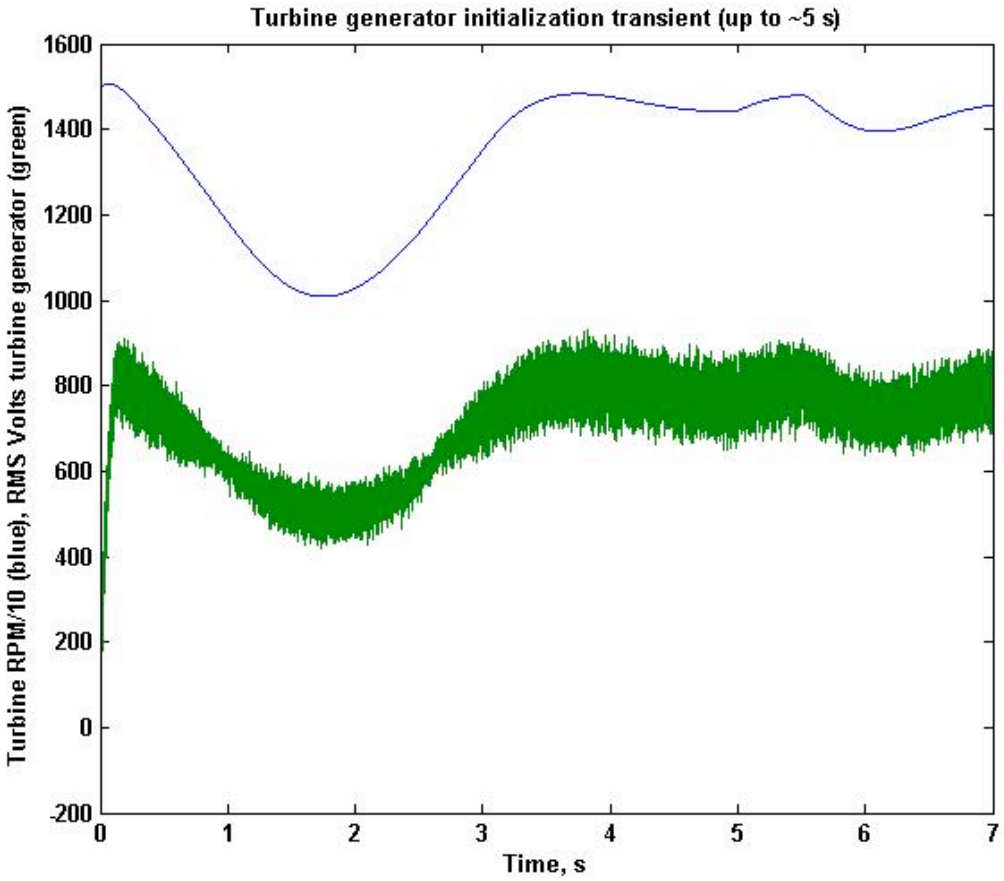

Figure 49. Initialization transient for the turbine rpm that is reflected in an unregulated voltage output from the permanent magnet turbine generator

Figure 49 shows the initialization transient for the turbine rpm during the first 5 s of the simulation that is reflected in an unregulated voltage output from the permanent magnet turbine generator. Although this initialization period (~ 5 s) is required by the software modeling the turbine, the system responds to it as if it were a true transient to be corrected.

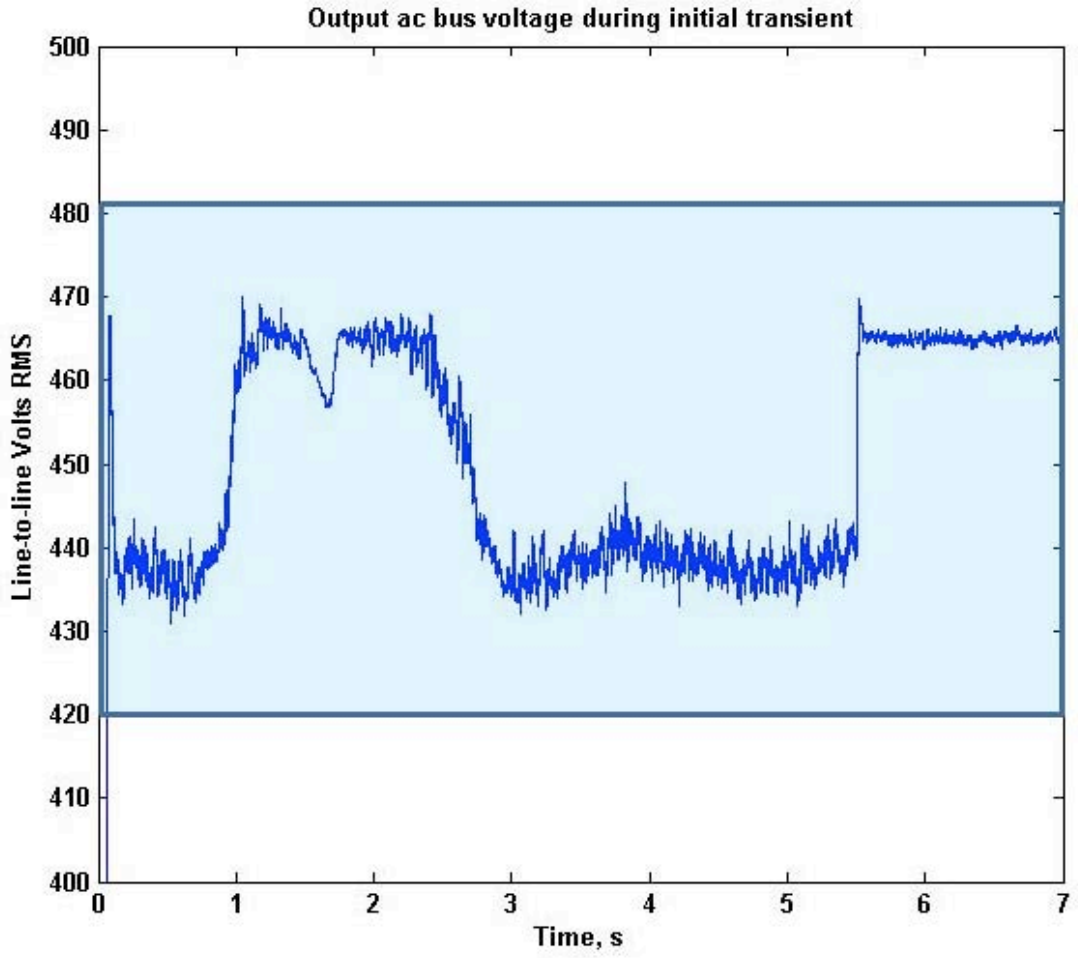

Figure 50. Line-to-line voltage on the ac bus showing effect of control system

Figure 50 shows precisely how the control system maintains the level of the output ac bus well within the limits dictated by MIL-STD-1399 even during these non-physical extreme transients in the power system. The figure shows the line-to-line RMS voltage output at the ac bus during system initialization (up to ~5 s). In this simulation, the ac load is doubled from 1.4 to 2.8 MW at time t = 5.5 s. The acceptable band ($\pm$ 7%) for general voltage fluctuation per MIL-STD 1399 is shown shaded in blue around the 450 V nominal voltage. In reality, in this case the tolerance band for transients would apply which is even broader ($\pm$ 16%), thus, the system is well under control.

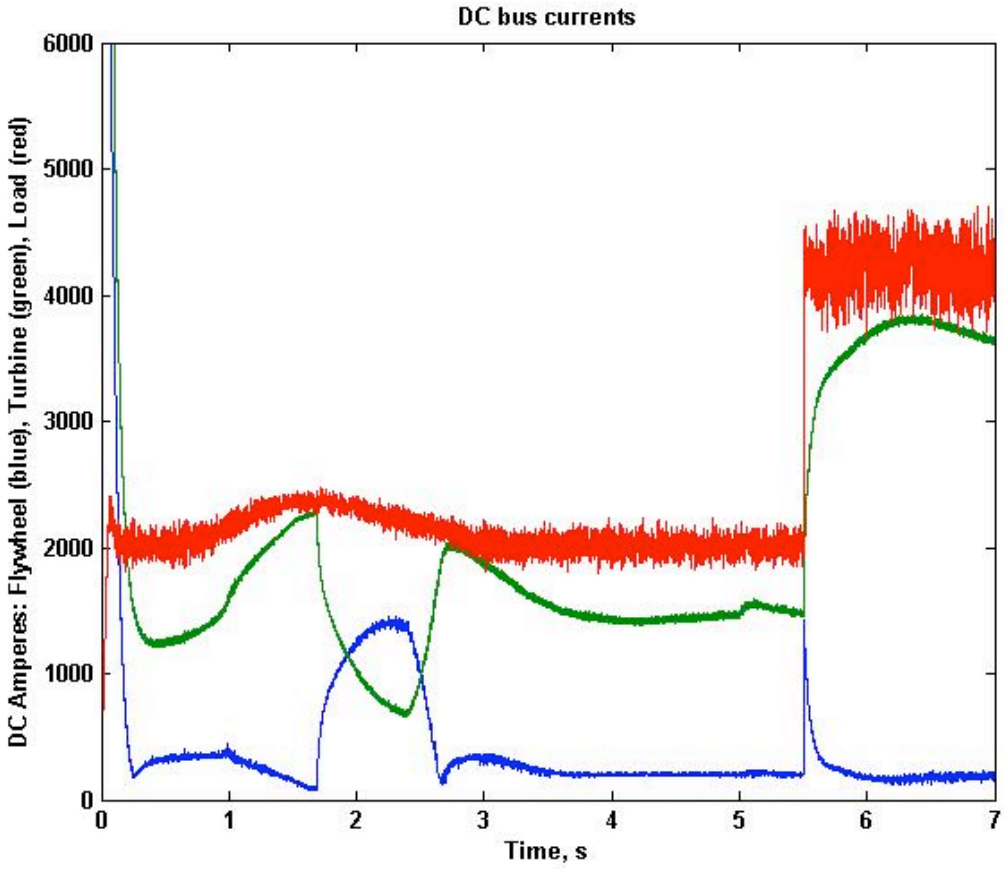

Figure 51. DC bus currents during initial transient

Figure 51 shows the dc bus currents during initial transient. It can be seen how the flywheel control system steps up the flywheel generators output (blue trace) when the turbine generator (green trace) fails to support the load (around t $\simeq$ 2 s) and during the step load transient at time t = 5.5 s.

The issue of filtering required to achieve the total harmonic distortion (THD) limits at the output ac bus has been a constant throughout the course of this program and a final attempt at settling it was made. After extensive evaluation, one thing remains clear: a system rated at 3 MW of output power requires a filtering system rated at 3 MW in order to meet the voltage regulation and THD limits specified in MIL-STD 1399. This is best accomplished with active filtering, from the standpoint of performance and eventual hardware size.

Modeling of effective active filters is extremely complex and computationally intensive and so was not included in the scope of this effort. An attempt was made early on to obtain information on its active filters from the potential supplier identified in the course of this work (i.e. American Superconductor) with the hope of being able to incorporate it into our simulation. Since no information was shared, this item is deferred to suggestions for future work. The output filters used in the simulation are of the conventional passive type, basically accomplished with reactors and capacitors. Although it is recognized that the eventual hardware will likely be of the active filter type, the passive filters used in the simulation have proven adequate to demonstrate the desired performance.

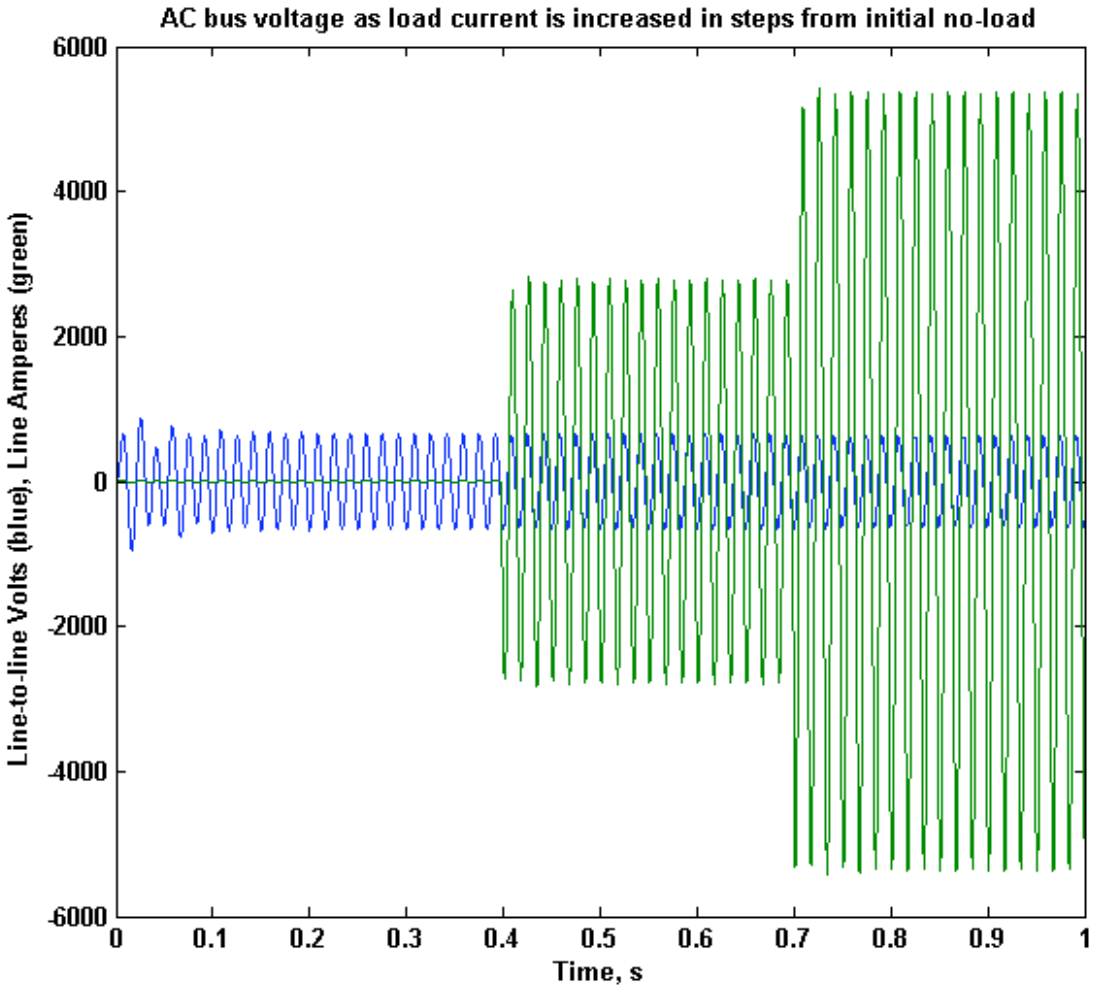

Figure 52. Line-to-line ac bus voltage as load current is stepped up from initial no-load

Figure 52 shows the line-to-line ac bus voltage (blue trace) as the load current (green trace) is increased in steps from the initial no-load condition. Figure 52 shows the ac bus total voltage RMS (blue trace) and the fundamental voltage only (green trace) as load current is stepped up from initial no-load. The blue and green traces overlap, indicating minimal harmonic contents. Total harmonic distortion (THD) is shown in the red trace magnified by a factor of 100 for scaling purposes. Thus, ignoring the initial settling transient ($t < 0.2$ s) the THD is always less than 4%.

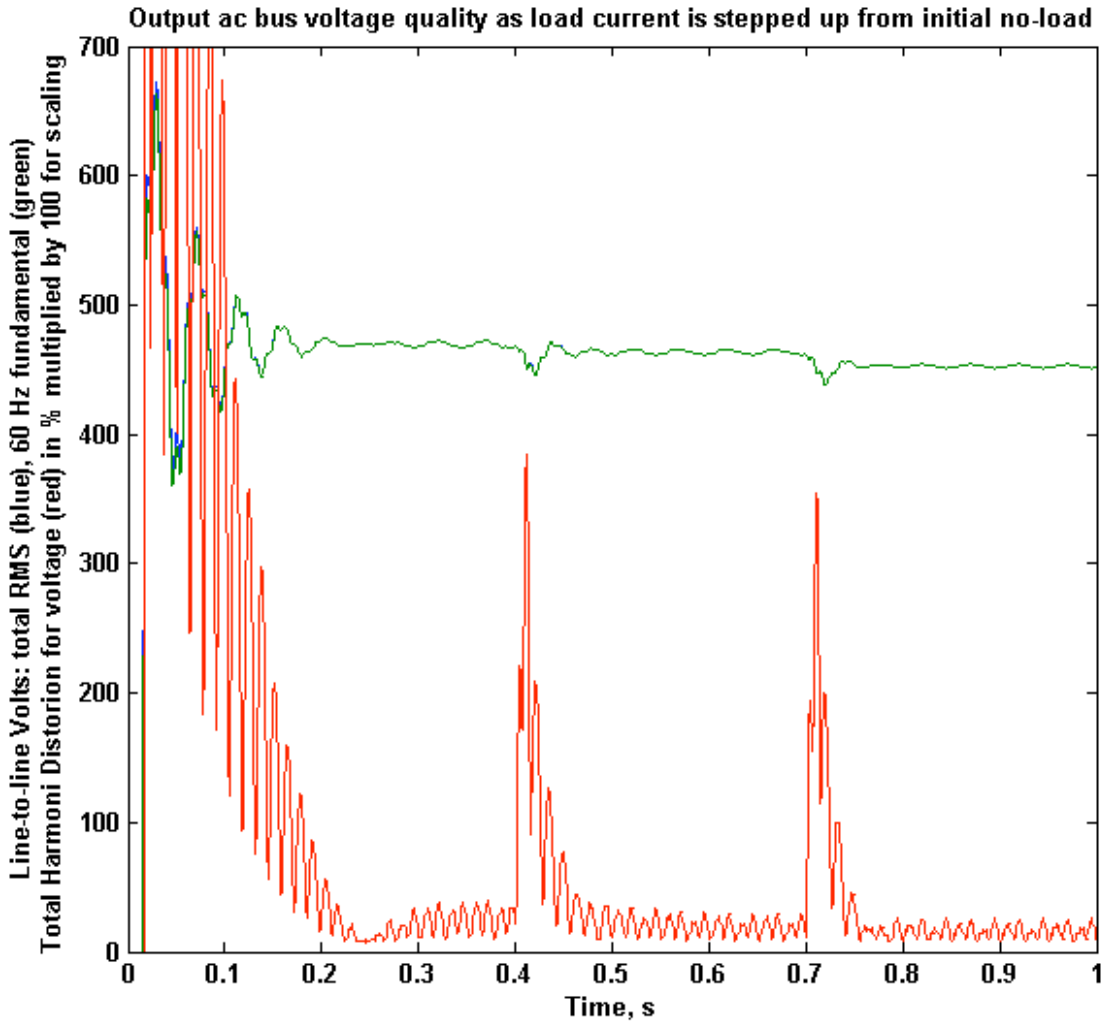

Figure 53. Fundamental current and total harmonic distortion (x100) during step load transients

Modeling Summary

The MatLab Simulink simulation developed under this contract enabled high fidelity modeling of the Megawatt Power Module concept for the DDG51 ship service generator system. The simulation includes a high fidelity model of the Rolls-Royce AE1107 twin shaft gas turbine as well as accurate representations of the permanent magnet generator, flywheel motor/generators, solid state power converters and output filters. Simulations included step load transients as well as high fidelity modeling of expected transient events such as across the line starting of induction motors with a variety of load/speed profiles. The modeling indicates that the proposed system will enable reliable single generator set operations using energy storage flywheels to provide load leveling and uninterruptible power to the ship service distribution grid in the event of a failure on the primary turbine generator set.

The MatLab Simulink model is a deliverable under this contract. A detailed User's Manual has been developed to document the simulation software and provide guidance for the use and modification of the simulation to explore other operating scenarios. The User's Manual for the MPM simulation is attached to this report as Volume 2.

Technology Demonstration and Development Planning

System Definition

This effort was conducted in the context of a planned demonstration of the Megawatt Power Module concept under ONR BAA07-029 titled Fuel Efficient and Power Dense Demonstrator for the Arleigh Burke DDG51 Class Ship. As part of this effort, UT-CEM and Rolls-Royce developed technology development and demonstration plans to mature the MPM concept through a prototype demonstration and Engineering Development Model (EDM) program.

The technology demonstration plan must balance cost, schedule and technical risk to work within the available funding and meet the timeline defined by the goal of implementation into the Flight 2A modernization program in 2015. The technology demonstration must also clearly show the functionality required to achieve the projected fuel savings and demonstrate these functions at power levels relevant for the DDG51 application. The technology development plans look at the activities needed to further mature the components and system and to qualify them for Navy service.

After reviewing multiple power system component and topology options, a system topology has been selected as the baseline system for a technology demonstration program. Figure 54 shows the basic block diagram for the demonstration system. Alternative system demonstration plans using different components and/or with reduced scope have also been developed (refer to the companion grant for details). In order to limit the cost of the technology demonstration, the use of existing equipment and/or facilities has been considered whenever possible.

UT-CEM and Rolls-Royce contacted potential suppliers for various elements of the demonstration system to explore alternative component designs and evaluate rough-order-of-magnitude (ROM) costs for demonstration prototypes. Based on these evaluations, Direct Drive Systems (DDS) was selected as the primary supplier for the high speed permanent magnet generator driven by the Rolls-Royce gas turbine. For the system demonstration, DDS is proposing the use of an existing 8 MW high speed PM generator design developed for commercial applications. The use of an existing PM generator design significantly reduces the

cost of a custom developed prototype while validating critical elements of the generator design that would be used in a follow-on Engineering Development Model (EDM) program. The EDM high speed generator would be a shorter version of the current DDS machine using essentially identical rotor and stator design and construction techniques.

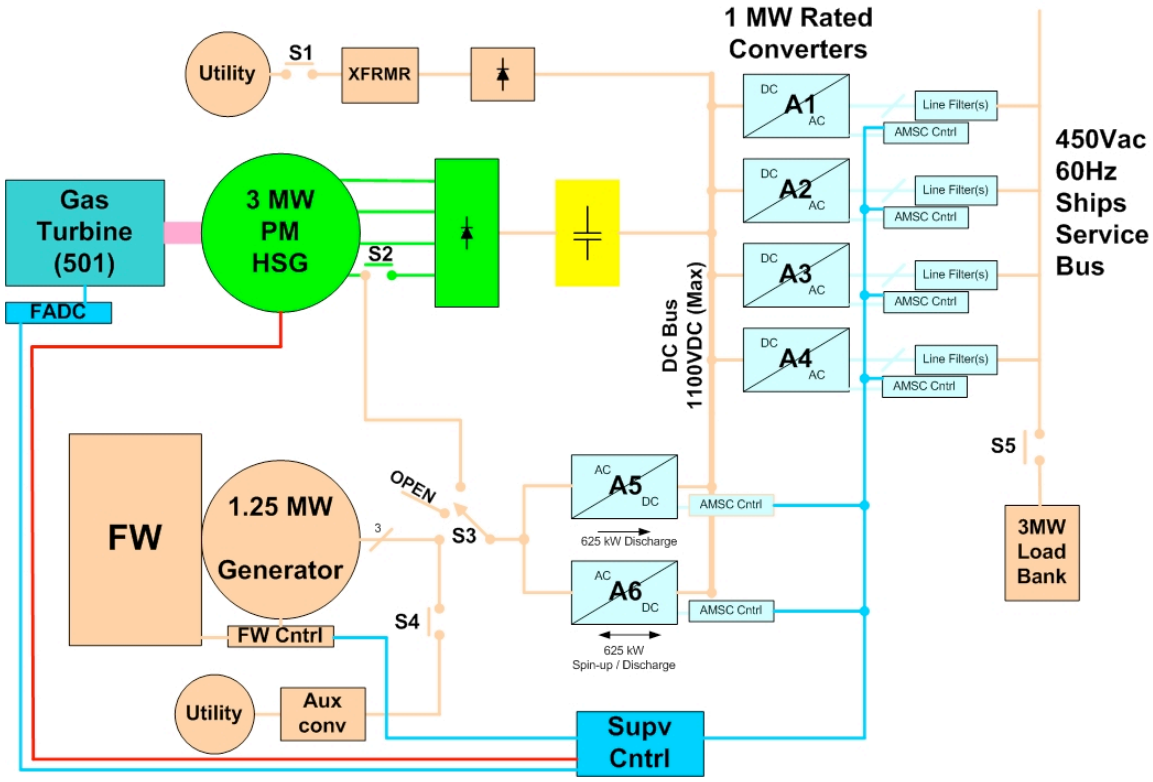

Figure 54. Basic block diagram of demonstration system

After exploring alternative designs for the power conversion system, UT-CEM and Rolls-Royce selected a relatively conventional rectifier/inverter topology using IGBT devices and passive filters to achieve the required power quality. The primary goal of the power conversion system for the technology demonstration was to use low-risk, proven technologies to enable the use of high speed, high frequency power generation while maintaining the required efficiency, power density, and power quality. Although alternative power conversion topologies may eventually offer modest increases in power density and efficiency, the systems evaluated in the study have not been demonstrated at the power levels required by the DDG51 ship service and

their use was deemed too risky for the current technology demonstration. ROM costs for the technology development activities required for these alternative power conversion systems were also beyond the scope of the envisioned system-level technology demonstration program.

After discussions with several commercial suppliers, American Superconductor Corporation (AMSC) was selected as the primary supplier for the power conversion system for the technology demonstration. AMSC developed a system of Power Electronic Building Blocks (PEBB's) in conjunction with ONR. Similar power converter systems up to 4 MVAR have been developed by AMSC for use in wind turbines, generator sets, power quality systems and military pulsed power systems. The power electronics for the technology demonstration program are from AMSC's PowerModule^{TM}PM2000 family that employs two low-risk modifications to the widely used PM1000 line: incorporation of 1,700 V IGBT devices and the use of a water cooled chill plate to increase power density. In addition to the primary inverters to supply the 450 Vac, 60 Hz distribution grid, AMSC equipment will also be used to interface the energy storage system to the dc bus and ac grid.

The major energy storage system components will be provided by UT-CEM and will leverage existing equipment from the Advanced Locomotive Propulsion System (ALPS) program wherever possible. The ALPS program developed a hybrid electric propulsion system for high speed passenger locomotives that has a similar topology to the proposed DDG51 ship service power system. The ALPS energy storage flywheel will be used to demonstrate the uninterruptible power supply and load leveling functions of the system. The UPS function enables single generator set operations which results in the majority of the fuel savings for the system.

For UPS operation, the energy storage system must be capable of providing secondary power into a "dead" bus, so the existing ALPS flywheel induction motor/generator was not well suited for this application. After reviewing alternative motor/generator technologies as discussed above, a Homopolar Inductor Alternator (HIA) was selected for the technology demonstration. The characteristics of the HIA are ideally suited to the flywheel motor/generator application and the HIA design is seeing increasing use in this application. The relatively simple construction of the HIA machine reduces development time and cost, and the demonstration costs will be further reduced by using some elements of the existing ALPS induction motor/generator for the HIA

prototype. The field winding of the HIA is located on the stator and the rotor is a robust solid steel structure. This construction eliminates the need for retention of permanent magnets and the risk of insulation or diode failures on a high speed rotor. The stationary field winding simplifies cooling and, unlike PM machines, provides external control of the generator output. This is a critical feature for high energy flywheels with a wide variation in operating speed and the need to control the output voltage or turn the machine off. During standby mode, the rotor EM losses are near zero, improving system efficiency and potentially enabling integration of the motor/generator into the flywheel for the EDM system.

Rolls-Royce will be responsible for development of the supervisory control system for the technology demonstration. The supervisory control system controls the overall operation of the power generation and energy storage systems and provides the user interface. Subsystem controllers will be developed for each of the major subsystems, including the power electronics, flywheel and flywheel motor/generator. UT-CEM will leverage experience developed during commissioning and testing of the ALPS propulsion system to support Rolls-Royce in this effort.

Demonstration of the Megawatt Power Module is planned to take place at the UT-CEM laboratory facility in Austin, Texas. This facility was developed to allow testing of the ALPS hybrid propulsion system and is ideally suited for the ship service power system technology demonstrations. Use of the existing test site will significantly reduce the technology demonstration program costs and will leverage the infrastructure developed for the ALPS program. The facility includes a remote EMI/RFI screened control room, a spin test bunker for testing of high energy rotating machines and a gas turbine test cell with supporting auxiliaries for testing of gas turbines in the 3 to 5 MW power range. The ALPS flywheel and its auxiliary and control systems are in place and operational in the spin test bunker, further reducing the cost of the technology demonstration.

The goal of the test program will be to demonstrate a fuel-efficient, multi-megawatt ship power system with energy storage in a high fidelity laboratory environment, maturing the advanced components and the overall system to TRL 6. The demonstration will consist of incremental testing of the major subsystems, followed by incremental testing of the fully integrated power system. The tests will demonstrate:

- Delivery of 3 MW at 0.8 pf from the gas turbine and PM generator
- Fuel consumption improvements relative to the existing AG9140
- Load leveling to mitigate the effects of load transients on the gas turbine generator
- UPS operation – 1.25 MW for 2.5 minutes

Demonstration of Flywheel Discharge

Early plans for the laboratory demonstration of the UPS functionality of the system chose a 1 MW rating for the new motor generator design, coupled to the existing UT/FRA flywheel. However, as the plans matured, the design rating for the new flywheel motor/generator (and associated power electronics) were increased to 1.25 MW. The reason for this change is to configure the demo system to more accurately represent a single flywheel unit of the objective system, while better matching the energy and speed parameters of the available demonstration flywheel. Configured this way, this equipment will be a partial system demonstration, not a sub scale system. The planned test will be performed at a substantial 50% of objective power, and 25% of objective energy.

The demonstration flywheel system will operate at 1.25 MW for 2.5 minutes, precisely representing one flywheel on one skid of a 4 FW, 5 minute, parallel / serial discharge configuration. This requires the motor generator, power electronics, and dummy load to be operated at the 1.25 MW level, and those requirements have therefore been carried forward to the respective components. However, this sizing also allows demonstration at 625 kW for 5 minutes, simulating the alternative parallel discharge configuration in the event that this topology is still under consideration during the time of the demonstrations. For either of these cases, the UT/FRA flywheel would be cycled between 12,500 and 7,500 rpm to meet the energy requirements (including surplus to cover system inefficiencies) of the 5 minute UPS demonstration. This range was selected to minimize technical risk and demonstrate the flywheel rotor tip speed used in the preliminary design of the flywheels for the DDG51 application.

This demonstration decision imposed changes to the design specification for the new flywheel motor/generator. The original preliminary power rating for the HIA motor generator design was 1 MW, operating over a range of 14,000 to 7,000 rpm. The electromechanical design

of the rotor and stator were therefore updated to accommodate the new power and operating speeds. Likewise, the requirements for the flywheel discharge power electronics were updated to reflect the higher power. These changes are described in more detail in previous sections of this report.

Starting Gas Turbine in Laboratory

The need in the system for a variable frequency drive (VFD), as a minimum, in order to be able to bring the flywheel back up to full speed after a discharge cycle provides the opportunity for using the same variable speed drive unit to start up the turbine. In principle, the VFD can be switched from the flywheel M/G to the turbine generator that now will be used temporarily as a motor to get the turbine up to speed. Of course, the control system will have to be programmed to provide the proper sequencing of events and suitable interlocks to accomplish the operation safely. After the turbine has been started, the VFD unit can be re-connected to drive the flywheel M/G. This idea is very useful in the case of the laboratory demonstrator, since the normal means for starting the turbine would not be available and use of the VFD unit is an effective way to accomplish it.

One issue to overcome is that of power rating mismatch between the VFD, rated in our case at 625 kW, and the turbine generator (now used as a motor) rated at 3 MW. However, since the turbine generator is expected to have four independent windings, it is possible to power only one of these windings, essentially reducing the machine's motoring rating to nominally 750 kW, well within the design short term overload capacity of the VFD. In any case, the turbine will require less than 200 kW to start so that the task should be feasible.

The schematic diagram showing the planned laboratory demonstrator with turbine starting via the VFD is shown in figure 54. The turbine supplier, Rolls-Royce, and the generator supplier, Direct Drive Systems, have been consulted on this idea and have both confirmed its feasibility based on the torque needed to start the turbine and the torque output expected from the motor operating on only one quarter of its windings.

Flywheel System Reliability and Maintenance Estimation

Background

As part of the preliminary design activity, UT-CEM and Rolls-Royce compiled information about the characteristics and maintenance requirements for the proposed power system and major components. This information will enable comparisons with the existing ship service power system and will also allow follow-on design efforts to focus on improving the key drivers for reliability and maintenance requirements. A portion of the information compiled in this section was developed based on the current design of existing components proposed for the initial technology demonstration and so are not specifically designed or optimized for the DDG51 application. It is expected that the component designs and reliability will be improved as DDG51 specific designs are developed. The sections below present the process used by UT-CEM for generation of information on the major components of the flywheel energy storage system. This level of detail was not available for the information prepared by potential suppliers for the high speed generator and power electronics systems. An example of the potential for reliability improvements with DDG51 specific designs is presented in the section on the motor/generator encoder. Available system level and component level supplier information is presented in tabular form.

Energy Storage System

The flywheel system is first described in an overview to provide a technical background for the design reliability of energy storage flywheels, followed by more detailed, quantified maintenance data estimates.

Flywheel Design Life

The main components of the energy storage flywheel have fundamentally high reliability and long design life. The primary energy storage component is the flywheel rotor, in which energy is stored kinetically. The robust flywheel rotor (fig. 55) is comprised of essentially three main structural parts- the graphite composite body (the primary inertia), the steel shafting, and magnetic bearings. The flywheel rotor is essentially a structural component, and apart from rotation, has no moving parts, no wearing parts, and its robust mechanical structure can be designed for a 35 year design life, with no performance degradation. As a point of comparison,

commercial flywheel UPS systems from Active Power, Inc., using steel flywheels at lower power than the DDG51 objective system advertise 740,000 hr MTBF, demonstrating that flywheel battery systems can achieve very high reliability.

Figure 55. Example composite rotor component for large energy storage flywheel

Comprehensive studies and tests performed by UT-CEM for NASA, DARPA, and DOT regarding graphite composite materials used in energy storage flywheels have shown that properly designed composite flywheels maintain their material properties stably for very long cycle life operation. For example, in accelerated life tests of over 112,000 deep charge/discharge cycles performed at operating temperature, a subject transit bus flywheel performed equally to a

"new" flywheel during overspeed tests intended to stress the material properties[4]. In another accelerated life study, a prototype space station flywheel was successfully tested to 375,000 cycles of deep discharge to represent 15 years of operating life[5]. In these cases, the composite materials showed little or no degradation in the form of fatigue or viscoelastic creep response. In the Naval power system application in which the flywheel accumulates a relatively small number of cycles, at lower discharge percentages, (assume 1,000 per year), fatigue cycle life on the order of what has been already demonstrated translate to 100's of years of design life. The long term viscoelastic response of the composite material is addressed by designing the rotor assembly interferences to maintain the required radial pre-stress at the end of the design life. Likewise, the steel shaft components can be designed with a predicted fatigue life that exceeds the needs of the Megawatt Power Module application. The magnetic bearing components on the rotor are passive steel structures that carry magnetic flux generated by the bearing stators. These rotor magnetic bearing components do not employ any electrical windings or permanent magnetic materials, and can therefore also be robustly designed for a design life exceeding 35 year service life of naval applications.

The other main components of the flywheel include the housing and vacuum enclosure, composite safety liner, and magnetic bearing stators. The housing and pressure vessel is a robust steel or stainless steel structure. The only vulnerabilities of the housing components pertain to vacuum sealing features—the electrical penetrations (for sensors and magnetic bearings) may develop benign vacuum leaks, and the rotating shaft seal and seal mount incur wear and require periodic maintenance.

The composite safety liner is a passive graphite/epoxy composite structure designed to absorb energy released in the unlikely event of a rotor composite ring failure. The liner structure requires no maintenance and incurs no wear in ordinary operation, lasting the lifetime of the flywheel.

---

[4] M.M. Flynn, J.J. Zierer, R.C. Thompson, "Performance Testing of a Vehicular Flywheel Energy System," Publication # 05P-131, Society of Automotive Engineers, SAE 2005.

[5] R.C. Thompson, J.H. Beno, "Final Report of the Technology Assessment of Space Flywheel Systems and Composite Rotor Safe-Life Technology Program, Phase 0", CEM publication # RF-197, June 2000.

The flywheel magnetic bearing system employs permanent magnets and electrical control coils mounted on the stator to position the rotor. The magnetic bearing stator components may be susceptible to long term insulation degradation, but will be designed with adequate insulation life for the lifetime of the flywheel. The bearing permanent magnets will not require any maintenance and will last the lifetime of the flywheel. Magnetic bearing position feedback sensors are non-contacting, high reliability sensors, but are neverthe`s potentially vulnerable to failure. To mitigate this risk, the feedback sensors will be designed for quick replacement. Further, the auxiliary rolling element bearing system (back up bearings) is designed to benignly catch the rotor in the event of a magnetic bearing system fault. These backup bearings have limited operating life, and therefore may require replacement after multiple touchdown events.

Flywheel Magnetic Bearing Control System MTBF

The magnetic bearing control system is comprised of electronic components including a microprocessor, servo amplifiers, and signal conditioning circuitry. This equipment will be military grade and ruggedized, but is nevertheless vulnerable to electronic faults, and may require preventative maintenance or scheduled replacement of components. The power amplifiers that supply current to the control coils in the magnetic bearing stators are critical components of the bearing power circuit. Industrial suppliers of commercial servo amplifiers publish maintenance data on their products, and high MTBF's and service lives are quoted:

Danaher / Kollmorgen servo amplifier MTBF = 3,000,000 hrs

Elmo Motion Controls MTBF = 550,000 hrs

Yaskawa MTBF = 400,000 hrs

Flywheel Motor Generator System Life

The flywheel motor generator component of the flywheel energy storage system is based on mature industrial motor technology with predictable, high reliability. It is worth noting that while the proposed specific topology (homopolar inductor alternator) is a somewhat unusual type of synchronous machine, the fundamental materials and construction techniques of this electric machine are essentially unchanged from conventional off-the-shelf military grade motors, and the user can therefore expect a similarly high level of reliability. The vulnerabilities of the flywheel motor generator include shaft coupling preventative maintenance (due to wear and

fretting), periodic shaft bearing replacement, potential for electrical insulation degradation, and shaft position encoder wear.

Flywheel Motor Generator Electrical Insulation Life

This section quantifies the life estimates for the flywheel motor generator stator electrical winding insulation. Winding insulation is assumed to be Class H (180^{o}C rated) with an expected temperature rise of 90^{o}C over an ambient of 50^{o}C during full power discharge cycling, resulting in a peak insulation temperature of 140^{o}C. If the motor/generator were running continuously at the insulation's rated temperature of 180^{o}C, a life of 20 years would be expected. Based on the widely used criterion in industry whereby insulation life doubles for every 10^{o}C reduction of running temperature, this would translate in our case into an expected life of

$$20 \text{ years} \times 2^4 = 320 \text{ years}$$

Thus, even allowing for the fact that the approximation may lose its value when extended over several intervals (here 4) away from the baseline, essentially for the life of the ship the motor/generator is not expected to experience insulation failures. Some minimal maintenance, however, is desirable. This will include periodic (yearly suggested) check of insulation resistance, both to ground and phase to phase. This should not take more than 1 or 2 hours. At longer intervals, a surge test may be advisable and an actual visual inspection of the windings (possibly every five years). This should take 6-8 hours.

Flywheel Motor Generator Shaft Encoder MTBF

A shaft encoder is currently planned for the laboratory demonstration of the Megawatt Power Module in order to synchronize the phasing of the power electronic drive with the motor true position. However, for the ultimate implementation, “sensor-less control” (which is common in industrial synchronous motor applications) will likely be used which would eliminate the position feedback encoder. Nevertheless, the MTBF for an encoder is estimated. Based on the manufacturer data sheet, the shaft encoder is rated with a Mean Time Between Failures (MTBF) of 17 years for the electrical parts or 10^{10} mechanical revolutions, whichever is shorter. In our case, the mechanical limit is the governing one. Thus, at 12,000 rpm operation (laboratory demonstration flywheel speed), the encoder's MTBF is calculated as follows:

$$12{,}000 \text{ rpm} \times 60 = 720{,}000 \text{ RPH (revolutions per hour)}$$

$$MTBF = 10^{10} / 720{,}000 = 13{,}889 \text{ hours @ } 4{,}000 \text{ operating hours per year}$$

$$MTBF = 3.5 \text{ operating years}$$

It must be noted that an encoder failure would not be per se catastrophic as the power electronic converters could revert to a sensor-less mode of operation until a convenient time is found for maintenance. This, of course, would have to be designed into the control system. The Mean Time To Repair (in our case, substitute) is expected to be less than 1 hour.

This exercise of computing the MTBF for the encoder identified that it is likely the lowest reliability component of the system. Considering this point, and recognizing that 'sensor-less control' of the power electronic drive is technically feasible, we will eliminate the encoder all together in the objective system design to eliminate this maintenance item and improve overall system reliability.

Flywheel Motor Generator Bearing MTBF

While the flywheel rotor operates on contactless active magnetic bearings, the present concept for the flywheel motor generator employs conventional rolling element bearings. These ball bearings wear due to phenomena such as rolling fatigue, lubrication contamination, misalignment, and corrosion, and will therefore need periodic replacement. Rolling element bearings have very predictable service life as a result of extensive maintenance history, and empirical equations for life prediction are well documented.

To find the MTBF life, the operating conditions (bearing load and operating speed) and bearing capacity are needed. For the objective system, the rotor weight is approximately 952 lb (distributed amongst four bearings), and the maximum operating speed is 19146 rpm. Timken duplex ball bearings of the size 50 mm ID x 80 mm OD x 16 mm thick were selected for the application with a rated capacity of 5500 lb at 10^6 cycle life. The following calculations were used to compute the MBTF for this combination of bearings and application conditions:

$$L_{10} = (\text{capacity} / \text{load})^3 * 10^6 / \text{rpm} / 60$$

$$L_{10} = (5500 / 238)^3 * 10^6 / 19146 / 60 = 10{,}743 \text{ hrs}$$

$$MTBF = 5*L_{10} = 53{,}715 \text{ hrs @ } 4{,}000 \text{ operating hours / year}$$

MTBF = 13.4 years of operation

A summary of the maintenance data pertaining to the flywheel energy storage system components (excluding power electronics) is shown in Volume 2. This information was used to generate a spare parts list, selecting components that have a relatively high likelihood of failure or frequent preventative maintenance schedule. The list of spares and the estimated inventory cost is tabulated in table 18.

Table 18. Summary of calculated and estimated flywheel system maintenance data

Maintenance Item	MTBF (Mean Time Between Failures, hrs)	Operating Years (Assume 4000 hrs/ yr)	MTTR (Mean Time To Repair)	MHTR/MTBF (Man Hours To Repair / MTBF)
FW Steel shaft	306,600	35	N/A	N/A
FW Composites	306,600	35	N/A	N/A
FW Mag bearing radial stator windings	306,600	35	32	2.09E-04
FW Mag bearing thrust stator windings	306,600	35	32	2.09E-04
FW Mag bearing feedback sensors	61,320	7	8	1.30E-04
FW Mag bearing control hardware	400,000	>35	8	2.00E-05
FW Auxiliary bearings	175,200	20	8	4.57E-05
FW Vacuum pump auxiliary system	61,320	7	4	6.52E-05
FW Vacuum seals for MG coupling end	61,320	7	8	1.30E-04
FW Vacuum seal for rotor cooling	61,320	7	4	6.52E-05
FW / MG Shaft coupling system	175,200	20	6	6.85E-05
FW Bellows support for seal	175,200	20	6	6.85E-05
Motor generator rotor	306,600	35	N/A	N/A
Motor generator stator	306,600	35	N/A	N/A
MG Armature windings	2,803,200	>35	32	1.14E-05
MG Field windings	2,803,200	>35	32	1.14E-05
Motor generator field control	400,000	>35	4	1.00E-05
MG rotor bearings	53,715	13	8	2.98E-04
MG Lubrication auxiliary system	61,320	7	4	6.52E-05
MG Instrumentation	61,320	7	4	6.52E-05
MG Shaft encoder	13,889	3.5	4	2.88E-04

Table 19. Summary of maintenance issues for flywheel energy storage system

Maintenance Item	MLDT (Mean Logistics Delay Time)	Notes and Assumptions
FW Steel shaft	N/A	Continuous duty 35 year design life, 4 men to replace
FW Composites	N/A	Continuous duty 35 year design life, 4 men to replace
FW Mag bearing radial stator windings	7 days (est)	Continuous duty 35 year design life on insulation, 4 men to replace
FW Mag bearing thrust stator windings	7 days (est)	Continuous duty 35 year design life on insulation, 4 men to replace
FW Mag bearing feedback sensors	10 hrs est (spare item)	Estimated instrumentation MTBF
FW Mag bearing control hardware	10 hrs est (spare item)	Typical MTBF published by amplifier manufacturers
FW Auxiliary bearings	10 hrs est (spare item)	20 year design life (est)
FW Vacuum pump auxiliary system	6 hrs est (spare item)	7 year operating life (est)
FW Vacuum seals for MG coupling end	10 hrs est (spare item)	7 year operating life (est)
FW Vacuum seal for rotor cooling	6 hrs est (spare item)	7 year operating life (est)
FW / MG Shaft coupling system	8 hrs est (spare item)	20 year operating life (est), 2 men to replace
FW Bellows support for seal	8 hrs est (spare item)	20 year operating life (est), 2 men to replace
Motor generator rotor	N/A	35 year design life, 2 men to replace
Motor generator stator	N/A	35 year design life, 2 men to replace
MG Armature windings	30 days (est)	Insulation life calculation based on operating temperature
MG Field windings	30 days (est)	Insulation life calculation based on operating temperature
Motor generator field control	7 days (est)	Typical MTBF published by servo amplifier manufacturers
MG rotor bearings	10 hrs est (spare item)	MTBF based on L50 life of bearings, computed, 2 men to replace
MG Lubrication auxiliary system	7 days (est)	7 year operating life (est)
MG Instrumentation	6 hrs est (spare item)	Estimated instrumentation MTBF
MG Shaft encoder	6 hrs est (spare item)	Calculated from manufacturer data, part may be eliminated

Table 20. List of spare parts inventory for flywheel energy storage system

Item Description	*Qty*	*Total*
Magnetic Bearing System		
Feedback sensors	4	$1,200
Control cabinet and hardware	4	$4,000
Auxiliary bearings	4	$2,000
Instrumentation and controls		
Vacuum sensors	2	$500
Control boards	1	$2,500
Vacuum and sealing system		
Vacuum pump auxiliary system	1	$2,500
Vacuum seals for MG coupling end	1	$15,000
Vacuum seal for rotor cooling	1	$7,500
FW / MG Coupling System		
Shaft coupling system	1	$10,000
Bellows support for seal	1	$2,000
Bearings / seals	4	$2,000
Shaft encoder	1	$800
TOTAL		**$50,000**

Rolls-Royce has compiled system level characteristics for a system to provide 2.5 MW of UPS power for a10 minute duration and a system to provide 2.5 MW of UPS power for a 5 minute duration. This information is presented in table 21. A summary of the component specifications for the 2.5 MW, 10 minute UPS duration system is presented in table 22.

Table 21. System level characteristics for 10 minute and 5 minute UPS duration

Characteristics - System Level - Option 2		
	2.5 MW for 10 Minutes	2.5 MW for 5 Minutes
• Salient Characteristics:		
Length, Width, Height	Same as Current AG9140RF Module (312.70" x 85.30" x 133.40")	Same as Current AG9140RF Module (312.70" x 85.30" x 133.40")
Maintenance Envelope (LxWxH)	Same as Current AG9140RF Module	Same as Current AG9140RF Module
Weight, Center of Gravity	121,940 Lbs	92,510 Lbs
Speed (rpm)	Optimized for maximum fuel efficiency	Optimized for maximum fuel efficiency
Exotic or Hazardous Materials?	No	No
Special Storage or Handling?	No	No
• Operational Characteristics:		
Mean Time Between Failure	2,253 Hrs	2,253 Hrs
Mean Time To Repair	4.1 Hrs	4.1 Hrs
Man-hours to Repair/Operating Hour	1.82×10^{-3}	1.82×10^{-3}
Mean Logistics Delay Time	TBD	TBD
• List of spares	See Individual Component Spares	See Individual Component Spares
• Equipment Rating: Normal and Emergency	Normal Operation: 3.0 MW @ 450V, 60 Hz, 0.8 PF, & 100F Flywheel Only Operation: 2.5 MW @ 450V, 60 Hz, 0.8 PF, & 100F for 10 min.	Normal Operation: 3.0 MW @ 450V, 60 Hz, 0.8 PF, and 100F Flywheel Only Operation: 2.5 MW @ 450V, 60 Hz, 0.8 PF, and 100F for 5 Minutes
• Efficiency Curve, including at Standby	See Individual Component Efficiencies	See Individual Component Efficiencies
• Time to Full Power:		
From Standby	60 Seconds	60 Seconds
From Secured	3 Minutes	3 Minutes
• Noise: Frequency(ies) and Level (dB)	The retrofitted AG9140RF will be designed to meet the same standard as the existing AG9140RF	The retrofitted AG9140RF will be designed to meet the same standard as the existing AG9140RF
• Operating Temp Range: Internal & External	32 to 104 F	32 to 104 F
• Failure Modes	See Individual Component Failure Modes	See Individual Component Failure Modes
• System Interface Requirements:		
Electrical Power: (Input)	Dark Ship Start: 28 VDC	Dark Ship Start: 28 VDC

Input Volts, Amps, Phases, Freq	Flywheels: 220 VAC, 45.5 A, 1 phase, 60 Hz Flywheel Motor/Generators: 460 VAC, 23.8 A, 3 phase, 60 Hz or 220 VAC, 22.7 A, 1 phase, 60 Hz FADC: 440 VAC and 28 VDC	Flywheels: 220 VAC, 45.5 A, 1 phase, 60 Hz Flywheel Motor/Generators: 460 VAC, 31.4 A, 3 phase, 60 Hz or 220 VAC, 22.7 A, 1 phase, 60 Hz FADC: 440 VAC and 28 VDC
Input Harmonic Limits	MIL-1399	MIL-1399
Backup Source?	Battery UPS	Battery UPS
• Electrical Power: (Output)		
Voltage, Amperage, Frequency, Ph	Entire Genset: 3.0 MW @ 450 VAC, 60 Hz, 3 phase Flywheels Only: 2.5 MW @ 450 VAC, 60 Hz, 3 phase for 10 minutes	Entire Genset: 3.0 MW @ 450 VAC, 60 Hz, 3 phase Flywheels Only: 2.5 MW @ 450 VAC, 60 Hz, 3 phase for 5 minutes
Output Harmonics	MIL-1399	MIL-1399
Backup Source	N/A	N/A
Applicable Spec or MILSTD	MIL-G-22077 and MIL-1399	MIL-G-22077 and MIL-1399
• Thermal - Cooling Required:		
Air – Volume, Pressure	Enclosure: 4500 CFM, 9" Pressure HSG: 7000 CFM, 60" Pressure and 1500 CFM, 100" Pressure in closed loop system	Enclosure: 4500 CFM, 9" Pressure HSG: 7000 CFM, 60" Pressure and 1500 CFM, 100" Pressure in closed loop system
Fluid – Type, Volume, Pressure	MIL-L-23699 Oil: 75 Lbs/min, 0 to 20 psig and 50 gpm, 70 psi Fresh water 97 gpm, 60 psi	MIL-L-23699 Oil: 75 Lbs/min, 0 to 20 psig and 50 gpm, 70 psi Fresh water 97 gpm, 60 psi
• Thermal Discharge:		
Air BTUs, Temp, Volume, Pressure	14,030 BTU/Hr from Genset to surrounding compartment	14,030 BTU/Hr from Genset to surrounding compartment
Fluid – Type, BTUs, Vol, Press, Temp	~200 gpm seawater (25-50 psig, 28-95 F)	~200 gpm seawater (25-50 psig, 28-95 F)
• Description of System Interfaces to the Ship and Auxiliary systems needed	Same as AG9140RF (need seawater, bleed air, fuel, and drainage connections and access to DDG 51 electrical grid, including 28 VDC line)	Same as AG9140RF (need seawater, bleed air, fuel, and drainage connections and access to DDG 51 electrical grid, including 28 VDC line)
• Expected Mounting Location of Components – include Type of Mount	Will be retrofitted onto existing AG9140RF module using same shock mounts in same location on ship	Will be retrofitted onto existing AG9140RF module using same shock mounts in same location on ship

Table 22. Component characteristics for 10 minute UPS duration

Characteristics - Option 2 - 2.5 MW for 10 Minutes							
Component Characteristics	501K GT	HS Generator	Flywheel	Flywheel M/G	Power Electronics	Supervisory Controls	Packager
• Salient Characteristics:							
Length, Width, Height	85.8"x 27"x 27"	84"x 64"x62"	90"L, 41.5"W, 41.5"H	33.1"L,25.8"W,25.8"H	TBD	26",54",54"	Information provided on preliminary layout drawings
Maintenance Envelope (LxWxH)	87.6"x 33"x 32"	TBD	130"L,81.5"W,81.5"H	73.1"L,65.8"W,65.8"H	TBD	TBD	See AG9140RF Technical Manuals
Weight, Center of Gravity	1545 Lbs	8755lbs	14715 lb, COG: 45.75"x, 0"y, 0"z ref flange face & CL	2368 lb, COG: 16"x, 0"y, 0"z ref flange face & CL	TBD	<1000 lbs	TBD
RPM	14340 rpm	15,000rpm	9573 - 19146 rpm	9573 - 19146 rpm	N/A	N/A	N/A
Exotic or Hazardous Materials?	No	No	No	No	No	No	No
Special Storage or Handling?	No	No	No	No	No	No	Environmentally controlled facility is recommended.
• Operational Characteristics:							
Mean Time Between Failure	12,232 Hrs (based on number of 501-K34 failures in the AG9140RF gensets between Jan 2007 and Jun 2007)	TBD	See Table 2.4	See Table 2.4	106,000 Hrs	>25000 hrs	12,232 Hrs (based on number of AG9140RF package component failures between Jan 2007 and Jun 2007, not including failures on components that would be removed during retrofit)
Mean Time To Repair	2.2 Man Hrs	TBD	See Table 2.4	See Table 2.4	2 Hrs	2.2 Man Hrs	2.2 Man Hrs
Man-hours to Repair/Operating Hour	1.80×10^{-4}	TBD	See Table 2.4	See Table 2.4	1.89×10^{-5}	8.80×10^{-5}	1.80×10^{-4}
Mean Logistics Delay Time	TBD	TBD	See Table 2.4	See Table 2.4	Externally Dependent	TBD	TBD
• List of spares	See USN Provisioning Parts Lists for 501-K34	complete generator	See Table 2.5	See Table 2.5	PM2000 Power Poles, customer standard stores		See USN Provisioning Parts Lists for AG9140RF
• Equipment Rating: Normal and Emergency	3.3 MW	100%	52 kWh / FW deliverable (208 kWh per skid)	625 kW / MG (2.5 MW per skid)	3.0 MW	N/A	N/A
• Efficiency Curve, including at Standby	See Figure 2.3	98%	N/A	94% at 9500 RPM, 96% at 14500 RPM, 95% at 19500 RPM	98% Full Power, 92% Half Power	N/A	N/A
• Time to Full Power:							
From Standby	60 seconds	as fast as the GT	500 ms	500 ms	<1 second	N/A	N/A
From Secured	60 seconds	as fast as the GT	1245 s (21 min)	1245 s (21 min)	TBD	FADC boot time (2 min)	N/A
• Noise: Frequency(ies) and Level (dB)	Compliant with BIW Purchase Spec 450-310-01A and MIL-STD-740	75db	160-319 Hz, 75dB (est)	160-638 Hz, 85 dB (est)	Not Measured	negligible	Compliant with BIW Purchase Spec 450-310-01A and MIL-STD-740
• Operating Temp Range: Internal & External	20 to 140 F	0 to 40 C	100°C int. / 49°C ext.	140°C int / 49°C ext.	0 to 50 C	20 to 122 deg F	Maximum internal: 250 degrees F Maximum external 140 degrees F.
• Failure Modes	See AG9140RF Technical Manuals - No FMECA	TBD	See Table 2.6	See Table 2.6	TBD	See AG9140RF Technical Manuals	See AG9140RF Technical Manuals
• System Interface Requirements:							
Electrical Power: (Input)	None	None	up to 10 kW control power & auxiliaries	up to 19 kW charge maintenance / 5 kW excitation, & auxiliaries	Draws all power directly from HSG and flywheels		
Input Vol, Amps, Phases, Freq	None	None	220 V, 45.5 A, 1 ph, 60 Hz	460 V, 23.8 A, 3 ph, 60 Hz / 220 V, 22.7 A, 1 ph, 60 Hz	450 VAC, 3 phase, 60 Hz	Normal: 440VAC and 28 VDC Dark Ship: 28 VDC	None
Input Harmonic Limits	None	None	MIL-1399	MIL-1399	TBD	N/A	None
Backup Source?	None	None	Battery UPS for controls and bearings	Battery UPS for field excitation	None Required		None
• Electrical Power: (Output)	N/A		N/A	625 kW / MG (2.5 MW per skid)			
Voltage, Amperage, Frequency, Ph	N/A	1100VDC,	N/A	600 Vl-lrms, 1402 Arms, 0-638 Hz, 3 ph	3.0 MW @ 450VAC, 60 Hz, 3 phase	N/A	N/A
Output Harmonics	N/A	TBD	N/A	MIL-1399 Compliant at 60 Hz bus		N/A	N/A
Backup Source	N/A	N/A	N/A	N/A		N/A	N/A
Applicable Spec or MILSTD	MIL-E-17341	TBD	N/A	MIL-1399		N/A	MIL-G-22077
• Thermal - Cooling Required:							
Air – Volume, Pressure	4500 SCFM, 9" Water	Blower 1 is 460V, 60Hz, 125hp, 60"static pressure, 7000 cfm	N/A	N/A	Negligible	N/A	4500 SCFM, 9" Water
Fluid – Type, Volume, Pressure	MIL-L-23699 Oil, 75 lbs/min max, inlet pressure - 0 to 20 psig	Blower 2 is 460V, 60HZ, 50hp, 100"static pressure, 1500 cfm	water, 10 gpm, 60 psi / skid	water, 28 gpm, 60 psi / skid	Water, 9 gpm/module (72 gpm total)	N/A	None
• Thermal Discharge:		Coolant pump for motor is 460V, 60Hz, 8hp, 50GPM, 70psi					
Air BTUs, Temp, Volume, Pressure	4500 SCFM, 9" Water	Fan for motor water-air heat exchanger is 460V, 60Hz, 12hp	N/A	N/A	Negligible	negligible	14,030 BTU/Hr from package to engine room
Fluid – Type, BTUs, Vol, Press, Temp	MIL-L-23699 Oil, 75 lbs/min max, pressure - 55 psig, 180 F max, 1800 BTU/min	Oil pump is 460V, 60Hz, 6hp.	water, 20 kW (1137 BTU/m), 10 gpm, 60 psi, 42°C outlet / skid	water, 56 kW (3185 BTU/m), 28 gpm, 60 psi, 42°C outlet / skid	2-3% of wattage	N/A	Sea water, ~200 gpm, 25 to 50 psig, 28 to 95 F
• Description of System Interfaces to the Ship and Auxiliary systems needed	No direct connection to ship auxiliaries required. All auxiliaries provided by package.	No direct connection to ship auxiliaries required. All auxiliaries provided by package.	The flywheel energy storage system will interface to the ship transparently through the electrical service system. Status and control will be facilitated through the updated RR9140 control panel. Auxiliaries for the flywheel include a magnetic bearing control system, control power, and cooling water.	The flywheel energy storage system will interface to the ship transparently through the electrical service system. Status and control will be facilitated through the updated RR9140 control panel. Auxiliaries for the motor/generator include a bearing lubrication skid, field exciter and cooling water. Flywheel charge maintenance requires a continuous low power demand from the electrical service.	No direct connection to ship auxiliaries will be required. All auxiliaries will be provided by package.	No direct connection to ship auxiliaries will be required. All auxiliaries will be provided by package.	Connections will be the same as on the AG9140RF (Package will need connections to the Seawater, Bleed Air, Fuel, and Drain Systems)
• Expected Mounting Location of Components – include Type of Mount	on shock mounts inside main enclosure	4 bolts at the base	Pedestal mounted to modified AG9140 skid, shock isolated	Flange mounted to FW on modified AG9140 skid		shock mounts	Location provided on preliminary layout drawing. Mounting to be hard or isolation as required.

Appendix 1. Homopolar Inductor Alternator Technology Literature Search

[1] Siegl, M.; Kotrba, V., “Losses and cooling of a high-speed and high-output power homopolar inductor alternator”, Electrical Machines and Drives, 1991. Fifth International Conference on (Conf. Publ. No. 341), 11-13 Sep 1991 Page(s):295 - 299

[2] McGrow, L.; Pollock, C., “Low cost brushless generators”, Industry Applications Conference, 1999.Thirty-Fourth IAS Annual Meeting. Conference Record of the 1999 IEEE, Volume 2, 3-7 Oct. 1999 Page(s):1229 - 1236 vol.2

[3] Jin He; Feng Lin, “A high frequency high power IGBT inverter drive for 45 HP/16,000 rpm brushless homopolar inductor motor” Industry Applications Conference, 1995. Thirtieth IAS Annual Meeting, IAS '95., Conference Record of the 1995 IEEE, Volume 1, 8-12 Oct. 1995 Page(s):9 - 15 vol.1.

[4] Clifton, D., et al, Assignee: Magnetic Bearing Technologies, Inc., “Integrated motor/generator/flywheel utilizing a solid steel rotor”, United States Patent Number 5,731,645, filed Feb 1996, issued March 1998.

[5] Perry Tsao; Senesky, M.; Sanders, S.R., “An integrated flywheel energy storage system with homopolar inductor motor/generator and high-frequency drive”, Industry Applications, IEEE Transactions on Volume 39, Issue 6, Nov.-Dec. 2003 Page(s):1710 – 1725.

[6] Pinkerton, J., Assignee: Active Power, Inc., “High inertia induction alternator”, United States Patent Number 5,929,548, filed Sept 1997, issued July 1999.

[7] Pinkerton, J., Assignee: Active Power, Inc., “High-efficiency inductor-alternator”, United States Patent Number 6,323,573, filed Mar 2000, issued Nov 2001.

[8] Lorilla, L.M.; Keim, T.A.; Lang, J.H.; Perreault, D.J., "Topologies for future automotive generators. Part I. Modeling and analytics", Vehicle Power and Propulsion, 2005 IEEE Conference, 7-9 Sept. 2005 Page(s):74 - 85

[9] Siegl, M.; Erdelyi, E.A., “Damper Bars and Their Influence in Operating Homopolar Inductor Alternators for Aerospace SuppliesÂ¿Part I: Determination of Saturated Time-Dependent Reactances”, Aerospace and Electronic Systems, IEEE Transactions on Volume AES-9, Issue 6, Nov. 1973 Page(s):925 – 931.

[10] Tsao, P.; Senesky, M.; Sanders, S., “A synchronous homopolar machine for high-speed applications”, Industry Applications Conference, 2002, 37th IAS Annual Meeting. Conference Record of the Volume 1, 13-18 Oct. 2002 Page(s):406 - 416 vol.1

[11] Hippner, M.; Harley, R.G., “High speed synchronous homopolar and permanent magnet machines comparative study” Industry Applications Society Annual Meeting, 1992., Conference Record of the 1992 IEEE, 4-9 Oct. 1992 Page(s):74 - 78 vol.1

[12] Walker, J.H., “The theory of the inductor alternator”, Proc. IEE Vol 89, 1942, pp 227-241.

[13] G. C. Jain, “ Design Aspects of a Homopolar Inductor Alternator”, IEEE Transactions on Power Apparatus and Systems, Vol. 83, pp. 1009-1015, October 1964.

[14] N. Ellis, F. A. Collins, “Brushless Rotating Electrical Generators for Space Auxiliary Power Systems,” National Aeronautics and Space Administration, Contract No. NAS 3-2783, Vol. 1, April 1965.

[15] Bornemann, H.J.; Tonoli, A.; Ritter, T.; Urban, C.; Zaitsev, O.; Weber, K.; Rietschel, H.; "Engineering prototype of a superconducting flywheel for long term energy storage" Applied Superconductivity, IEEE Transactions on Volume 5, Issue 2, Part 1, Jun 1995 Page(s):618 - 621 .

[16] Colling, D.; "Soft magnetic structural alloys for elevated-temperature applications" Magnetics, IEEE Transactions on Volume 7, Issue 1, Mar 1971 Page(s):91 - 102 .

[17] Das Gupta, A.K.; Dash, P.K.; "Derivation of the Basic Constants of Three-Phase Inductor Alternators in Terms of Winding Parameters" IEEE Transactions on Power Apparatus and Systems Volume PAS-88, Issue 5, Part Part-I, May 1969 Page(s):566 - 574 .

[18] Das Gupta, A.K.; Dash, P.K.; "Transient Analysis of One Type of Inductor Alternator Under Unsymmetrical Short Circuits" IEEE Transactions on Power Apparatus and Systems Volume PAS-88, Issue 5, Part Part-I, May 1969 Page(s):575 - 579 .

[19] Dash, P.K.; "Transient Performance of Three-Phase Inductor-Type Synchronous Generators: Part I-Symmetrical Short Circuit" IEEE Transactions on Power Apparatus and Systems Volume PAS-92, Issue 3, May 1973 Page(s):1149 - 1156 .

[20] Dash, P.K.; Das Gupta, A.K.; "Design Aspects of Three-Phase Inductor Alternators" IEEE Transactions on Power Apparatus and Systems Volume PAS-88, Issue 11, Nov. 1969 Page(s):1718 - 1724 .

[21] Dash, P.K.; Das Gupta, A.K.; "Inductance Coefficients of Three-Phase Inductor Alternators: Part IÂ¿Analytical Study" IEEE Transactions on Power Apparatus and Systems Volume PAS-88, Issue 11, Nov. 1969 Page(s):1725 - 1730 .

[22] Goodier, E.R.T.; Pollock, C.; "Homopolar variable reluctance machine incorporating an axial field coil" Industry Applications, IEEE Transactions on Volume 38, Issue 6, Nov.-Dec. 2002 Page(s):1534 - 1541 .

[23] Haller, T.; Mischler, W.; "A comparison of linear induction and linear synchronous motors for high speed ground transportation" Magnetics, IEEE Transactions on Volume 14, Issue 5, Sep 1978 Page(s):924 - 926 .

[24] Hwang, H.H.; Sarma, C.K.; "Unbalanced Operations of Three Phase Inductor Alternators with Damper Winding" IEEE Transactions on Power Apparatus and Systems Volume PAS-91, Issue 6, Nov. 1972 Page(s):2286 - 2294 .

[25] Jokl, A.L.; Amstutz, L.I.; Erdelyi, E.A.; "Nonsymmetrical, Nonlinear Aerospace Alternators on Nonlinear Loads" Aerospace and Electronic Systems, IEEE Transactions on Volume AES-11, Issue 3, May 1975 Page(s):298 - 315 .

[26] Kumaresan, N.; Subbiah, M.; "High frequency industrial power supplies using inductor alternators driven by bio-mass gasifier based systems" TENCON 2003. Conference on Convergent Technologies for Asia-Pacific Region Volume 1, 15-17 Oct. 2003 Page(s):273 - 277 Vol.1 .

[27] Lorilla, L.M.; Keim, T.A.; Lang, J.H.; Perreault, D.J.; "Topologies for Future Automotive Generators – Part II: Optimization" Vehicle Power and Propulsion, 2005 IEEE Conference 7-9 Sept. 2005 Page(s):831 - 837 .

[28] McGrow, L.; Pollock, C.; "The use of inductor alternators with electronic regulation for DC generation" Electrical Machines and Drives, 1999. Ninth International Conference on (Conf. Publ. No. 468) 1-3 Sept. 1999 Page(s):381 - 385 .

[29] Ochije, K.N.; Pollock, C.; "A controlled PWM AC/DC converter for a high-speed brushless generator for minimum kVA rating" Industry Applications, IEEE Transactions on Volume 40, Issue 3, May-June 2004 Page(s):861 - 868 .

[30] Ochije, K.N.; Pollock, C.; "Design and control of AC/DC converter for a high speed brushless generator for minimum kVA rating" Industry Applications Conference, 2003. 38th IAS Annual Meeting. Conference Record of the Volume 2, 12-16 Oct. 2003 Page(s):701 - 708 vol.2 .

[31] Ochije, K.N.; Pollock, C.; "Simulink model of controlled power factor flux switching generator system for embedded power generation" Industry Applications Conference, 2005. Fourtieth IAS Annual Meeting. Conference Record of the 2005 Volume 4, 2-6 Oct. 2005 Page(s):2657 - 2664 Vol. 4 .

[32] Ochjie, K.N.; Pollock, C.; "Design/performance of a flux switching generator system for variable speed applications" Industry Applications Conference, 2005. Fourtieth IAS Annual Meeting. Conference Record of the 2005 Volume 3, 2-6 Oct. 2005 Page(s):1567 - 1574 Vol. 3 .

[33] Pillai, K.P.P.; Nair, A.S.; Bindu, G.R.; "Analysis of train lighting brushless alternator with skewed rotor for harmonic minimization" Power Engineering Conference, 2005. IPEC 2005. The 7th International 29 Nov.-2 Dec. 2005 Page(s):1171 - 1175 Vol. 2 .

[34] Pollock, C.; Pollock, H.; Barron, R.; Sutton, R.; Coles, J.; Moule, D.; Court, A.; "Flux switching motors for automotive applications" Industry Applications Conference, 2003. 38th IAS Annual Meeting. Conference Record of the Volume 1, 12-16 Oct. 2003 Page(s):242 - 249 vol.1 .

[35] Schenk, K.E.; Fuchs, E.F.; Trutt, F.C.; "Load Analysis of Nonlinear Homopolar Inductor Alternators" IEEE Transactions on Power Apparatus and Systems Volume PAS-92, Issue 2, March 1973 Page(s):442 - 448 .

[36] Schenk, K.F.; Jokl, A.L.; "High-Speed Homopolar Inductor Alternators of Minimum Leakage Reactance" Aerospace and Electronic Systems, IEEE Transactions on Volume AES-6, Issue 4, July 1970 Page(s):491 - 497 .

[37] Senesky, M.K.; Tsao, P.; Sanders, S.R.; "Simplified modelling and control of a synchronous machine with variable-speed six-step drive" Applied Power Electronics Conference and Exposition, 2004. APEC '04. Nineteenth Annual IEEE Volume 3, 2004 Page(s):1803 - 1809 Vol.3 .

[38] Subbiah, M.; Adikesavan, A.S.; Krishnamurthy, M.R.; "Comments on "Single-Winding Single-Phase Inductor Alternator"" Aerospace and Electronic Systems, IEEE Transactions on Volume AES-14, Issue 2, March 1978 Page(s):386 - 388 .

[39] Subbiah, M.; Krishnamurthy, M.R.; "Certain Design Aspects of Single-Winding Three-Phase Inductor Alternators" Aerospace and Electronic Systems, IEEE Transactions on Volume AES-10, Issue 5, Sept. 1974 Page(s):648 - 658 .

[40] Subbiah, M.; Krishnamurthy, M.R.; "Single-Winding Single-Phase Inductor Alternator" Aerospace and Electronic Systems, IEEE Transactions on Volume AES-12, Issue 6, Nov. 1976 Page(s):689 - 697 .

[41] Venkataratnam, K.; Bhattacharya, T.K.; Sengupta, M.; "Theory, performance prediction and indirect sensing of rotor position of a switched reluctance motor under saturation" Electric Power Applications, IEE Proceedings- Volume 146, Issue 6, Nov. 1999 Page(s):667 - 677 .

[42] Yen, K.K.; Yang, C.-H.; Wu, F.Y.; "Dynamic commutation voltages in a reciprocating linear inductor alternator" Aerospace and Electronic Systems, IEEE Transactions on Volume 28, Issue 2, April 1992 Page(s):413 - 419 .